DEVELOPMENT OF NON-DESTRUCTIVE INFRARED FIBER OPTIC METHOD FOR ASSESSMENT OF LIGAMENT AND TENDON COMPOSITION

A Dissertation
Submitted to
the Temple University Graduate Board

In Partial Fulfillment
of the Requirements for the Degree
DOCTOR OF PHILOSOPHY IN BIOENGINEERING

by
Mugdha Vijay Padalkar
Diploma Date (May 2016)

Examining Committee Members:
Dr. Nancy Pleshko, Department of Bioengineering
Dr. Ruth Ochia, Department of Bioengineering
Dr. Mary Barbe, Department of Anatomy and Cell Biology, Temple University School of Medicine
Dr. Theresa Freeman, Department of Orthopaedic Surgery, Division of Orthopaedic Research, Thomas Jefferson University

ABSTRACT:

More than 350,000 anterior cruciate ligament (ACL) injuries occur every year in the United States. A torn ACL is typically replaced with an allograft or autograft tendon (patellar, quadriceps or hamstring), with the choice of tissue generally dictated by surgeon preference. Despite the number of ACL reconstructions performed every year, the process of ligamentization, transformation of a tendon graft to a healthy functional ligament, is poorly understood. Previous research studies have relied on mechanical, biochemical and histological studies. However, these methods are destructive. Clinically, magnetic resonance imaging (MRI) is the most common method of graft evaluation, but it lacks adequate resolution and molecular specificity. There is a need for objective methodology to study the ligament repair process that would ideally be non- or minimally invasive. Development of such a method could lead to a better understanding of the effects of therapeutic interventions and rehabilitation protocols in animal models of ligamentization, and ultimately, in clinical studies. Fourier transform infrared (FT-IR) spectroscopy is a technique sensitive to molecular structure and composition in tissues. FT-IR fiber optic probes combined with arthroscopy could prove to be an important tool where minimally invasive tissue assessment is required, such as assessment of graft composition during the ligamentization process. Spectroscopic methods have been used to differentiate normal and diseased connective tissues, but have not been applied to investigate ligamentization, or to investigate differences in tendons and ligaments. In the proposed studies, we hypothesize that infrared spectroscopy can

provide molecular information about the compositional differences between tendons and ligaments, which can serve as a foundation to non-destructively monitor the tissue transformation that occurs during ligamentization.

Keywords:

Anterior cruciate ligament, histology, infrared spectroscopy, ligamentization, magnetic resonance imaging, mechanical properties, multivariate analysis, partial least square discriminant analysis, patellar tendon, reconstruction,

DEDICATION

I dedicate my dissertation to Neeraj, my dear husband, without whom this dream was not possible! Thanks for making me this person who is respected by everyone. I equally owe this thesis to my dad, who is my inspiration, my loving mom, who always stood by me, my sisters, the perfect role models one could ask for and my brother, who is my biggest strength.

***And** to the wonderful city of Philadelphia…My home away from home!*

ACKNOWLEDGEMENT

I would like to take a moment to look back at my journey and thank each and every individual I met during my time at Temple University. First of all I would like to thank Temple University for accepting me as a graduate student. I also would like to thank Vice provost office for the Fellowship. I feel so fortunate to have had four successful, talented, strong female members on my thesis committee. I would like to thank my adviser, Dr. Nancy Pleshko, my committee members Dr. Barbe, Dr. Ochia and Dr. Freeman for guiding me through this journey to be a better researcher.

My life is full of wonderful coincidences. Long ago, I graduated with a bachelor degree and declared, I will never take a class again. Met Neeraj, fell in love with him and decided to go for a Master's degree. I got married and within a month I came to America with my wonderful husband, Neeraj. I was still trying to figure out everything things; new language, new country (and cooking, of course!) and on the top of that was applying for graduate school. After several rejections, I came to meet Dr. Chen in Mechanical Engineering department and that afternoon changed my life! He introduced me to Dr. Peridier. She welcomed me with a big smile. She looked at it for a moment and kept it aside and started talking to me about my life. When I told her I recently got married and came here, she said," You are going through so many changes at the same time and I can see how hard it must be!" It was the first time someone had looked at me as a person and not as a prospective student. First time in so many months I felt accepted. There were no teaching assistant position available at that time. But she insured me that if anything comes up, I will be the first one to get a call and she did. Thank you Dr. Peridier!

The other night, Neeraj and I were talking about the movie ‘Martian’ and I said to him,” if I get stuck on the Mars I will just give up!” He looked at me and said, “No, you will call Dr. Pleshko and you guys will work it out!” such is your presence in my life Dr. Pleshko. When someone says that my adviser is like my mom it feels very cliché! But when every time when students from other lab come to you for advice, I always got the jealous feeling of sharing your affection with them. Thank you for always being there for your students! You are the best adviser any PhD student can ask for.

I would like to thank my current and former TISL lab members (Ramya, Heejin, Farzad, Nicholas, Kenny, Rutvin, Yusra, Yosef, James, Meenakshi) for helping me in this journey. I am so grateful to Padraig Glen who helped me in my dissections without whom the vegetarian in me wouldn’t have survived! I was very fortunate to learn from Dr. Cushla McGoverin, Dr. Arash Hanifi and Dr. Uday Palukuru. I would also like to thank Dr. Soslowsky, Dr. Snehal Shetye, and Dr. Mike Hast for allowing me to use their mechanical testing facility at University of Pennsylvania.

As I said, my life is full of coincidences and if I have to tie all these coincidences I can only think of the existence of the All mighty! Every time I lost hope, I stumbled upon a new opportunity, a new guiding hand!

Thank you!

Dr. Mugdha Padalkar

TABLE OF CONTENTS

Contents

LIST OF ABBREVIATIONS

Anterior cruciate ligament (ACL)

Magnetic resonance imaging (MRI)

Fourier transform infrared (FT-IR)

Fourier transform infrared imaging spectroscopy (FT-IRIS)

Medial collateral ligament (MCL)

Anteromedial bundle (AMB)

Posterolateral bundle (PLB)

Mid infrared (Mid-IR)

Near infrared (NIR)

Proteoglycans (PG)

Attenuated total reflectance (ATR)

Multiplicative scatter correction (MSC)

Extended multiplicative scatter correction (EMSC)

Standard normal variate (SNV)

Principal component analysis (PCA)

Partial least squares regression (PLS)

Linear discriminant analysis (LDA)

Partial least squares discriminant analysis (PLS-DA)

Posterior cruciate ligament (PCL)

Polymethylmethacrylate (PMMA)

Dimethylmethylene blue (DMMB)

Sulfated glycosaminoglycan (sGAG)

LIST OF FIGURES

LIST OF TABLES

CHAPTER 1

1. BACKGROUND AND LITERATURE REVIEW:

1.1 ACL injury and reconstruction:

The anterior cruciate ligament (ACL) is a dense connective tissue that connects the femur with the tibia. The primary function of the ACL is to resist anterior tibial translation and rotational loads. The incidence of ACL injuries is increasing, with a current annual incidence of 350,000 injuries per year in the United States alone [4]. ACL injuries often result in instability of the knee joint and an early onset of osteoarthritis (OA) [5].

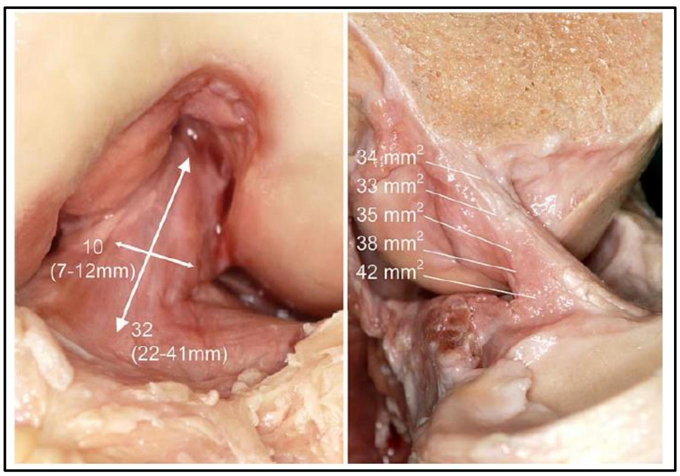

Figure 1: Gross anatomy of anterior cruciate ligament [3]

It was found that the thickness of ACL varies from the mid-substance (middle region) to the insertion sites. The thickness of ACL near the femoral insertion site is~ 3.54 mm whereas the thickness in the mid substance is~ 3.4 mm [1]. The average human ACL is 32 mm in length from femoral insertion to tibial insertion site, its width is 7-12 mm and the thickness is ~ 3 mm [3, 6]. It is made of two bundles, the anteromedial bundle (AMB) and the posterolateral bundle (PLB) [7]. There are some

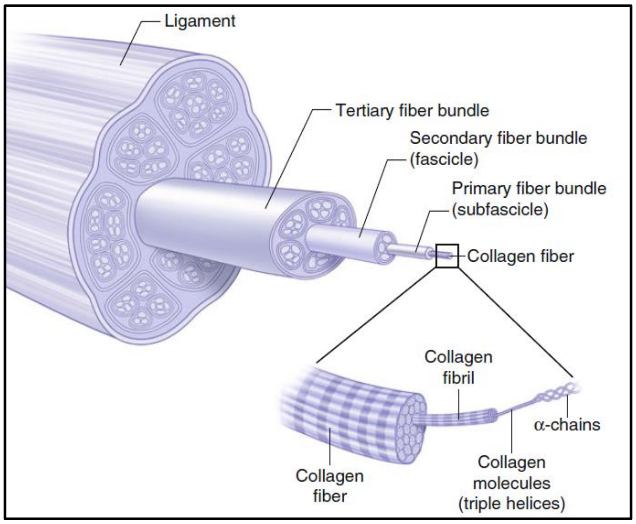

Figure 2: Schematic representation of ligament structure[1]

studies stating that ACL is made of three or more bundles [8], but here the assumption of two bundles will be made. These two bundles play an important role to insure the proper function of ACL**.** The AMB is tighter in flexion and lax in extension. The length of the bundles changes during flexion and extension. In terms of the function of the ACL, the AM bundle presents the opposition to anterior translation of tibia. The PM bundle is shown to carry significantly lower force when compared to the AMB [9]. The primary cell type in an ACL is fibroblast, but cell morphology is location specific [1]. The cells in the proximal part of the ACL are round and ovoid, the middle part has fusiform and spindle-shape fibroblasts and the distal part of the ACL has ovoid fibroblasts [3]. The ACL is composed of collagen (70%), water (60-80%), glycosaminoglycan, and elastic components.

Collagen: The ACL has a unique hierarchical structure as shown in Figure 2 [1]. The main biochemical component of this structure is collagen type I. A group of collagen fibrils comprise a collagen fiber, a group of fibers comprise a sub-fascicle, and groups of sub-fascicles comprise fascicles. In addition to collagen bundles, fascicles are packed with proteoglycans and elastin. Finally, bunches of fascicles wrapped in an epiligament forms a ligament [1]. There is some collagen II, present in the ACL near the insertion sites where ligament meets the bone, and collagen III (12%) and V [3].

The primary function of the collagen in the ACL is to resist tension. It also plays an important role at the insertion sites to avoid failure of insertion site under force. The insertion site is composed of four distinct zones, ligament, fibrocartilage, mineralized fibrocartilage and bone. The collagen fibers span the all zones and keep the material together. This arrangement makes the force transition from ligament to bone smoother [10].

Glycosaminoglycan: One of the main components of non-collagenous proteins are the glycosaminoglycans (GAGs) [11, 12], which are negatively charged and serve to bind water. These are responsible for the shock absorbing ability to the ligament.

Water: Ligaments contain ~60-70% water. Water along with non-collagenous proteins form a gel like structure. Ligaments are viscoelastic tissues. The viscoelastic behavior of the ligament results from a combination of interactions of water, collagen and GAGs. The GAGs are responsible for the flow of water through the collagen network. It is hypothesized that the collagen fibers are interconnected via GAGs and are submerged in gel of non-collagenous proteins and as the load is applied on the tissue it exerts forces on the collagen fibers [13].

1.2 Ligament Healing and Reconstruction

ACL, being an intra-articular tissue, has very little capacity to repair itself [14]. It is known that the extra-articular tissues, such as the medial collateral ligament (MCL) can heal themselves Previous studies have looked at this healing variation in intra- and extra- articular tissues from different approaches, such as the cellular response to the wound, the formation of new extracellular matrix, or the presence of blood vessels in the vicinity of the injured tissue. It was found that the cellular response is present in both tissues but the extracellular matrix formation is rapid in extra-articular tissues. A recent study was conducted to investigate the healing response of an ACL and MCL. A wound was created in ACL and MCL tissues in a canine model and monitored for 6 weeks. The tissues were evaluated based on immunochemistry (for fibrinogen, fibronectin, PDGF-A, TGF-b, and FGF) histological scoring system. It was found that the biggest difference between the mechanisms of healing of these ligaments was the formation of gap (a blood clot) between the wound sites [14]. Another study found that the fibroblasts in ACLs are different from the fibroblasts in MCL [15]. There is, however, a lot of information still required about why intra-articular tissues cannot heal while extra-articular tissues do have potential to heal. As ACL has very little capacity to heal, the best solution is to reconstruct a torn ACL with either allografts from donors or autograft tendons, such as patellar tendon, hamstring tendon and quadriceps tendon [16]. In the following paragraphs, the advantages and disadvantages of the available graft choices are discussed. The use of allograft reduces the surgery time as there’s no need to harvest a replacement tendon, but there is a risk of disease transmission, bacterial infection and compromised mechanical properties due to storage [16]. It has been shown that the methods of graft preservation such as freeze drying, thawing cycles and sterilization affect the mechanical properties of the graft tissue.

Graft Choices: Autograft tendons are often used for ACL reconstruction, especially the patellar tendon. The patellar tendon is the gold standard choice. However, recently, hamstring tendons have been used for ACL reconstructions. The patellar tendon graft is considered as the preferred choice because of its mechanical properties, anatomical location, which is similar to its desired use as a bone-patellar tendon-bone graft, and the fact that its use, which involves taking just a region of the tendon, doesn't affect the stability of the knee joint. However, it may cause donor site morbidity, muscle weakness, patellar tendonitis, knee pain and arthrofibrosis [16, 17]. A hamstring autograft has reduced donor site morbidity but has a longer period of bone to tissue integration [16]. Quadriceps tendon is also emerging as a choice for ACL reconstruction.

Although autografts do provide a good solution for ACL reconstruction, they nevertheless they do present some problems such as donor site morbidity and muscle weakness, and thus tissue engineering of the ligament could be another solution. There have been several studies showing promising results in ligament tissue engineering, which will not be discussed in detail here, but is further described in this review [18].

For the scope of this thesis, only ACL reconstruction with patellar tendon is discussed in detail.

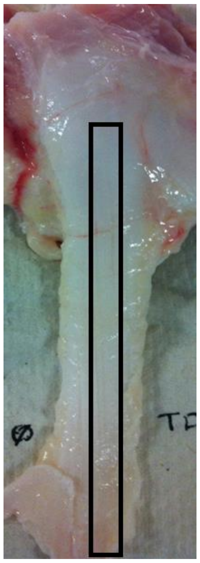

Figure 3: Patellar tendon graft harvest: The surgeons use either the mid third or the medial or lateral third part of the tendon for ACL reconstruction.

ACL reconstruction surgery is performed arthroscopically, which is a minimally invasive surgery. Three small incisions are made in the anteromedial, anterolateral and accessory anteromedial regions. These three portals are used to insert surgical tools and the arthroscope during the surgery. In the case of ACL reconstruction with a patellar tendon, surgeons either harvest the middle, lateral or medial third part of the tendon as a graft as shown in Figure 3. The graft is typically ~10mm in length. This bone-patellar tendon-bone graft is then arthroscopically reconstructed in the articular space [19].

Differences between ACL and patellar tendon: Even though the patellar tendon is the gold standard choice for ACL reconstruction, there are similarities as well as differences between ACLs and patellar tendons. ACL and patellar tendon both are dense connective tissues, but the ACL connects the femur to the tibia (intra-articular) and the patellar tendon connects the patella to the tibia (extra-articular). ACLs and patellar tendons both display a crimped structure due to the collagen fiber arrangement. The primary function of an ACL is to provide stability to the knee against twisting and pivoting motions [1] , whereas the patellar tendon provides straightening power to the knee joint. Biochemically, ACLs and tendons both have ~70% (dry weight) collagen and ~ 60-80% water content. ACL has ~88% type I collagen and 12% type III collagen, but tendons have only ~5% type III collagen [20]. Biochemically, the biggest difference between an ACL and the patellar tendon is the proteoglycan (PG) content. ACL has ~9% PG content and patellar tendon has only ~3%. The collagen fiber arrangement in these two tissues is different as well; collagen fibers are parallel to long axis in tendon and in ligaments, collagen fibers are oriented in different planes [10, 21].

1.3 Ligamentization

It has been shown that the grafted tendon undergoes transformation due to new environment (synovial fluid) and mechanical forces, and remodels into a structure similar to an ACL. This process is known as ligamentization [22]. Ligamentization has been studied in different animals such as sheep, pig and rabbit [22-24]. Previous studies have relied heavily on biochemical and histological analysis [2, 22] to study the progress of the ligamentization process.

Ligamentization stages: Ligamentization has been divided into 3 main stages: early stage, remodeling stage and a maturation stage [25, 26]. The ligamentization process is discussed here in terms of cell repopulation, shape of the cell, nucleus orientation, production of extracellular matrix and vascularity.

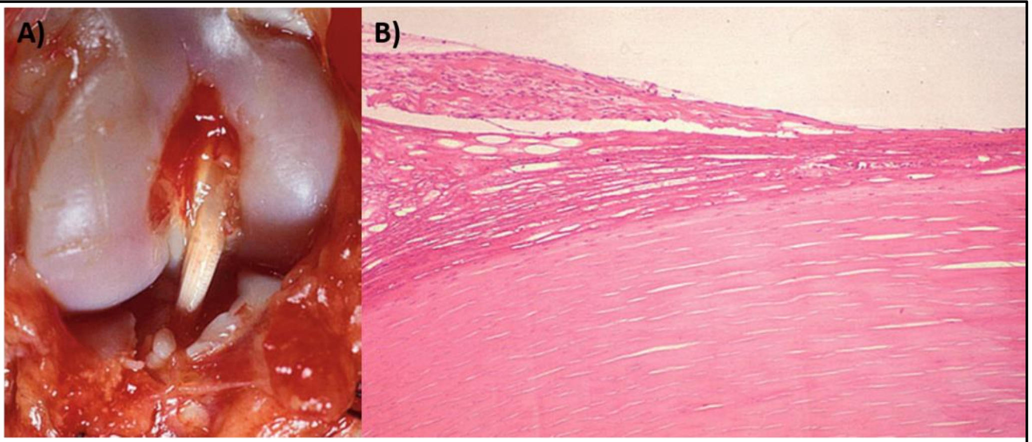

First week. (**a**) Gross pathology. (**b**) Avascular and acellular graft

Figure 4: In an animal model, the first week the graft shows hypocellularity[2]

In the first stage of ligamentization (Figure 4), the graft shows hypocellularity, random collagen orientation and no crimp pattern, as would be seen in a native ACL.

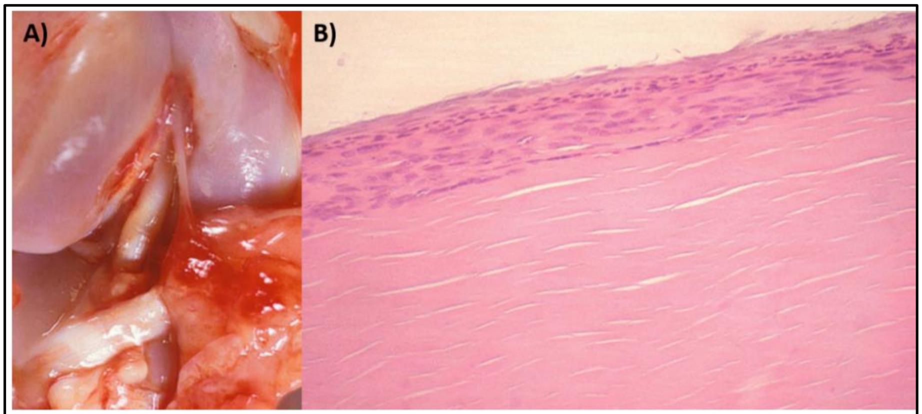

Second week. (**a**) Gross pathology. (**b**) Peripheral portion of the graft repopulated with cells

Figure 5: In the second week of ligamentization, the cells start repopulating from the peripheral region of the graft [2]

The second stage Figure 5, which is a remodeling stage, is characterized by hypercellularity at the periphery of the graft, repopulation of the tendon graft with fibroblast and synovial cells, longitudinally oriented collagen fibers (although not throughout the tissue), the shape of the cell nuclei more similar to ACL, but still no

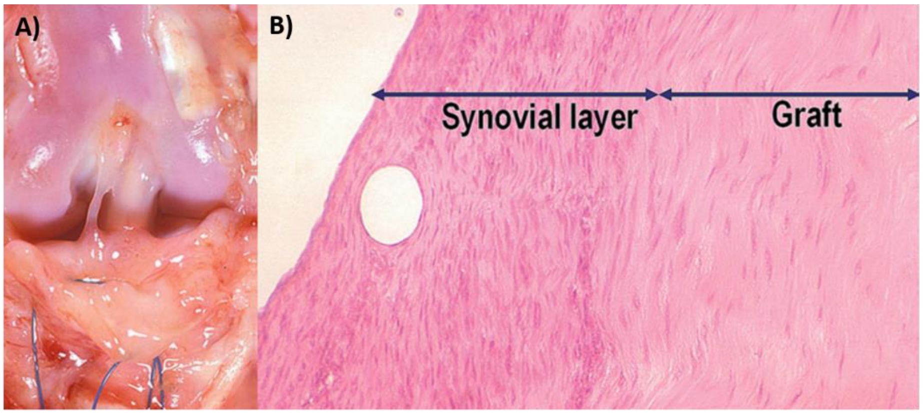

Third week. (**a**) Gross pathology. (**b**) Entire graft repopulated by cells

Figure 6: In the final stage of ligamentization, graft shows uniform crimp pattern [2]

crimp pattern is seen. As the final ligamentization stage approaches (Figure 6), the graft shows uniform crimp collagen orientation, cell shape like native ACL, and cellularity decreases as in native ACL [26]. It should be noted that the cells repopulate at the periphery of the graft first and progress towards the center of the graft.

In humans, very few studies have looked at the histology of the remodeling graft due to the destructive nature of this method. However, in a detailed review of the human ligamentization process [25]**,** the graft was found to have increased vascularization in the early stage of ligamentization, even though it reduced toward the final stage of remodeling. The cells of the graft showed hypercellularity and were metabolically active at the early stage. Toward the end of the remodeling process the cells were longitudinally aligned. Similar to animal ligamentization models, the collagen in human ligamentization was randomly organized in the initial stages but had parallel orientation at the end of the process [25]. The ligamentization process can take more than a year after reconstruction surgery [27].

1.4 Current methods of evaluation:

Clinically, arthroscopic evaluation has been the gold standard to diagnose and treat intra-articular tissue damage such as in articular cartilage [28], ACL [29], and meniscus [30]. Arthroscopy allows the surgeon to have a look at the intraarticular tissue with a minimally invasive procedure. In this procedure, three or more small insertions are made near knee area. Through these insertions, arthroscopic surgical instruments, a camera and a fiber optic probe are inserted into the knee. Thus arthroscopy provides a visualization tool to diagnose intra-articular tissues. The surgery is minimally invasive, therefore the recovery time is greatly reduced, compared to an open surgery. However, arthroscopic evaluations are generally observer dependent, which results in the decision making process being quite subjective.

Another method that has been used to study the ligamentization process in animal models as well as in human reconstructed ACL is histological analysis [2, 22]. In humans, biopsies are obtained from the reconstructed graft during second look arthroscopy [25], although this is not very common. In a histological analysis, tissues are fixed in formalin, embedded in paraffin and sectioned on histology slides. These slides are then deparaffinized in xylene and graded alcohol solutions, stained with haematoxylin and eosin and are examined microscopically. Remodeling of the graft is studied for neovasculization, cell morphology, and changes in extracellular matrix [25]. There is a scarcity of human ligamentization studies due to destructive nature of the assessment i.e. biopsies of remodeling graft. Especially in human ACL reconstruction the biopsies may hinder the graft remodeling. The biopsies are often limited to 2-3mm diameter hence they may not represent the entire tissue [25]. The findings from these few studies have shown that the ligamentization process differs from that of animal models [25], as the time line to recovery is slower. Better understanding of the ligamentization process could improve the postoperative therapies and rehabilitation protocols. A non-destructive method could be useful in animal models as well. It will allow longitudinal studies of the same tissue in the same animal, as every tissues response to the remodeling process can be slightly different.

1.5 Biomechanics of the ligament:

Along with the chemical changes that occur during ligamentization, mechanical properties of the remodeling graft are often of interest. It has been shown that the

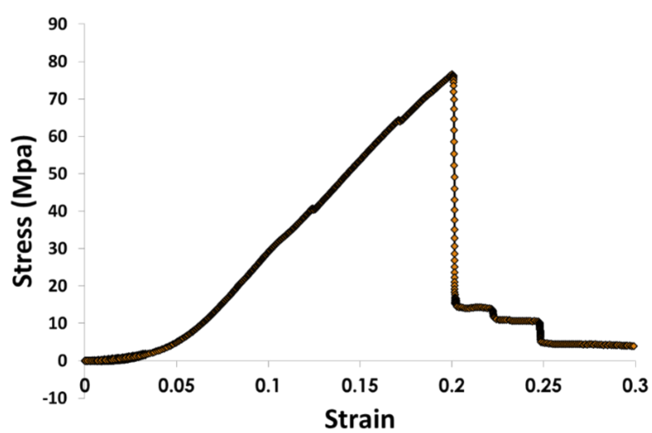

Figure 7: Stress strain diagram for typical tensile test of a ligament

graft never returns to the 100% of its mechanical strength. In order to understand and improve the mechanical properties of the remodeling graft, the mechanical properties of the normal tissue must be studied. The common method to study mechanical behavior of the ligament is the tensile test. In this test the ligament is loaded along the long axis of the fiber. Usually a bone-ligament-bone complex is tested, and the load versus elongation is recorded. The commonly studied mechanical properties of the ligament are ultimate load, failure load, modulus and energy absorbed to failure (area under the load versus time curve). Often the load and displacement curve is converted to a stress versus strain curve to get elastic modulus of the tissue, maximum stress, maximum stress and energy density [31]. The stress is defined as the force divided by area and the strain is elongated length divided by original length.

The stress -strain behavior of a ligament is pictured in Figure 7. It can be divided into three regions: toe region, linear elastic region and ligament failure region. The mechanical properties of ACLs can be explained based on the crimp pattern, which primarily reflects collagen fibril structure. Due to the crimp pattern, a ligament can elongate more without stress as it "uncrimps", and this results in the toe region. Once the fibrils straighten, the stress-strain relationship is linear. Then, as the load on the fiber exceeds beyond the elastic region, ligament failure occurs [1, 32]. The stress strain behavior of the ligament can be explained as the change in strain rate. In the toe region the strain is 1-3%, in the linear region which is more representative of the physiologic region the strain is 3-5% and if the strain increases more than 8-10% the ligament rupture [31, 33]. Typically, 4-10% strain is used to test ligaments and tendons.

Biomechanical properties of the ACL have been studied extensively [34, 35]. It has been shown that a human ACL can withstand 450N during normal activity (such as, running and walking) and 2000N before failing [1].

Since ACL and tendon are viscoelastic tissues, their mechanical behavior is rate dependent and history dependent and therefore studied for force relaxation, creep and hysteresis [31, 33]. In animal studies, mechanical testing has been as a method to compare the different surgical methods of ACL reconstruction [36-38]. Even though load to failure tests are common, there are several publications advocating the fatigue test as well since ligaments undergo repetitive loadings [39].

All biomechanical data about the remodeling graft or the native tissue has been obtained from experimental data on dissected tissues. In-vivo mechanical behavior of the tissue could provide physiologically more relevant information. There have been efforts to determine mechanical properties of the ligament and tendon in-vivo in the human during regular activity. Ultrasound and sonographic images have been used to measure mechanical properties in-vivo. Sonography was used to obtain the dimensions of the tendon, while the force was measured with a dynamometer. The findings from this study were yielded similar results to the percent strain shown in experimental data [33]. These studies show promising results which can be applied clinically, but had some limitations as well. It is hard to start the test with 0% strain and 0N force on the tendon. The cross-sectional area obtained from the sonography images were two dimensional areas, compared to the actual three dimensional volume of the tendon. And, the protocols need highly skilled personal to carry out the test each time [40, 41].

Ideally, we would like a non-destructive method for assessment of graft composition, where outcomes correlate to mechanical properties of the tissue that could be implemented in a clinical setting. Magnetic resonance imaging (MRI) provides a non-destructive tool for evaluation of ACL tears, preoperative measurements of the graft and postoperative follow up [42]. However, MRI lacks adequate spatial resolution and molecular specificity. Further, correct alignment of ACLs with the imaging plane is required to avoid partial volume averaging artifacts [43]. The partial volume artifact can be defined as an artifact which occurs when the tissue under investigation is only partially accessible. It has been shown that even though MRI had great accuracy in identifying ACL tears, it failed to differentiate between complete and partial ACL tears [44]. There are several challenges that still need to be resolved regarding the interpretation of the MR images, such as correlation of signal intensity of the graft after reconstruction to the graft health [43, 45, 46].

1.6 Infrared spectroscopy:

Fourier transform infrared (FT-IR) spectroscopy is a technique sensitive to molecular structure and composition changes in tissues, and is based on molecular vibrations. The electromagnetic spectrum is divided into different types of waves with different frequencies including radio, microwave, infrared (IR), visible, ultraviolet, x-ray and gamma ray. The infrared region lies between the visible and microwave region. The infrared portion of the electromagnetic spectrum can be further divided into three regions; far infrared (in the frequency (wavenumber, cm^{-1}) range 400-100 cm^{-1}), mid infrared region (mid-IR) (in the wavenumber range 4000-400 cm^{-1}), and the near infrared (NIR) (in the wavenumber range 12000-4000 cm^{-1}). Above absolute zero temperature all molecules vibrate at frequencies in the mid-infrared range. The necessary condition for infrared absorption is a change in dipole moment of the molecular bond. In IR absorption, molecules absorb light of a given frequency which is characteristic to their functional groups.

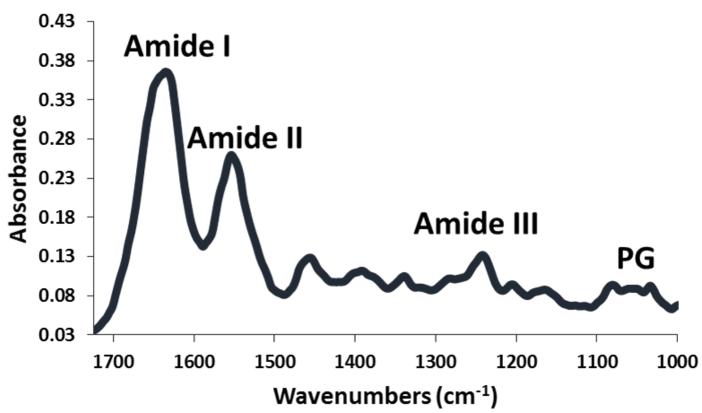

Figure 8: Typical mid infrared spectrum from cartilage showing absorbances from collagen (Am I (Amide I), Am II (Amide II) and AM III (Amide III)) and proteoglycan (PG)).

Mid infrared (mid-IR) spectroscopy of connective tissues is well understood and it has been extensively used to study musculoskeletal tissues [47, 48]. A typical mid-IR spectrum from cartilage is shown in Figure 8 where collagen absorbances are present at 1650 (amide I), 1550 (amide II), and 1240 cm^{-1} (amide III), which result from vibrations of the peptide bonds (also present to lesser amounts in proteoglycans, (PG)), and by collagen side chains at 1338 cm^{-1}, and PG sugar ring vibrations, 985–1140 cm^{-1} [47]. Mid-IR band assignments for connective tissues are summarized in Table 1 [47, 49].

Table 1: Typical mid-IR and NIR absorbances

FREQUENCY	ABSORBANCE	MODES OF VIBRATION
1650 CM^{-1}	Amide I	C=O stretching
1550 CM^{-1}	Amide II	N-H bending and C-N stretching
1338 CM^{-1}		Arises from collagen CH2 side chain
1240 CM^{-1}	Amide III	C-N stretching mode
1140 CM^{-1}	Proteoglycan	Sugar ring stretching
4608 CM^{-1}	Collagen	Asymmetric C-H stretch and C-H deformation combination
5200 CM^{-1}	Water	Combination of the OH-stretching band and the O-H bending band (2ν1,3+ν2)
6890 CM^{-1}	Water	First overtone of the OH-stretching band (2ν1,3)

The drawback of mid-IR is its limited depth of penetration, up to ~10 µm only [50, 51]. Nevertheless, mid-IR fiber optic probes have previously been used to differentiate between normal and pathologic connective tissues. It was found that the ratio of amide II / 1338 cm^{-1} was significantly higher in degraded cartilage compared to normal cartilage. Spectral changes were observed in amide I, II and 1338 cm^{-1} between normal and degraded cartilage [52]. A recent study by our group has also shown that the fiber optic probe spectral parameters correlate with cartilage histological grading [53]. To obtain spectral data related to tissue composition at high spatial resolution, ~ 6 micron, an FTIR spectrometer with a microscope attachment and an array detector, infrared spectral imaging, can be used to acquire spectral images from histological tissue sections. [54].

In contrast to mid-IR, near infrared (NIR) spectroscopy has a greater depth of penetration, up to the mm to cm range, depending on the wavelength (frequency) of data collection [55, 56]. NIR is rapidly emerging as a non-destructive tool to study connective tissues, especially cartilage. The NIR spectrum consists of overtones and combination bands of the fundamental molecular vibrations found in the mid-IR region. There are two dominant water peaks in the NIR region, centered at 5200 and 6890 cm^{-1} , which arise from combinations of the OH-stretching band and the O-H bending band ($2\nu1,3+\nu2$), and first overtone of the OH-stretching band ($2\nu1,3$), respectively [57]. Although water peaks dominate the NIR spectrum, several matrix peaks have also been identified and were shown to correlate with matrix in cartilage as listed in Table 1 [58]. NIR has been shown to distinguish between normal and enzymatically degraded tissue [59], histological grading systems such as Mankin score system [60, 61] and mechanical properties of cartilage [62]. In one study, when compared with MRI and arthroscopy, NIR had better intra-observer agreement to predict early cartilage degeneration [63]. Together, these studies strongly support the use of FT-IR fiber optic probes combined with arthroscopy as an important tool for the non-destructive evaluation of tissue, such as graft composition during the ligamentization process. However, the optimal wavelength region for these analyses has yet to be established.

Several studies have shown that the depth of penetration of NIR radiation is wavelength dependent, and varies with tissue type. Lammertyn et al. demonstrated that the depth of penetration of NIR radiation varied from 2-3 mm at 900-1900 nm (5263 cm^{-1}-11111 cm^{-1}) to 4 mm at 700-900 nm (11111 cm^{-1} -14285 cm^{-1}) in an apple thickness study [55]. In another study, the depth of penetration into a neonatal head ranged from 6.3-8.5 mm in the 700-900 nm (11111 cm^{-1} -14285 cm^{-1}) spectral range [56]. Until now no studies have looked at the depth of penetration of NIR radiation in a connective tissue. This is important so that we can assess whether molecular absorbances interrogated during fiber optic data collection arise from tendon or ligament only, or from underlying bone or other tissues.

Mid-IR and NIR are complementary methods to each other. Previous studies in the food industry have shown that combining NIR and mid-IR spectra together could result in better differentiation of products [64, 65]. Mid-IR spectroscopy can give surface information but NIR spectroscopy can give information through the depth of the tissue. Water content of connective tissues can be a good indicator of tissue health [66, 67]. It has been shown that the water content of the cartilage increases from 60 to 90% as osteoarthritis progresses [68]. Water in connective tissue can be classified as bound water or free water. Bound water can be defined as the water molecule bound to collagen or other matrix components such as proteoglycans. Free water is the water trapped in the matrix. In the mid-IR, the water peak overlaps with the strong protein amide I absorbance, whereas the NIR region is dominated by water peaks at 5200 cm^{-1} and 6890 cm^{-1}. Our recent study has shown that in cartilage, the water peak at 5200 cm^{-1} arises from a combination of free and bound water, and the water peak at 6890 cm^{-1} arises from free water [69]. It was shown that the gravimetrically-determined water content of the cartilage correlated significantly with both water bands, 5200 and 6890 cm^{-1}, and therefore these bands could be used to predict water content. As the molecular composition of ligaments and tendons differ, a combination of mid-IR and NIR could result in better differentiation of these tissues, and possibly better evaluation of the ligamentization process.

Infrared spectroscopic studies of ACL and tendon:

Even though mid-IR spectroscopy has been extensively used to study cartilage and bone, there are very few studies that have utilized spectroscopy to study ligament and tendon. However, to our knowledge there is no study which has utilized NIR spectroscopy to study either ACL or patellar tendon. Attenuated total reflectance (ATR) spectroscopy has been used to differentiate normal versus torn rotator cuff tendons and sizes of the tear [70]. The findings from that study showed that FTIR was able to differentiate between normal and torn tendon. The matrix content in torn tendon was altered and were distinguishable by differences in proteoglycan content, lipid content and collagen. Mid-IR spectral imaging has been used to characterize the ligament-bone interface in an ACL, and changes in collagen, proteoglycan and mineral distribution and collagen orientation at the bone ligament interface were observed. It was found that the matrix distribution, such as mineral, proteoglycan and collagen fiber orientation varied between the femoral and tibial interface [54].

Spectral data analysis:

Several factors introduce nonlinearity into NIR spectral data such as noise, light scattering and baseline shifts, and spectra are usually pretreated to remove these effects. These methods are called preprocessing methods. The most commonly used preprocessing techniques are multiplicative scatter correction (MSC), extended multiplicative scatter correction (EMSC), standard normal variate (SNV), detrending and second derivatives. MSC accounts for additive and multiplicative scatter effects and EMSC accounts for wavelength dependent scattering. Second derivative is used to eliminate baseline shifting and to resolve overlapping peaks [71-73].

In spectroscopy, two main approaches are used for data analysis; univariate analysis and multivariate analysis. In univariate analysis, the integrated area under an absorbance peak, or the peak height, area typically used for correlations to other outcome parameters. Or, the peak height or areas are related to the relative composition of a specific molecular species. However, in multivariate analysis, multiple frequencies, including at times the entire spectral region (multiple variables) are used for analysis. In mid-IR spectroscopy, the absorbance peaks are well defined, but in NIR, the absorbance peaks are broad. Therefore, univariate analysis for NIR spectra is difficult. Most frequently used multivariate methods in spectroscopy are principal component analysis (PCA), partial least squares regression (PLS) and linear discriminant analysis (LDA). In the studies presented here, we use partial least squares discriminant analysis (PLS-DA). PLS-DA, a variant of the classic PLS regression method used in multivariate statistics, is used to classify the X matrix variables based on the Y binary reference variables matrix. In order to use PLS-DA, the Y reference variable are split into multiple binary variables based on number of classes used. PLS-DA uses PLS regression on these newly created Y variables to predict the class membership of X variables. The results of the PLS-DA indicate the percentage of X variables correctly predicted to belong to a particular class. In order to get more information on how and which wavenumbers contributed to the discrimination, factors or the latent variable of the model are studied. These factors show the most variation in the two samples [72].

1.7 Current challenges related to ACL repair and rehabilitation:

Despite the number of ACL reconstructions performed every year, ligamentization is not completely understood. There is a consensus regarding the steps in the ligamentization process, but there is no consensus over the end period of the process. Further, patients who undergo ACL reconstruction can suffer from graft laxity, stiffness and complete ACL reconstruction failure [74]. Currently, graft remodeling is assessed by both patient's response (a subjective method) and the range of motion of the knee (an objective method). These are indirect methods of ligamentization assessment. Different rehabilitation protocols are proposed in the literature but there is no agreement on which protocol provides the best outcome [75]. This is partly due to the fact that there is no objective method of outcome evaluation of the graft remodeling process. A non-destructive method of assessment could provide a better understanding of the molecular changes that occur during successful graft remodelling, as well as the molecular changes that underlie failed ACL reconstruction.

CHAPTER 2

2 HYPOTHESIS AND SPECIFIC AIMS:

Based on this background we hypothesized that infrared spectroscopy could be used to monitor molecular changes during the ligamentization process. Improved understanding of the compositional changes that occur during ligamentization could lead to improved therapeutic and rehabilitation protocols. Here, we lay the groundwork for eventual evaluation of ligamentization by demonstrating the infrared spectroscopy is sensitive to compositional differences in ligaments and tendons.

2.1 Specific aims of this thesis:

1) Determine the optimal infrared spectroscopic method (using mid or near IR, or combined) to differentiate between ligament and tendon based on molecular composition differences in these tissues. This will establish the optimal method for eventual evaluation of the ligamentization process.

2) Establish the depth of penetration for the NIR fiber optic probe radiation. This is important so that clinically, we can assess whether molecular absorbances arise from tendon or ligament only, or from underlying tissues as well.

3) Correlate infrared spectral data obtained from ligament regions with varying composition with mechanical properties. This will validate that infrared spectral data correlate to functional properties of ligaments.

Together, these studies from this thesis will lay the foundation for a minimally invasive method for evaluation of healing ligament injuries, which will ultimately aid in clinical decision making.

CHAPTER 3

3.0 SPECIFIC AIM 1

Determine the optimal infrared spectroscopic method (using mid-IR or NIR, or combined spectral regions) to differentiate between ligament and tendon based on molecular composition differences in these tissues.

Significance: In order to ultimately use infrared spectroscopy to monitor the ligamentization process, it is important to investigate whether infrared spectroscopy can differentiate between ACL and patellar tendon, the most common tissue used for grafting a torn ACL. **The findings from this study were partially published in Padalkar, M. McGoverin, C., Onigbanjo Q., Spencer, R., Barbash, S., Kropf, EJ. Pleshko, N. Infrared Fiber Optic Probes for Evaluation of Musculoskeletal Tissue Pathology. Proc. SPIE; Photonic Therapeutics and Diagnostics X; Vol 8926, Article # 89263Y, 2014**

Initially, during the course of this thesis, we evaluated the performance of NIR, mid-IR and NIR and mid-IR combined together to differentiate between ligament and tendon. However as the study progressed it was found that mid-IR spectroscopy resulted in better differentiating between ligament and tendon when compared to the NIR, or to mid-IR and NIR combined. Therefore the manuscript results only include the mid-IR spectral data. Here within the thesis, the results from NIR, and from NIR and mid-IR combined are also presented.

3.1 Materials and methods:

3.1.1: Tissues

Bovine ACLs (n=14), patellar tendons (n=14) were dissected from freshly slaughtered 2-14 day old calves (Research 87, Boylston, MA). Mid infrared and near infrared fiber optic data were collected immediately after dissection on the fresh tissue.

3.1.2: Near infrared fiber optic probe and data collection

NIR spectra were obtained from ACL and patellar tendon using a 3 mm diameter silica glass diffuse reflectance NIR probe (Art Photonics, Berlin, Germany) coupled to a Matrix-F infrared spectrometer with a TEInGaAs detector (Bruker, MA). Care was taken to collect NIR data from the same locations as mid-IR data. NIR data were collected in diffuse reflectance mode from 4000-8000 cm^{-1} at 16 cm^{-1}, and 128 co-added scans.

3.1.3: Fourier transform infrared imaging spectroscopy (FT-IRIS) data collection

FT-IRIS data were collected to aid in understanding the NIR data and the compositional differences along the ACL. After NIR and mid-IR probe data sampling, tissues were fixed in 10% buffered formalin and cut cross-sectionally and longitudinally into regions of interest prior to embedding in paraffin for tissue sectioning. The tissues were sectioned to 4 μ m onto Low-e slides (Kevley, OH) for FT-IRIS data collection and onto plus slides for histology study. FT-IRIS data were acquired in the mid-IR region (750–2000 cm^{-1}, 8 cm^{-1} spectral resolution, 25 μ m pixel resolution and 2 co-added scans) using a Spectrum SpotLight 400 FT-IR Imaging system (PerkinElmer, CT).

3.1.4: Fiber optic spectra processing

Spectra were processed using Unscrambler 10.1 (CAMO, Woodbridge, NJ). Spectra were pretreated with a multiplicative scatter correction (MSC) followed by second derivative (Savitzky Golay, 3rd polynomial order, 13 point smoothing for mid-IR and 51 point smoothing for NIR data). A concatenated matrix was formed with NIR and mid-IR spectra where rows are comprised of NIR and mid-IR spectral absorbances from the same sample as well as the same location. The mid-IR and NIR spectra were pretreated separately. Combined spectra were normalized by the standard deviation at each wavelength in the entire spectral collection. Hotelling T^2 and influence plots were used to identify outliers [72]. Separate partial least square discriminant analysis (PLS-DA) models with full cross validation were performed to differentiate ACL versus patellar tendon using NIR spectra, mid-IR spectra and NIR and mid-IR combined together. Several different wavenumber regions were investigated to find the optimal spectral region. The results were compared based on the percent of correctly classified spectra into ACL and tendon.

3.1.5: FT-IRIS data analysis

Integrated areas under the Amide I, and 1338 cm^{-1} absorbances, reflecting total protein and collagen, respectively, were calculated. The ratio of 1660 cm^{-1} over 1690 cm^{-1} were calculated as an indicator of collagen maturity [76], a parameter related to collagen crosslinking.

3.2 Results

PLS-DA models based on mid-IR, NIR and the combination of mid-IR and NIR spectra were able to differentiate ACL versus tendon samples to different degrees (Table 2). Mid-

IR alone was able to differentiate 90% of the samples into ACL and tendon correctly, and NIR alone resulted in 80% correct classification. The best classification was obtained with standard normal variate pretreatment. Use of mid-IR and NIR slightly increased the correct classification of ligament and tendon. We found that mid-IR alone was able to differentiate between ligament and patellar tendon, and that addition of NIR helped, but the increase in correct classification was not significant.

Table 2: *Partial least squares discriminant analysis (PLS-DA) results comparing the performance of mid-IR, NIR and the combination of mid-IR and NIR for tendon ligament discrimination. Columns indicate the methods of preprocessing multiplicative scatter correction (MCS) and second derivative and standard normal variate (SNV) used and rows show the performance of each model.*

	Msc+ Second Der	**Msc+ Second Der**	**Msc+ Second Der**	**Snv +Detrend**
Spectral range	mid-IR	mid-IR	mid-IR	mid-IR
% Correct Classification	90%	90%	90%	92%
Factors*	9	9	9	12
Spectral range	NIR all (4000-10000)	mid-IR+4000-6000	NIR 5000-8000	NIR (4000-10000)
% Correct Classification	81%	94%	82%	84%
Factors	5	5	5	15
Spectral range	mid-IR+NIR	NIR 4000-6000	mid-IR 1500-1800, NIR 4000-6000	mid-IR +NIR
% Correct Classification	92%	80%	91%	93%
Factors	6	11	7	11
***[72]**				

FT-IRIS data (Figure 9) showed regional variations of matrix components, even within cross-sections at different points along the ACL length. Higher mean values of PG were observed at the insertion sites compared to midsubstance, and mean collagen intensity was lowest at the femoral insertion site and higher in the tibial insertion region. Further, collagen maturity at the insertion sites was lower than in the midsubstance. The variation in composition of PG and collagen are consistent with a previous study [77].

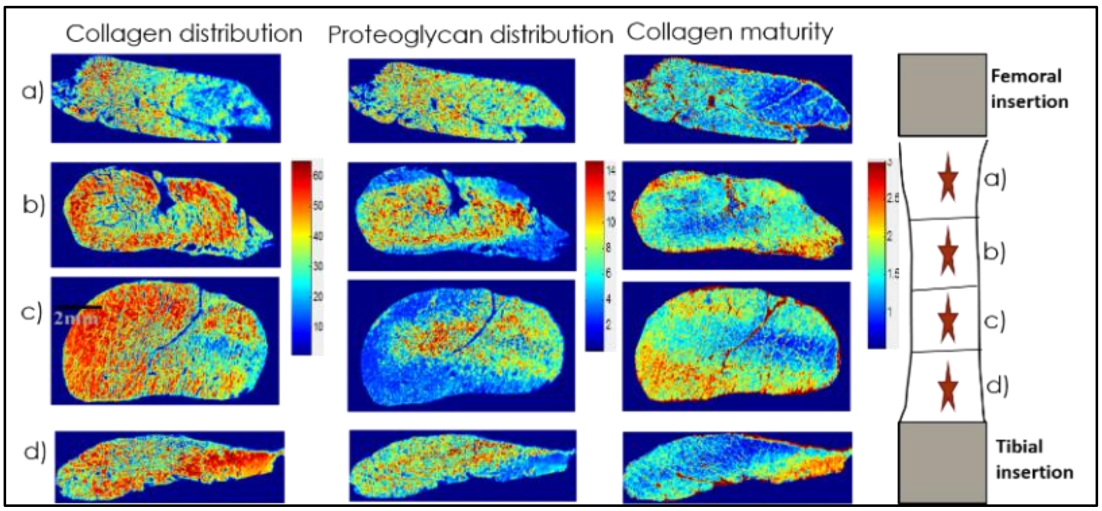

Figure 9: Typical distribution of collagen, proteoglycan and collagen maturity in cross-sections of a bovine ACL where a and d are femoral and tibial insertion sites, respectively, and b and c are midsubstance. The color bar indicates highest and lowest values by red and blue, respectively.

Manuscript to be submitted to American Journal of Sports Medicine

3.3 Mid infrared fiber optic evaluation of ligament and tendon composition: an enabling technology for arthroscopy

M. V. Padalkar[1], C.M. McGoverin[2*], H.J. Yang[1], S. Barbash[3], E.J. Kropf[3], N. Pleshko[1]

[1]Dept. of Bioengineering, College of Engineering, Temple University, Philadelphia, PA

[*2]Department of Physics, University of Auckland, Auckland, New Zealand

[3]Dept. of Orthopaedic Surgery and Sports Medicine, Temple University, School of Medicine, Philadelphia, PA, United States.

*current address

3.4 What is known about the subject:

The incidence of anterior cruciate ligament (ACL) injuries is increasing, with a current annual incidence of 350,000 injuries per year in the United States alone. ACL, being an intra-articular tissue, has very little capacity to repair itself. A torn ACL is typically reconstructed with either allograft from donors or autograft tendons, such as patellar tendon, hamstring tendon and quadriceps tendon. It has been shown that the grafted tendons undergo transformation due to the new environment and mechanical forces, and eventually change into a structure similar to an ACL, through a process known as ligamentization. Ligamentization has been studied in different animals such as sheep, pig and rabbit by histology and biochemical evaluations of the grafted tendon. However, due to destructive nature of the assessment, i.e. biopsies of the remodeling graft, there is a scarcity of human ligamentization studies. A non-destructive method for evaluation of ligamentization in clinical setting, as well as in animal studies, would enable modification of rehabilitation and therapeutic protocols, and yield insight into the remodeling process.

3.5 What this study adds to existing knowledge

Efforts are being made to enhance information that can be gained from intra-articular tissues during arthroscopy [78]. Arthroscopic evaluations can be highly subjective, based on the perspective of the surgeons performing surgical procedures. Findings from this study will aid in development of a non-destructive method, infrared fiber optics, to assess molecular composition of ligaments and tendons. This will improve understanding of the changes that occur during ligamentization, and could lead to advancement of biologic adjunctive therapies and postoperative rehabilitation protocols. In an animal study, fiber optic probe evaluations would allow longitudinal study of the healing graft in the same animal, resulting in a more complete analysis of molecular changes during ligamentization. The long term goal of this study will be to develop a protocol to use infrared fiber optic probes in combination with second look arthroscopy to assess molecular changes in the human graft tissue.

3.6 Abstract:

Despite the number of anterior cruciate ligament (ACL) reconstructions performed every year, the process of ligamentization, transformation of a tendon graft to a healthy functional ligament, is poorly understood. Currently, histology is the gold standard method to assess the remodeling of the graft tissue in animal studies. Ideally, a non-destructive method for assessment of graft composition could be implemented in a clinical setting. Magnetic resonance imaging (MRI) provides a non-destructive tool for evaluation of ACL tears, preoperative measurements of the graft and postoperative follow up. However, MRI lacks high spatial resolution, and has limited molecular specificity. Fourier transform infrared (FT-IR) spectroscopy exhibits a high degree of specificity to molecular structure and compositional changes in tissue. In this current study, we investigated the feasibility of infrared spectroscopy to differentiate between ligament and tendon as a first step toward development of infrared spectroscopy tools to study ligamentization. Mid infrared (Mid-IR) fiber optic data were collected from freshly dissected bovine ACLs (n=15) and patellar tendon (n=16) in the frequency range of 1000-1800 cm^{-1}. Partial least squares discriminant analysis (PLD-DA) was used to differentiate between ligament and tendon. It was found that PLS-DA based on Mid-IR spectral data resulted in 94% correct classification. The basis of discrimination was primarily differences in the frequency range of 1500-1600 cm^{-1} and 1000-1100 cm^{-1} which is dominated by collagen absorbances. This study provides a foundation to develop a minimally invasive method for evaluation of changes that occur in the graft during ligamentization, which will ultimately aid in understanding the ligamentization process. Improved understanding of ligamentization could lead to better therapeutic interventions and post-operative protocols.

Keywords: Anterior cruciate ligament reconstruction, ligamentization, infrared spectroscopy, fiber optics, magnetic resonance imaging, partial least squares discriminant analysis

3.7 Introduction:

The frequency of anterior cruciate ligament (ACL) injuries is increasing, with a current annual incidence of ~350,000 injuries per year in the United States alone [4]. ACL, being an intra-articular tissue, has very little capacity to repair itself [14]. A torn ACL is typically reconstructed with either allograft from donors or autograft tendons, such as patellar tendon, hamstring tendon and quadriceps tendon [16]. It has been shown that the grafted tendons, exposed to new types of mechanical forces in the intra-articular synovial fluid environment, undergo transformation into a structure similar to an ACL, a process known as ligamentization [22]. Ligamentization has been studied in different animals including sheep, pig and rabbit [22-24]. Previous studies have relied heavily on biochemical and histological analysis [2, 22] to evaluate the progress of ligamentization process. However, these methods are destructive, and therefore have restricted use for the study of ligamentization clinically in human subjects.

Clinically, arthroscopic evaluation has been the gold standard to diagnose and treat intra-articular tissue damage such as in articular cartilage [28], ACL [30], and meniscus [29]. However, arthroscopic evaluations can be highly observer dependent and rely on visual, rather than compositional, information. Ideally, a non-destructive method for assessment of graft composition could be implemented in a clinical setting. Magnetic resonance imaging provides a non-destructive method for ACL tear detection and post-operative follow up [42]. However; it suffers from several disadvantages, such as low spatial resolution, low molecular specificity, and partial volume averaging artifacts. It was found that in MRI studies, changes in intensity of the remodeling graft still needed to be correlated with histology to understand the mechanism of ligamentization [43, 45, 46].

In contrast, Fourier transform infrared (FT-IR) spectroscopy exhibits a high degree of specificity to molecular structure and compositional changes in tissue. The mid infrared (mid-IR) spectral absorbances from connective tissues are well understood and have been used to study connective tissues for over 30 years [47, 48]. An FT-IR spectrometer with a microscope attachment, infrared spectral imaging, can be used to acquire spectral images from histological tissue sections and to study regional differences within the tissue at high spatial resolution, ~ 6 micron. When a fiber optic probe is attached to the spectrometer, spectral data could be directly obtained from tissues with minimal sample preparation, making them ideal for clinical use. Our group has utilized spectral imaging as well as infrared fiber optic probes to study musculoskeletal tissues. Recent studies by our group have studied cartilage degeneration and repair with Mid-IR fiber optic probes [79]. Previous studies by our group have shown that Mid-IR fiber optic probe spectral parameters correlate with cartilage histological grading [52, 53]. Therefore, these studies strongly support the use of FT-IR fiber optic probes as an important tool for the non-destructive evaluation of tissue, such as changes in graft composition during ligamentization process. Infrared fiber optic probe designed specifically to glide through arthroscope ports could be used during second look arthroscopy to get visual information about the tissue and its chemical composition.

In this current study, we hypothesize that infrared spectroscopy could provide tools to study ligamentization in an animal model as well as in a clinical setting. Here, we investigated the feasibility of mid infrared spectroscopy to differentiate between ligament and tendon as a first step toward development of non-destructive infrared spectroscopy tools to study ligamentization. Since patellar tendon is the gold standard choice for ACL reconstruction [16], mid-IR fiber optic data were collected from bovine ACL and patellar tendon and partial least squares discriminant analysis (PLS-DA) was used to differentiate between ACL and patellar tendon composition.

3.8 Materials and methods:

3.8.1 Tissue

Bovine ACLs (n=15), patellar tendons (n=16) were dissected from freshly slaughtered 2-14 day old calves (Research 87, Boylston, MA). The data were acquired in four batches of three ACLs and patellar tendons. Mid-IR fiber optic data were collected on fresh samples.

3.8.2 ATR fiber optic data collection:

Mid-IR data were collected using a Thermo Scientific Nicolet iS5 FT-IR spectrometer with a TGS detector fitted with a fiber optic coupler (Harrick Scientific Products, Inc., Pleasantville, New York), and a silver halide ATR-loop mid-infrared fiber optic probe with a 6 mm diameter (Art Photonics, Berlin, Germany). The experimental setup is as shown in the Figure 10. Even though the probe used in this study was 6 mm diameter, we have another 1 mm diameter probe which can glide through the portals used during arthroscopy. Spectra were ratioed to an air background. Spectral data was acquired from four different locations of ACL and patellar tendon; femoral and tibial insertion and mid substance. At each location 3 replicate spectra were recorded resulting in 12 spectra from each tissue. Spectra were collected at 8 cm^{-1} spectral resolution, with 32 co-added scans in the frequency range of 1000-1800 cm^{-1}.

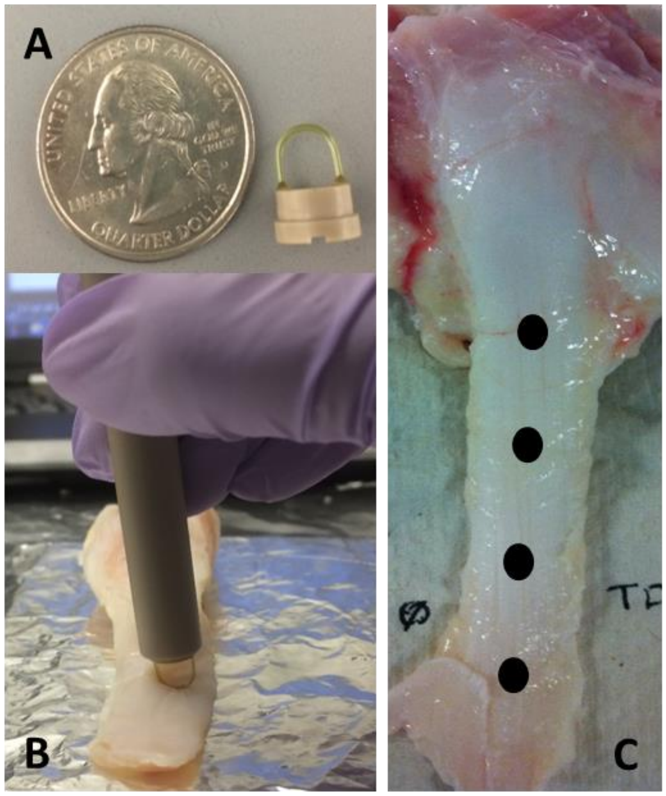

Figure 10: Experimental set up: The diameter of the probe used here was 6 mm (A). Spectra were collected from four different locations of anterior cruciate ligament and patellar tendon as shown in the figure (B). The black spots represent the location of data collection (C).

3.8.3 Fourier transform infrared imaging spectroscopy (FT-IRIS) imaging data collection

FT-IRIS data were collected to aid in understanding the compositional differences between ACLs and patellar tendons. Fiber optic measurements were limited to surface evaluation of the tissues [80], but IR imaging data of cross-sections of ACLs and patellar tendons (n=3) allow assessment of the distribution of components through the full tissue depth. After mid-IR fiber optic probe data sampling, tissues were fixed in 10% buffered formalin and cut cross-sectionally into 2mm Segments prior to embedding in paraffin for tissue sectioning. The tissues were sectioned to 3 μm thickness onto silicon wafers (Fuzere Manufacturing Co. Sunnyvale, CA) for FT-IRIS data collection and onto plus slides for histology studies. FT-IRIS data we acquired in the mid-IR spectral region (transmission mode,750–2000 cm^{-1}, 8 cm^{-1} spectral resolution, 50 μm pixel resolution and 2 co-added scans) using a Spectrum SpotLight 400 FT-IR Imaging system (PerkinElmer,Shelton, CT).

3.8.4 Histology:

Tissue sections were deparaffinized in xylene and series of graded alcohols and stained with hematoxylin and eosin to evaluate general cellular detail, and with Alcian blue to stain specifically for proteoglycan [81].

3.9 Data processing:

Fiber optic spectra were processed using Unscrambler 10.1software (CAMO, Woodbridge, NJ). Several different spectral preprocessing methods were investigated to optimize the spectra for multivariate analysis, including multiplicative scatter correction (MSC), extended multiplicative scatter correction (EMSC), baseline correction, normalization and second derivative (savitzky golay, 3rd polynomial order, 13 point smoothing) [72]. In addition, several spectral regions were investigated. Some of the tissues (both ACL and patellar tendon) showed a fat absorbance at 1740 cm^{-1}, and therefore models were created that excluded the spectral region of fat absorbance.

Partial least squared discriminant analysis (PLS-DA), a variant of the classic PLS regression method used in multivariate statistics, was used to differentiate between ACLs and patellar tendons. PLS-DA is used to classify the X matrix variables based on the Y binary reference variables matrix. In order to use PLS-DA, the Y reference variables are split into multiple binary variables based on number of classes used. In this case there were two classes, ACL and patellar tendon. PLS-DA uses PLS regression on these newly created Y variables to predict the class membership of X variables based on a threshold [82], which for differentiation in our study was assigned as 0.5. The results of the PLS-DA indicate the percentage of X variables correctly predicted to belong to a particular class. PLS2 regression models with leave one out cross-validation were prepared using 2/3rd of the spectral data, and 1/3rd of the data were used to validate the prediction ability of the models Hotelling T^2 and influence plots were used to identify the outliers [72]. The results were compared based on the percent of correctly classified spectra.

3.10 FT-IRIS spectral imaging processing:

FT-IR spectral images of ACL and patellar tendon were analyzed using ISYs 5.0 software (Malvern Instruments, UK). The images were masked based on the Amide I absorbances such that pixels not related to tissue were not included in the analysis. Absorbance bands were baselined and images of integrated areas under the Amide I (1594–1712 cm^{-1}) (total protein) and 1338 cm^{-1} (collagen) absorbances and 985-1140 cm^{-1} for PG [47] were generated to show the distribution of the specific molecular component of interest. Mean values of integrated areas and standard deviations were recorded for each image. A Student t-test was used to evaluate statistical significance at $p<0.05$.

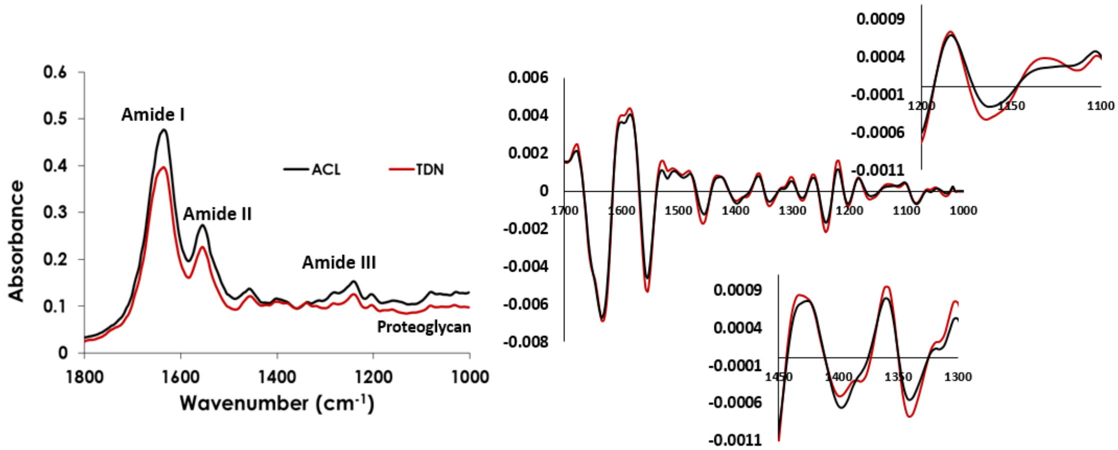

Figure 11: typical MIR spectrum of an ACL (black) and patellar tendon (red). Second derivative spectra showed subtle differences in the spectral range 1300-1450 cm^{-1} and 1000-1200 cm^{-1}.

3.11 Results:

Mid-IR spectra (fiber optic and imaging) from ACL and patellar tendon were dominated by collagen peaks at 1650 (amide I), 1550 (amide II), 1338 (side chains) and 1240 cm^{-1} (amide III) which result from vibrations of the peptide bonds and by proteoglycans, (PG), sugar ring vibrations or collagen glycosylation between 985–1140 cm^{-1}[47]. Raw spectra of these tissues were qualitatively very similar, but when second derivative spectra were analyzed, subtle differences were seen in the collagen and glycosylated proteins absorbance Figure 11.

3.11.1 PLS-DA:

PLS-DA was able to differentiate ligament and patellar tendon composition (Table 3) the best results of 94% discrimination were obtained using extended multiple scatter correction (EMSC) preprocessing and second derivative transformation.

Table 3: Results of partial least squares discriminant analysis to differentiate anterior cruciate ligament and patellar tendon.

	MODEL	**PREDICTION**
RAW SPECTRA	82.75%	91%
BASELINE	87.45%	90%
MSC	85.71%	91%
EMSC	86.51%	94%
MSC AND 2ND DERIVATIVE	85.88%	93%
EMSC AND 2ND DERIVATIVE	86.67%	92%

The loadings (which reflect the spectral features that contribute to the model) for the PLS-DA model based on EMSC preprocessing of ACL and tendon were dominated by collagen absorbances at Amide I, II and III (Figure 12).

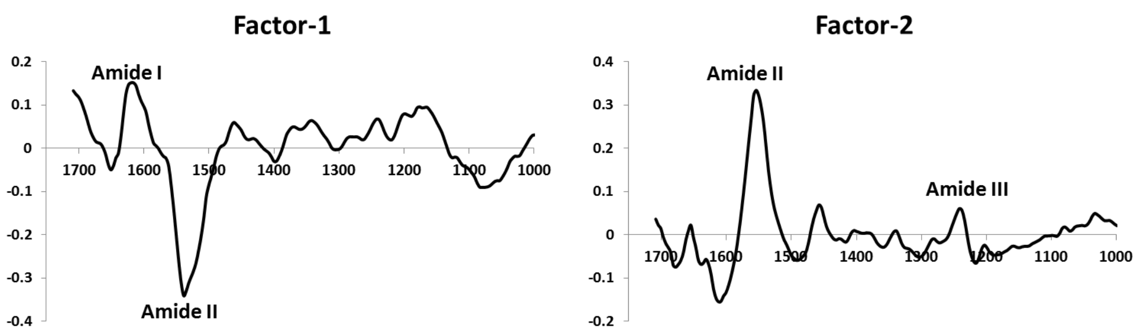

Figure 12: Loadings for the PLS-DA model of ACL and patellar tendon classification. Factor 1 and 2 are shown here.

3.11.2 Spectral image analysis:

FT-IRIS images showed a greater amount of total protein and collagen in patellar tendons compared to ACLs (Figure 14). In addition, the matrix component distribution is more uniform in tendon compared to ligament. The variation in the ligament composition is observed both within and between the bundles.

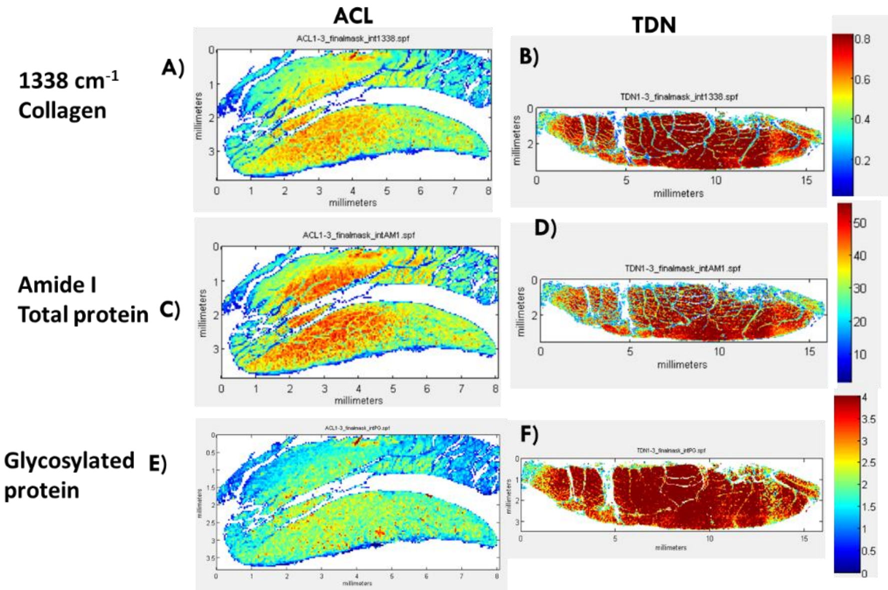

Figure 13: Representative spectral images of integrated areas under the Amide I and 1338 cm^{-1} absorbance, reflecting total protein and collagen, in ACL (A) and tendon (B) Cross-sections were obtained from the mid-section of each tissue. The color bar indicates the scale for component concentration, where red represents higher and blue represents lower concentration

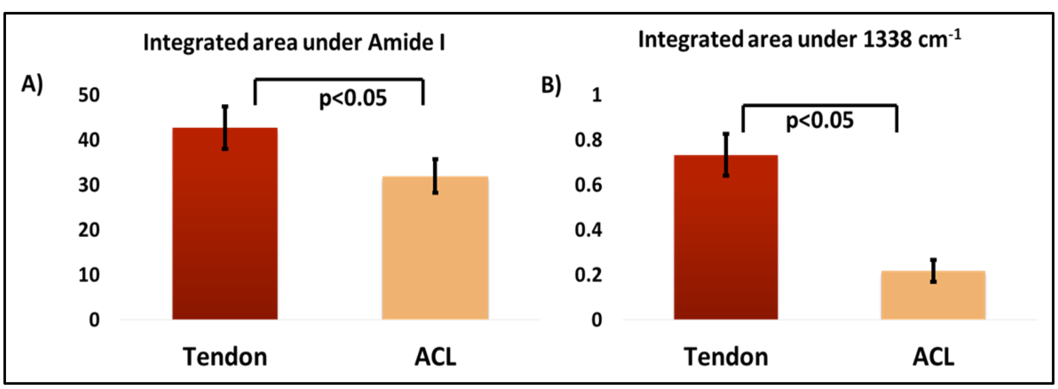

Figure 14: Mean values and standard deviations from FT-IRIS data of the integrated areas under Amide I and 1338 cm^{-1} in patellar tendon were significantly higher than

3.12 Discussion:

There are very few studies in the literature which have directly investigated compositional differences between ACLs and patellar tendons. One of the first studies showed that tendon had higher collagen content but lower proteoglycan compared to ligament. It was also found that ACL had higher metabolic activity, more DNA content and more type III collagen content. However, this study used biochemical and histological analysis which are destructive methods [20]. Here, we present the first study to investigate differences between ligament and patellar tendon composition using non-destructive fiber optic infrared spectroscopy, followed by infrared spectral imaging analysis of full depth composition. Our results showed that patellar tendon had significantly higher collagen content when compared to the ACL, in agreement with the literature [20]. The collagen fiber arrangement in these two tissues is different as well; collagen fibers are parallel to long axis in tendon and in ligaments, collagen fibers are oriented in different planes [10, 21]. However, these differences were not investigated in the current study.

Another difference between ACL and patellar tendon composition is the amount of elastin present [83]. Our group has previously studied collagen and elastin infrared spectra in a pig aorta model. It was found that there are several similarities and subtle difference between the elastin and collagen spectra in the 1040–1100 cm^{-1} and 1380–1420 cm^{-1} regions [84]. However, it is difficult to differentiate between ligament and patellar tendon in our models based on elastin content solely, due to the relatively low amounts present, less than 1-2 % in ligament and tendon.

One of the major disadvantages of mid-IR spectroscopy is its limited depth of penetration. It has been shown that mid-IR radiation in ATR mode can penetrate only up to ~10μ maximum, therefore only giving surface information [50, 51]. However, a previous study by our group showed that infrared fiber optic spectra correlated with the full depth histology in cartilage [53]. In addition, during ligamentization, molecular and chemical changes in the graft have been shown to start from the peripheral surface [85]. Therefore, the mid-IR ATR fiber optic probe could be ideal to study remodeling in the graft tissue.

The current gold standard for assessment of the ligamentization process in animal is histological analysis of the remodeling graft [26, 86]. It should be noted that these methods are destructive; hence evaluation cannot be performed on of the same tissue over time. In an animal study, fiber optic probes would allow longitudinal study of the healing graft in the same animal resulting in better understanding of the changes during ligamentization. Notwithstanding the 400,000 ACL reconstruction surgeries performed every year in United States, very few human ligamentization studies are present in the literature due to the destructive nature of the assessment, i.e. biopsies of remodeling graft. The findings from these few studies have shown that the ligamentization process in humans differs from that of animal models [25, 87]. Infrared fiber optic probes in combination with second look arthroscopy could provide a non-destructive tool to study ligamentization in a clinical environment.

In the future, near infrared (NIR) spectroscopy could also be used to study ligamentization. NIR has been emerging as a nondestructive modality for cartilage evaluation [60, 88]. It is a well-known fact that NIR penetrates to a much greater depth, ~mm to ~cm. It was found that the depth of penetration of NIR radiation into articular cartilage varies throughout the spectral range, 4000-10000 cm^{-1}, from 0.5 mm to 5 mm. It has also been shown that NIR spectra correlate with cartilage matrix composition [58, 69, 89], thickness [90], degradation enzymatically [59], as well as histological grading, including the Mankin score system [60, 61]. In addition, several studies around the world are advocating the use of NIR probes arthroscopically to evaluate early degeneration [88].

One drawback of our study was that a pressure sensor was not used during the fiber optic data collection. In fiber optic data collection, increased pressure could lead to better surface contact between the tissue and fiber optic probe. This in turn could lead to higher spectral absorbances [91]. The fiber optic probes used in this study were hand held therefore the pressure applied during the data collection may have varied. In order to confirm that the data collection method didn't confound our results, a separate spectral data set of ACLs and patellar tendons was acquired with a custom made pressure sensor, and a constant pressure of 0.25-0.3 lbs. was applied during data collection. We did find that the differences between ACL and patellar tendons found in this data set were consistent with the current data set presented here.

Clinically, evaluation of ligamentization by infrared fiber optics would have several challenges. Data would be collected arthroscopically, therefore it will be hard to keep the pressure same for data collection. However, the use of these probes are very straight forward, therefore there will not be need for skilled users. During standard arthroscopy procedures, the knee joint is filled with pressurized saline which rinses off the synovial fluid to give the surgeon a clear view of the ACL, and keeps the joint open. In this case the probe will be surrounded by saline, which may interfere during data collection. Future in vivo experiments are required to address these questions.

3.13 Conclusion:

The results from this study showed that mid infrared spectroscopy was able to differentiate ACL and patellar tendon composition. A non-destructive modality will improve understanding of the changes that occur during ligamentization and could lead to advancement of surgical reconstruction techniques, biologic adjunctive therapies and postoperative rehabilitation protocols. In an animal study, fiber optic probes would allow longitudinal study of the healing graft in the same animal resulting in better understanding of the changes during ligamentization. Better understanding of ligamentization could lead toward improved therapeutic interventions and post-operative protocols.

3.14 Acknowledgments:

Special thanks to Padraig Glenn, Nicholas Caccese and Meenakshi Patel for their help with tissue harvesting and data collection.

CHAPTER 4:

4.0 SPECIFIC AIM 2

Establish the depth of penetration for the NIR fiber optic probe radiation.

Significance: It is known that NIR radiation has greater depth of penetration than mid-IR radiation. Several studies have shown that the depth of penetration of NIR radiation is wavelength dependent, and varies with tissue type. Lammertyn et al. demonstrated that the depth of penetration of NIR radiation varied from 2-3 mm at 5263 cm^{-1}-11111 cm^{-1} to 4 mm at 11111 cm^{-1} -14285 cm^{-1} in an apple thickness study [55]. In another study, the depth of penetration in a neonatal head ranged from 6.3-8.5 mm in the 11111 cm^{-1} -14285 cm^{-1} spectral range [56]. Until now, none of the studies have looked at the depth of penetration of NIR radiation in a connective tissue. This is important so that we can assess whether molecular absorbances obtained by fiber optic probe arise from tendon or ligament only, or from underlying bone (or posterior cruciate ligament in case of mid substance) as well. To address this, we first evaluated penetration depth of NIR radiation into cartilage. The findings from that study were published in **Padalkar, M. V., and Nancy Pleshko. "Wavelength-dependent penetration depth of near infrared radiation into cartilage." Analyst 140.7 (2015): 2093-2100 (included below). Subsequently, penetration of NIR radiation into ligaments and tendons was investigated.**

Wavelength-Dependent Penetration Depth of Near Infrared Radiation into Cartilage

M.V. Padalkar,[a] and N. Pleshko[a]

[a] Department of Bioengineering, Temple University, Philadelphia, PA

Corresponding Author: Dr. Nancy Pleshko

Email: npleshko@temple.edu

Analyst 140.7 (2015): 2093-2100.

4.1 Abstract

Articular cartilage is a hyaline cartilage that lines the subchondral bone in a diarthrodial joint. Near infrared (NIR) spectroscopy has been emerging as a nondestructive modality for evaluation of cartilage pathology. However, studies of the depth of penetration of NIR radiation into cartilage are lacking. The average thickness of human cartilage is about 1-3 mm, and it becomes even thinner as OA progresses. To ensure that the spectral data collected is restricted to the tissue of interest i.e. cartilage in this case, and not from the underlying subchondral bone, it is necessary to determine the depth of penetration of NIR radiation in different wavelength (frequency) regions. In the current study we establish how the depth of penetration varies throughout the NIR frequency range (4000-10000 cm^{-1}). NIR spectra were collected from cartilage samples of different thicknesses (0.5 mm to 5 mm) with and without polystyrene placed underneath. A separate NIR spectrum of polystyrene was collected as a reference. It was found that the depth of penetration varied from ~1 mm to 2 mm in the 4000-5100 cm^{-1} range, to ~3 mm in the 5100-7000 cm^{-1} range, and to ~5 mm in the 7000-9000 cm^{-1} frequency range. These findings suggest that the best

NIR region to evaluate cartilage only with no subchondral bone contribution is in the spectral range from 4000-7000 cm^{-1}.

4.2 Introduction:

Articular cartilage is a hyaline cartilage that lines the subchondral bone in a diarthrodial joint. It is composed primarily of collagen type II, proteoglycans, cells and water. Cartilage has zonal organization with respect to depth, and is typically divided into a superficial, middle, deep and calcified zone. The cell morphology, collagen fiber orientation and composition varies throughout the zones [92]. Water and collagen content vary from being greatest at the surface to lowest in deep zone. However, proteoglycan content has the opposite trend, with a lower content at the surface and higher content in the deep zone. The primary function of cartilage is to provide frictionless motion and act as a shock absorber. The mechanical properties of cartilage are due to its composition where collagen provides tensile strength and proteoglycans are responsible for compressive stiffness. The primary functions of water in cartilage are shock absorption during loading, transport of nutrients, and lubrication [93].

Osteoarthritis (OA) is a progressively disabling disease characterized by wear and tear of cartilage. Approximately 27 million adults in United States are estimated to have OA, with prevalence correlated with age and obesity [94]. The pathology of OA is characterized by a damaged collagen network, loss of proteoglycan, and an increase in water content, often resulting in fibrillation and thinning of articular cartilage [95]. Articular cartilage is avascular and acellular therefore it has very little capability to repair itself [96]. Clinically, arthroscopy has been used as a 'Gold Standard' to diagnose and treat intra-articular tissues, such as cartilage [28], meniscus [29], and ligament [30] injuries. During standard arthroscopy procedures, the knee joint is filled with pressurized saline to keep the joint open as well as wash off the synovial fluid to give surgeons a clear view of cartilage. Surgeons can view the cartilage with the arthroscope on a monitor and make a decision on the quality of the cartilage. However, arthroscopic evaluations can be observer dependent [97, 98]. More quantitative outcome measures are under development [99], including advanced magnetic resonance imaging (MRI) analyses. MRI has a long, though not entirely successful, record in the noninvasive evaluation of cartilage [100-102]. Limitations of the MRI approach include limited spatial resolution, lack of molecular specificity, and the difficulties of partial volume averaging effects. Thus, the detection of thin fissures, cartilage flaps, and shallow defects can present a substantial challenge [103, 104]. Further, MRI is not typically utilized intra-operatively.

Fourier transform infrared (FT-IR) exhibits a high degree of specificity to molecular structure and compositional changes in tissue. The mid infrared (mid-IR) spectral absorbances from connective tissues are well understood, but mid-IR radiation exhibits a penetration depth of only ~10 microns through tissue, restricting its utility to the study of surface characteristics and degradation [50, 51]. Near infrared (NIR) spectroscopy has been emerging as a nondestructive modality for cartilage evaluation [88, 105, 106]. It has been shown that NIR spectra correlate with cartilage matrix composition [58, 69, 89], thickness [90], mechanical response of intact and artificially degraded cartilage [107], degradation enzymatically [59], traumatic degradation [108], as well as histological grading schemes, such as the Mankin score [61, 109]. In addition, several studies are advocating the use of

NIR probes arthroscopically to evaluate early degeneration [105, 106]. It is a well-known fact that NIR penetrates to a much greater depth, ~mm to ~cm [55, 56]. Several studies have shown that the depth of penetration of NIR radiation is wavelength dependent, and varies with tissue type. Lammertyn et al. demonstrated that the depth of penetration of NIR radiation varied from 2-3 mm at 900-1900 nm (5263 cm^{-1}-11111 cm^{-1}) to 4 mm at 700-900 nm (11111 cm^{-1} -14285 cm^{-1}) in an apple thickness study [55]. In another study, the depth of penetration in a neonatal head ranged from 6.3-8.5 mm in the 700-900 nm (11111 cm^{-1} -14285 cm^{-1}) spectral range [56]. Previous NIR studies with cartilage have looked at the depth of penetration of NIR in cartilage [59, 90], with the primary goal being to ensure that the NIR radiation penetrates through the sample thickness. However, studies of the depth of penetration of NIR radiation at different wavelengths in cartilage are lacking. The average thickness of human cartilage is about 1-3 mm, and it changes according to the location of cartilage [110, 111] with age [112], and with disease, thinning as OA progresses. In order to ensure that the spectral data collected is restricted to the tissue of interest i.e. cartilage in this case, and not from the underlying subchondral bone, it is necessary to determine the depth of penetration of NIR in different wavelength regions. In the mid-IR, bone has a strong phosphate absorbance at 900-1200 cm^{-1} [47] which can be used to differentiate the tissue from cartilage. However, in the NIR spectral region of interest, there is no phosphate absorbance present. Therefore, the motivation of the current study was to establish how the depth of penetration varies throughout the NIR frequency range (4000-10000 cm^{-1}) in cartilage.

4.3 Material and methods

4.3.1 Material:

Cartilage plugs of 5 mm diameter (n=5) were harvested from freshly dissected newborn bovine knee joints (Research 87, Boylston, MA). These plugs were cleaned to completely remove bone and were cut into varying thicknesses, ranging from 0.5 mm to 5 mm using a tissue cutter (Zivic Instruments, Pittsburgh, PA). The thickness of each cartilage slice was measured three times with a caliper (Fisher Scientific, Pittsburgh, PA) and averaged. Three to five replicates for each tissue thickness were investigated.

4.3.2 Near infrared fiber optic probe data collection

NIR spectra were obtained using a 3 mm diameter silica glass NIR fiber optic reflectance probe (Art Photonics, Berlin, Germany) coupled to a Matrix-F infrared spectrometer with a TE-InGaAs detector ((Bruker, MA). Background spectra were collected from a mirrored surface. Sample spectra were collected from different thickness cartilage samples in contact mode with and without a polystyrene plate underneath at 16 cm^{-1} spectral resolution, with 256 co-added scans in the 4000-10000 cm^{-1} frequency range. A reference spectrum was collected from the polystyrene plate (thickness: 0.54 mm) to identify peaks of interest. A mirrored surface was placed underneath the polystyrene, and underneath the cartilage samples when data was collected from cartilage alone. This results in a data collection mode of transflectance for samples 1 mm or thinner. As the sample thickness increases, diffuse reflectance increasingly dominates the spectra.

4.3.3 Near infrared imaging data collection

NIR spectral imaging data were collected from 1 mm thick cartilage samples (n=3) to investigate the zonal distribution of water and matrix components. The sections were cut longitudinally to obtain all the zones of the cartilage in one image. To assess water distribution, cartilage sections were placed on glass slide, covered with a glass coverslip and sealed with tape. NIR images were collected in transmission mode on a Perkin Elmer spotlight 400 spectrometer (Perkin Elmer, Shelton, CT) at 32 cm^{-1} spectral resolution, 16 co-added scans and at 50 µm spatial resolution in the 4000-7800 cm^{-1} frequency range. For matrix distribution the samples were air dried and imaged using the same parameters. Transmittance spectra were ratioed to a background obtained through the glass slide and converted to absorbance for data analysis. The image acquisition time was approximately 15 minutes per sample.

4.4 Data analysis

NIR Spectra were processed using Unscrambler 10.1 (CAMO, Woodbridge, NJ). NIR spectra from cartilage with different thicknesses were analyzed to understand the effect of an increase in thickness on the NIR spectrum. For the data analysis the NIR spectral range was divided into 3 regions: 4000-5100 cm^{-1}, 5100-7000 cm^{-1} and 7000-9000 cm^{-1}. Polystyrene peaks were identified and assessed to determine the depth of penetration in each region separately. Spectra from cartilage samples with and without polystyrene plate underneath were compared to determine the depth of penetration of NIR. Spectra were first visually compared to see if the polystyrene peaks were visible in the raw cartilage spectrum when the polystyrene plate was placed underneath during data collection. Further, second derivative spectra were analyzed (Savitzky Golay, 31 point smoothing) to improve the assessment of the presence of polystyrene in the cartilage spectra.

4.5 Spectral Image analysis

Images of integrated areas under the NIR water absorbances centered at 5200 and 6890 cm^{-1} were generated using ISYs 5.0 software (Malvern Instruments, UK) to assess the distribution of water in cartilage. Similarly, integrated images for matrix distribution through different regions were generated from the 4384 cm^{-1} (combination of collagen and proteoglycan) absorbances[58].

4.6 Results

4.6.1 Cartilage NIR spectra with varying thickness

Cartilage NIR fiber optic spectra were dominated by water absorbances at 5200 cm^{-1}, 6890 cm^{-1} and 8500 cm^{-1} and matrix peaks at ~5600 cm^{-1}. Cartilage spectra with different thickness were compared to see the effect of increasing thickness on the spectra (Figure 15). It was observed that as the thickness of the cartilage increased, the water absorbance band at 6890 and 8500 cm^{-1} broadened. We observed that not only did the peaks change as the thickness of the cartilage changed, the mode of data acquisition also changed. When the thickness of the cartilage was less than 1 mm, the mode of data collection was transflectance, as the radiation could pass through the sample and reflect from the mirror back through the tissue. However, as the thickness of the cartilage increased the mode of data collection was dominated by diffuse reflectance.

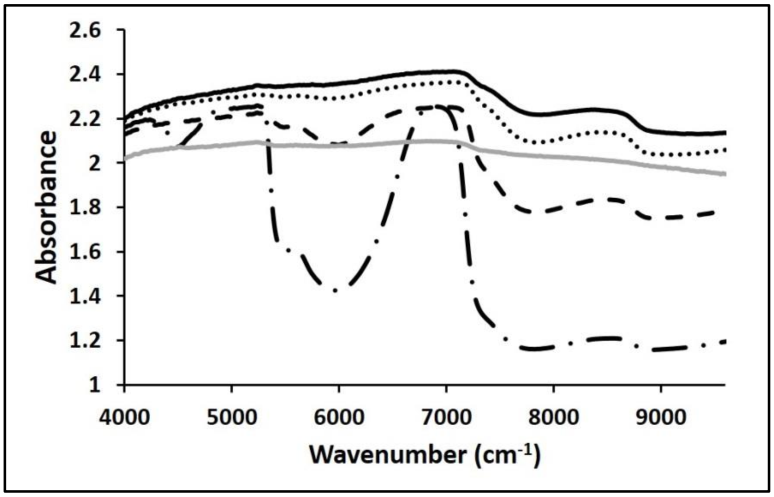

Figure 15: NIR cartilage spectra from 1 mm (long dash dot), 2 mm (black dash), 3 mm (dots) and 4 mm (solid black) thick samples. A diffuse reflectance spectrum (solid grey) obtained from a 1 mm thick cartilage sample on a dark surface is added for comparison of transflectance (long dash dot) to diffuse reflectance in the thin sample.

4.6.2 Comparison of raw and second derivatives of the NIR spectra from cartilage of varying thickness with polystyrene underneath:

The NIR spectrum of polystyrene (Figure 16) displays several distinct peaks (4048, 4245, 4330, 4612, 4663, 5668, 5949, 6078, 8270, and 8741 cm^{-1}) in the 4000-9000 cm^{-1} spectral region.

The primary reason behind utilizing polystyrene in this study was the fact that it had sharp peaks in the three regions of interest in the NIR spectrum. To assess the depth of penetration of NIR in region 1, polystyrene absorbances at 4612 and 4663 cm^{-1} were assessed. Similarly, for regions 2 and 3, polystyrene absorbances at 5959 and 8741 cm^{-1} were assessed, respectively.

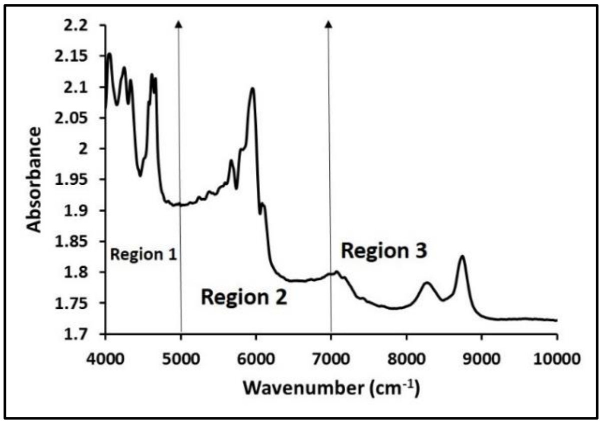

Figure 16: NIR spectrum of polystyrene. The NIR spectra were divided into 3 regions; region 1 (4000-5000 cm^{-1}), region 2 (5000-7000 cm^{-1}) and region 3 (7000-9000 cm^{-1}).

The NIR spectrum of polystyrene, cartilage of 0.5 mm thickness with polystyrene underneath and without polystyrene underneath are shown in Figure 17. The polystyrene peaks are clearly visible in all three regions of the NIR spectra of cartilage with the polystyrene plate underneath, which confirmed that the depth of penetration is at least 0.5 mm.

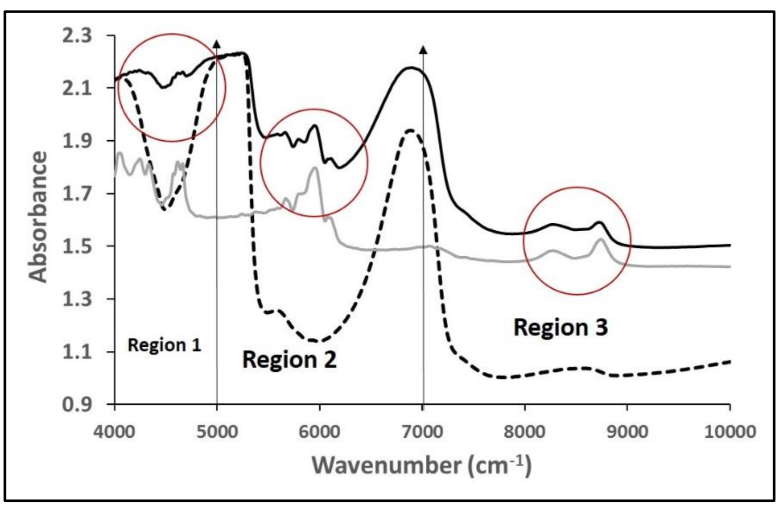

Figure 17: Comparison of raw NIR spectra from 0.5 mm thick cartilage sample with polystyrene (solid black) and without polystyrene underneath (dotted black) along with

polystyrene spectrum (solid grey). The influence of the polystyrene peak is highlighted with red circles in the three regions.

When raw spectra from a 1 mm thick cartilage specimen with and without polystyrene were

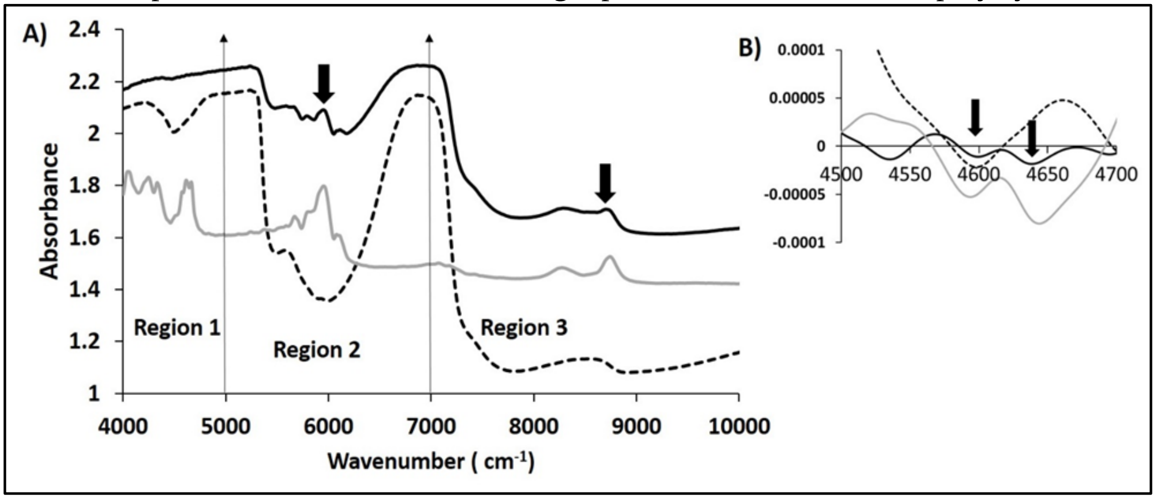

Figure 18: (A) Comparison of raw NIR spectra from 1 mm thick cartilage with polystyrene (solid black) and without polystyrene (dotted black) along with polystyrene spectra (solid grey). Influence of polystyrene on NIR spectra of 1 mm cartilage in region 2 and region 3 is highlighted by arrows. B) Second derivatives of NIR spectra from 1 mm thick cartilage with polystyrene underneath (solid black) and without polystyrene (dotted black) along with polystyrene spectra (solid grey) are compared in region 1. The polystyrene spectrum was divided by a factor of 10 to bring all spectra on the same scale.

compared (Figure 18), it was observed that the polystyrene peaks in region 1 was no longer visible, but the polystyrene peaks in region 2 and region 3 were clearly observed.

Second derivatives of the cartilage spectra with and without polystyrene were assessed to obtain more accurate data on penetration. It was found that in the second derivative of 1 mm cartilage with polystyrene underneath, polystyrene peaks were in fact still evident.

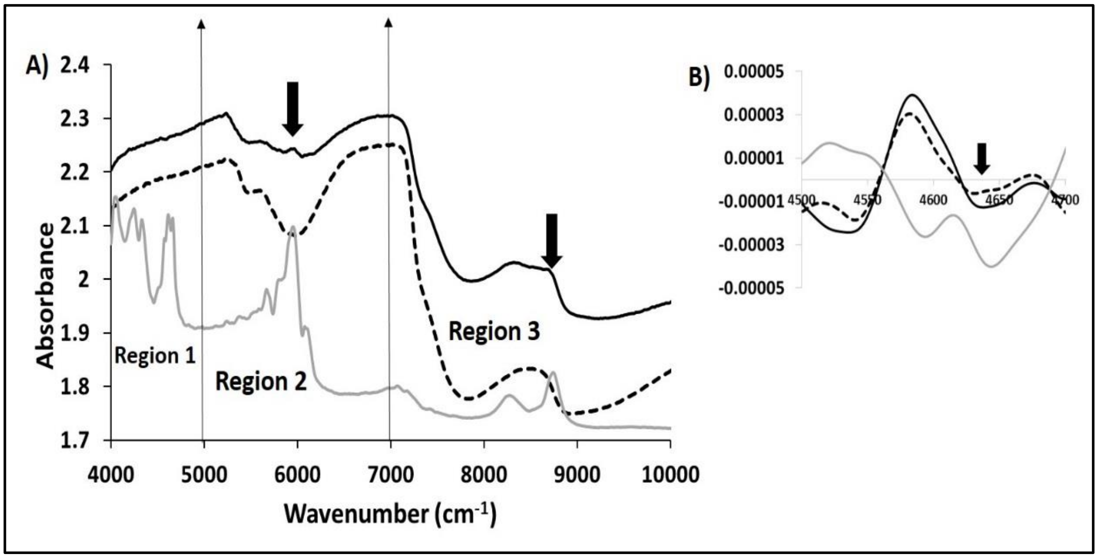

Figure 19: (A) Comparison of raw NIR spectra from 2 mm thick cartilage with polystyrene (solid black) and without polystyrene (dotted black) along with polystyrene spectra (solid grey). Influence of polystyrene on NIR spectra of 2 mm cartilage in region 2 and region 3 is highlighted by arrows. B) Second derivatives of NIR spectra from 2 mm thick cartilage with polystyrene (solid black) and without polystyrene (dotted black) along with polystyrene spectra (solid grey) compared in region 1. The polystyrene spectrum was divided by a factor of 10 to bring all spectra on the same scale.

Similarly, we compared 2 mm thick cartilage spectra with and without polystyrene underneath (Figure 19). It can be seen that the polystyrene peaks were not visible in region 1 but were still seen in regions 2 and 3, even though their intensity was reduced compared to the 1 mm cartilage with polystyrene underneath. When second derivatives were evaluated, we could barely see polystyrene in region 1, indicating the NIR penetration was reaching its limit.

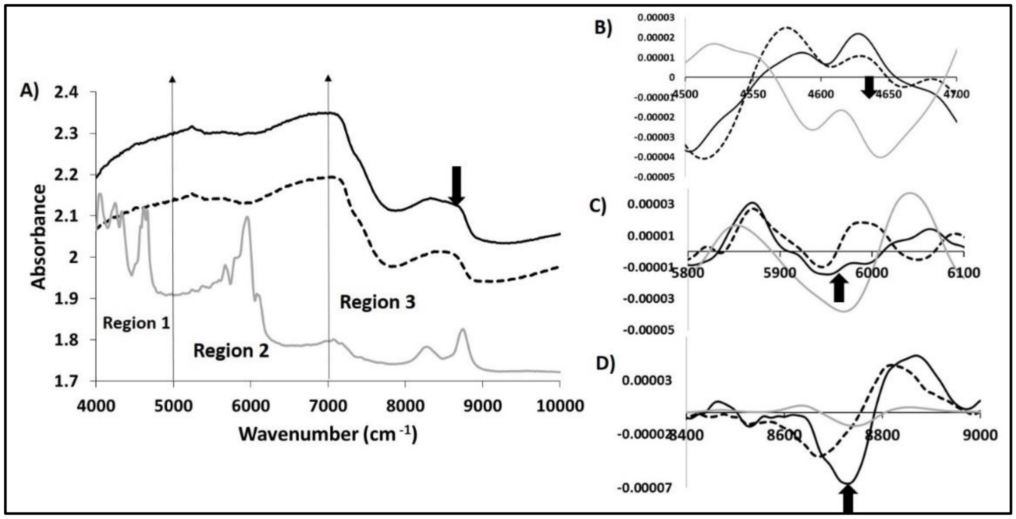

Figure 20: (A) Comparison of raw NIR spectra from 3 mm thick cartilage with polystyrene (solid black) and without polystyrene (dotted black) along with polystyrene spectra (solid grey). Second derivatives of NIR spectra from 3 mm thick cartilage with polystyrene (solid black) and without polystyrene (dotted black) along with polystyrene spectra (solid grey) compared in region 1 (B), region 2(C) and region 3(D). The polystyrene spectrum was divided by a factor of 10 to bring all spectra on the same scale.

In 3 mm thick cartilage with polystyrene underneath, polystyrene peaks were seen only in region 3 of the raw spectrum Figure 20). The evaluation of second derivative spectra showed that the polystyrene peak in region 1 was not seen at all, whereas in region 2 it was approaching its penetration limit. However, the polystyrene peak in region 3 was clearly observed.

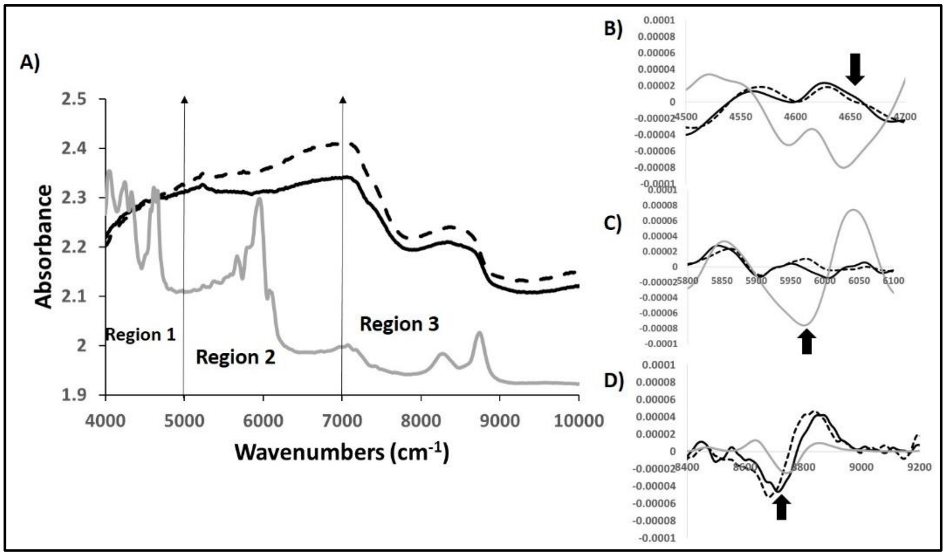

Figure 21 : (A) Comparison of raw NIR spectra from 4 mm thick cartilage with polystyrene (solid black) and without polystyrene (dotted black) along with polystyrene spectra (solid grey). Second derivatives of NIR spectra from 4 mm thick cartilage with polystyrene (solid black) and without polystyrene (dotted black) along with polystyrene spectra (solid grey) compared in region1 (B), region 2(C) and region 3(D). The polystyrene spectrum was divided by a factor of 10 to bring all spectra on the same scale.

The raw NIR spectra of 4 mm thick cartilage with and without polystyrene underneath looked very similar to each other (Figure 21). The polystyrene peaks were not seen in any region of the spectrum obtained from cartilage with polystyrene underneath. Evaluation of second derivative spectra showed that region 1 and region 2 had no polystyrene absorbances, but region 3 clearly showed a polystyrene peak. We also observed that the second derivative NIR spectra of cartilage with and without a polystyrene plate underneath were very similar in regions 1 and 2 as thickness increased, indicating no polystyrene penetration.

4.6.3 NIR image analysis results

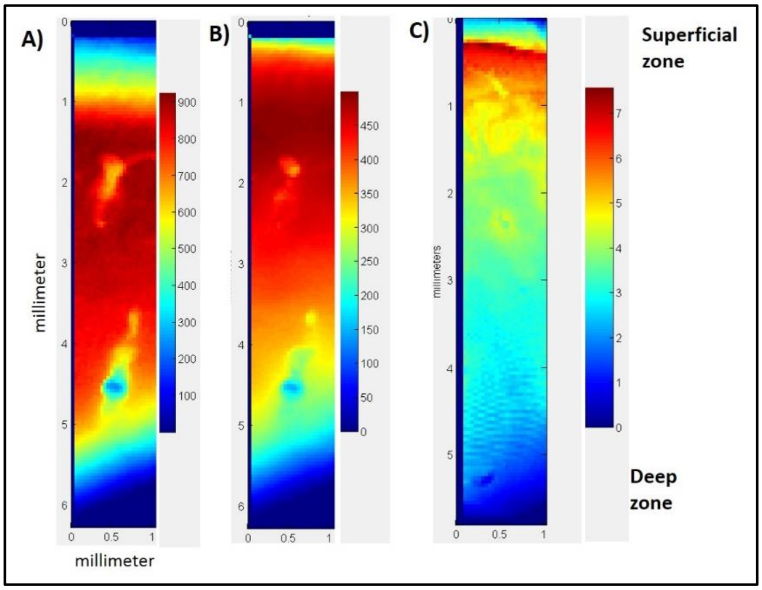

Figure 22: Distribution of water (A and B) and matrix components (C) through the cartilage depth. A) Integrated area map of the 5200 cm-1 (bound and free water) NIR absorbance B) Integrated area map of the 6800 cm-1 (free water) NIR absorbance and C) Integrated area map of the 4384 cm-1 (combination of collagen and proteoglycan) NIR absorbance. Color bar shows the integrated area scale for each absorbance.

FTIR images of cartilage showed the distribution of water and matrix content across all the zones of cartilage (Figure 22). The free water content (B) was greatest just below the superficial zone, into the middle zone, and decreased towards the deep zone. The bound plus free water (A) showed a similar distribution, except for quite near the surface. The reduction in water content towards the deep zone is consistent with literature reports [93]. The matrix content similarly was greater near the superficial zone, but decreased to a much greater extent into the middle and deeper zones.

4.7 Discussion

The current study showed that the depth of penetration of NIR radiation varies throughout the NIR spectral range in cartilage from 0.5 mm to 5 mm. In region 1 (4000-5000 cm^{-1}), the NIR depth of penetration was at least~1 mm, but approached the penetration limit at 2 mm. In region 2 (5000-7000 cm^{-1}), the NIR depth of penetration was ~3 mm whereas in region 3 (7000-9000 cm^{-1}) it was found to be greater than 4 mm.

Our results suggest that since the normal cartilage thickness of human cartilage is between 1-3 mm, the NIR absorbances obtained from the tissue will arise from cartilage, as well as from the subchondral bone underneath it, if the correct spectral range is not investigated. In NIR spectra, it is difficult to differentiate between bone and cartilage absorbances as the NIR region investigated does not display a phosphate absorbance. NIR absorbances from bone and cartilage, primarily water and organic matrix components, are at similar wavenumbers, though bone has sharper spectral features [61]. Therefore, the spectral region from 4000-7000 cm^{-1}, where the depth of penetration is ~3 mm, could be an ideal region for cartilage assessment. However, the spectral contribution from the higher wavenumbers could be useful for certain investigations focused on obtaining information from the subchondral bone.

A recent study from our group investigated the depth of penetration of bovine nasal cartilage (BNC) in the 4000-7000 cm^{-1} spectral region [61]. Here BNC samples were cut into different thickness from 0.34 to 5.76 mm and a parafilm absorbance peak at 5774 cm^{-1} was used to assess the depth of penetration. It was found the depth of penetration of NIR radiation for BNC in the spectral range 5000-7000 cm^{-1} was ~5 mm. In the current study where articular cartilage was used, the depth of penetration was ~3 mm in the same spectral range. The main differences between BNC and articular cartilage is the zonal organization in articular cartilage, and alignment of collagen fibrils. Thus, the difference between NIR depths of penetration is likely attributable at least in part to these features. Another difference between that study and the current study is the fact that our polystyrene plate was 0.54 mm thick whereas the parafilm was only ~ 0.1 mm thick. This difference in plastic thickness would result in a change in overall pathlength the NIR radiation travels through the samples and underlying plastic, resulting in what appears to be reduced penetration depth through the cartilage. However, since the thickness of 0.54 mm is closer to what would be observed for subchondral bone, the results from the current study more closely resemble the physiological condition. A previous study by Spahn et al. used a ratio of the NIR water absorbance band at 7017 cm^{-1} to the 8510 cm^{-1} matrix absorbance, and considered this as an indicator of cartilage water content [88]. According to our results, the depth of penetration of NIR radiation at this spectral range is greater than 5 mm. Therefore the spectral absorbance collected in this region not only resulted from the cartilage but also from the subchondral bone underneath.

The NIR spectral range we used in this study was from 4000-10000 cm^{-1}. The absorbances in this region arise from combination, first and second overtones of the fundamental vibrations in the mid-infrared regions. The absorbance intensity is inversely proportional to the order of overtone thus making the analysis difficult and complicated [113, 114]. A recent study from our group showed that the absorbances from cartilage matrix components, (collagen type II and chondroitin sulfate), in the 4000-5000 cm^{-1} spectral region, could be used to assess cartilage composition [58]. Similarly, we showed that the water absorbance at 5200 cm^{-1} , which arises from bound and free water, and the 6890 cm^{-1} free water absorbance, could be used to assess water content [69]. Together, these studies show that the NIR spectral region from 4000-7000 cm^{-1} could prove to be an important region to assess cartilage quality based on matrix composition, and thus provide support for focusing on this region for evaluation of tissue pathology.

Recently, NIR has been used to develop a non-destructive method to determine the thickness of cartilage [90]. In that study, NIR spectra were collected from 1.2 mm to 2.4 mm thick cartilage samples from bovine samples. Partial least square (PLS) models with various NIR spectral ranges from 4000-12000 cm^{-1} were built to correlate NIR spectra with the cartilage thickness, with the results of the PLS varying from 53% to 93% for correct thickness prediction. The best results were from the 5350-8850 cm^{-1} region, and the lowest correlation from higher wavenumbers, i.e. 8000-12000 cm^{-1}. According to our results, the depth of penetration of NIR radiation in this range is more than 4 mm. Therefore the absorbance in this range are a combination of cartilage and the subchondral bone, and possibly primarily from subchondral bone, which could result in a poor thickness prediction. However, it's also possible that the differences in subchondral bone contributions in the spectra could aid in the thickness assessment in the lower frequency region.

There were some limitations of our study, including the fact that the tissue sections were cut parallel to the cartilage surface, and thus differences in organization or composition in different zones could impact the results. In essence, this means that samples of different thicknesses could contain either, e.g., both superficial and middle zone cartilage, or only middle or deep zone cartilage, or middle plus deep zone cartilage. Our results from the imaging data analysis showed that the distribution of water and matrix components varies among the different zones. This is most relevant to our fiber optic studies if thinner cartilage tissues are evaluated in the lower frequency NIR spectral regions, and there could be a question as to whether having the dense, collagenous superficial zone intact would result in reduced penetration depth. To address this, a separate experiment was conducted in a similar manner as the rest of the study with 1 mm samples that contained superficial and middle zone cartilage to assess whether the zonal differences did in fact affect the depth of penetration. We found that the NIR spectra collected from these samples on top of polystyrene showed polystyrene peaks in all regions, in agreement with the results presented previously (data not shown). Another issue to address is the fact that we did not evaluated degraded tissue samples. Degraded cartilage is less dense and fibrillated due to the loss of proteoglycans and damage to the collagen fibers. In this case, it is possible that the depth of penetration would be even greater through the tissue, compared to normal cartilage. Thus, it's possible that we should consider further limiting the spectral range of analysis for such samples if we want to exclude the contribution of subchondral bone. Human adult normal and degraded cartilage should be evaluated in future studies to confirm the depth of penetration of NIR radiation in these physiologically relevant tissues.

Potential applications of NIR probe evaluation of cartilage include for animal model studies, where a non-destructive method could be used to understand the effects of therapeutics and rehabilitation protocols in longitudinal studies. Clinically, intra-articular injuries are the most common injuries in young athletes, such as meniscus and ligament tears [115]. Currently, arthroscopic evaluation is the gold standard method for investigation of symptoms related to early stages of cartilage degeneration. However, they can be somewhat subjective as they rely on the perception of the surgeon performing the procedure. The use of NIR probes has the potential to play an important role in monitoring early degeneration of cartilage for the high risk patients, such as those with prior anterior cruciate ligament or meniscus injury. Since the data obtained is less subjective than that from visual arthroscopy, it is possible that more precise results on how to stage cartilage could be obtained. Further, since arthroscopy is currently the preferred method for evaluation of intra-articular tissues, addition of NIR fiber optic probe data, which could be obtained through an arthroscopic port, could prove to be an important tool to study the pathology of injury and repair. Improved understanding of the features of the NIR spectra is critical for implementation of this methodology for tissue evaluation.

4.8 Conclusion

The results from this study demonstrated that the depth of penetration of NIR radiation into articular cartilage varies throughout the spectral range, 4000-10000 cm^{-1}, from 0.5 mm to at least 5 mm. The optimal NIR frequency range to ensure the absorbances being evaluated are only from cartilage and not from the subchondral bone is no higher than 7000 cm^{-1}.

4.9 Acknowledgements

This study was supported by NIH AR056145 and EB000744.

4.10 Part II: Establish the depth of penetration of NIR radiation into ligament and tendon.

4.10.1 Materials:

Medial collateral ligaments (MCLs, n = 3, ~ 1 mm thick) were harvested from Dutch-Belted female rabbits ~ 6 months of age under an IACUC-approved protocol, and stored in PBS and PI at -20°C until NIR data collection. To obtain wide range of different thicknesses, rabbit MCL and bovine anterior cruciate ligament (ACL) and patellar tendon (n=3) were used in this study. Further, ACL and tendons were cut into 1 mm, 2 mm and 3 mm thick slices with blades (longitudinal direction). The thickness of the MCLs and ACLs and tendons were recorded three times with a caliper (Fisher Scientific, Pittsburgh, PA) and averaged.

4.10.2 Near infrared fiber optic probe data collection:

NIR spectra were obtained using a 3 mm diameter silica glass NIR fiber optic diffuse reflectance probe (Art Photonics, Berlin, Germany) coupled to a Matrix-F infrared spectrometer with a TE-InGaAs detector ((Bruker, MA). Spectra were collected from different thickness ligament samples with and without polystyrene plate underneath at 16 cm^{-1} spectral resolution, 126 co-added scans in the 4000-10000 cm^{-1} spectral range. Light pressure was applied during data collection to ensure proper contact. A reference spectrum was collected from the polystyrene plate (thickness: 1mm) to identify peaks of interest.

4.11 Data analysis:

NIR spectra were processed using Unscrambler 10.1 (CAMO, Woodbridge, NJ). NIR spectra from ligament with different thickness were analyzed to understand the effect of increases in thickness on the NIR spectrum. For the data analysis near infrared spectral range was divided into 3 sub-ranges: 4000-5000 cm^{-1}, 5400-7000 cm^{-1} and 8000-9000 cm^{-1}. In these three regions polystyrene peaks were identified and followed to determine the depth of penetration in each region separately.

Spectra from ligament with and without polystyrene plate were compared to determine the depth of penetration of NIR radiation. Raw spectra were first visibly compared to see if the polystyrene peaks were visible in the ligament spectrum when polystyrene plate was placed underneath during data collection. Further, spectra were pretreated with second derivative (Savitzky Golay, 31 points smoothing) and compared.

4.13 Results

The average thickness of rabbit MCL was ~ 1mm. When the raw NIR spectra from the

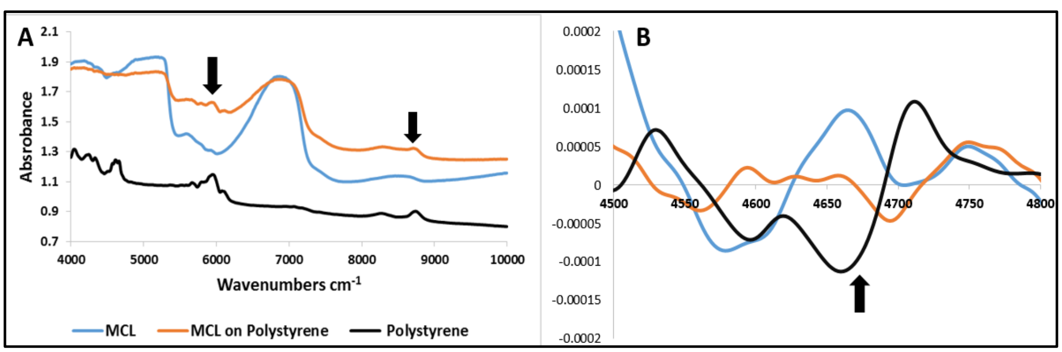

Figure 23: Comparison of NIR spectra of rabbit MCL with (orange) and without polystyrene underneath (blue). A polystyrene spectrum is added as a reference (black). The black arrows are indicating the influence of polystyrene on MCL spectrum.

MCL with and without polystyrene were compared, it was seen that polystyrene peaks were visible in the 5000-7000 cm^{-1} region and in the 7000-10000 cm^{-1} region (Figure 23). However, the polystyrene peak was not visible in the 4000-5000 cm^{-1} region. Therefore we looked into the second derivatives in this region. When the second derivative spectra of MCL with and without polystyrene were compared in the 4000-5000 region, the polystyrene peaks were not seen in the MCL spectra with polystyrene underneath. However, we observed some slight peak shifts indicating the NIR penetration reaching its limit in region 1.

4.12.1 Tendon and ACL:

To investigate different tissues thickness, we collected NIR data from ACL and patellar tendon. The NIR spectra of different tendon thicknesses with polystyrene underneath are shown in the Figure 24.

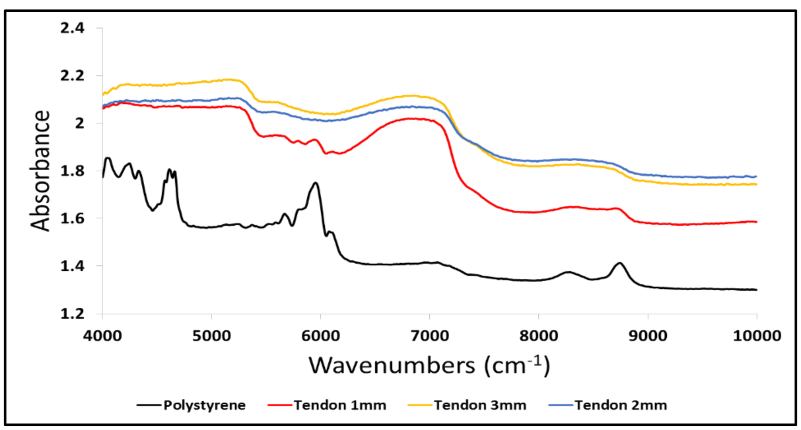

Figure 24: NIR spectra of tendon sample with different thickness with polystyrene (black) underneath. In the 1mm (red) sample you can clearly see the influence of polystyrene on the tendon spectrum. However, it is not seen in 2 mm (yellow) and 3mm (blue) raw spectra.

We observed that in 1 mm thick tendon slices, polystyrene peaks were clearly seen in the raw spectrum at 5959 cm^{-1} and 8778 cm^{-1}. The polystyrene peaks were not seen visually in the spectral range of 4000-5000 cm^{-1}. When we compared the second derivatives of NIR spectra of tendon 1 mm slice with and without polystyrene in the 4000-5000 cm^{-1} range, we observed that the polystyrene peaks were still not seen in the NIR spectra of tendon collected on polystyrene.

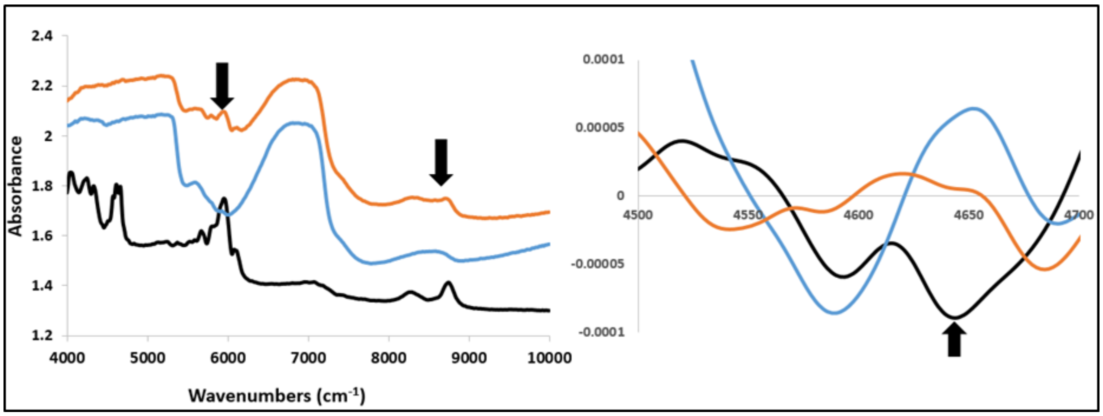

Figure 25: Comparison of 1mm thick tendon slice with (orange) and without polystyrene (blue) underneath. Arrows are pointing to the influence of polystyrene underneath. A reference spectrum of polystyrene (black) is added. Comparison of second derivative spectra in the range 4000-5000 cm^{-1} did not show polystyrene when the spectra were collected with polystyrene underneath.

In the 2 mm and 3 mm thick tendon spectra with polystyrene underneath, it was seen that the polystyrene peaks were not visually apparent in any range of the NIR spectra. As the thickness of the tendon slice increased, the NIR spectra of tendon with and without polystyrene looked very similar to each other. When we compared the second derivatives of NIR spectra of tendon 2 mm slice with and without polystyrene in the 5100-6000 cm^{-1} range, we observed that the polystyrene peaks were still not seen in the NIR spectra of tendon collected on polystyrene. In contrast, the polystyrene peaks in 8000-9000 cm^{-1} range were clearly seen.

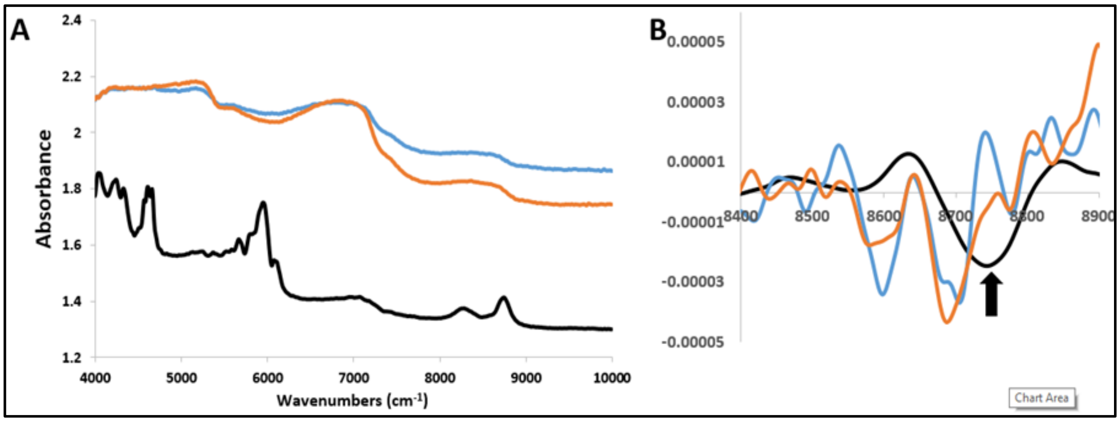

Figure 26: (A) Comparison of raw NIR spectra from 3 mm thick tendon with polystyrene underneath (orange) and without polystyrene (blue) along with polystyrene spectra (black). Second derivatives of NIR spectra from 3 mm thick tendon with polystyrene (orange) and without polystyrene (blue) along with polystyrene spectra (black) compared in 8000-9000 cm^{-1} (B). The polystyrene spectrum was divided by a factor of 7 to bring all spectra on the same scale.

In the 3mm spectrum of tendon with polystyrene underneath showed no clear polystyrene suggesting that the depth of penetration of NIR radiation reaching its limits.

For ACL the depth of penetration of NIR radiation into the tissue followed same trend as tendon. In 3 mm thick ACL, the polystyrene peaks were not visible in raw spectra of ACL with and without polystyrene. Therefore we looked into the second derivatives. When the second derivatives of the NIR spectra were compared in the range of 5000-6000 cm^{-1} it was found that the polystyrene peaks were not seen however, in the 8000-9000 cm^{-1} we could clearly see the effect of polystyrene peak underneath as shown in figure 29(C).

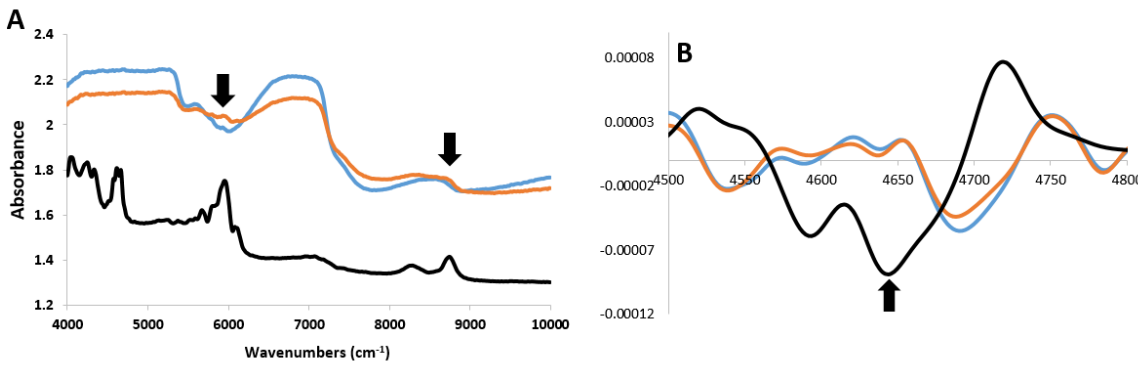

Figure 27: Comparison of 1 mm thick ACL with (orange) and without (blue) polystyrene underneath. The influence of polystyrene in ACL spectrum is shown with the arrows. A polystyrene spectrum (black) is added for reference. B) Comparison of the second derivative of the 1 mm thick ACL in 4000-5000 cm^{-1} spectral range. It was seen that the influence of polystyrene was not seen in the spectrum indicating the limit of NIR radiation.

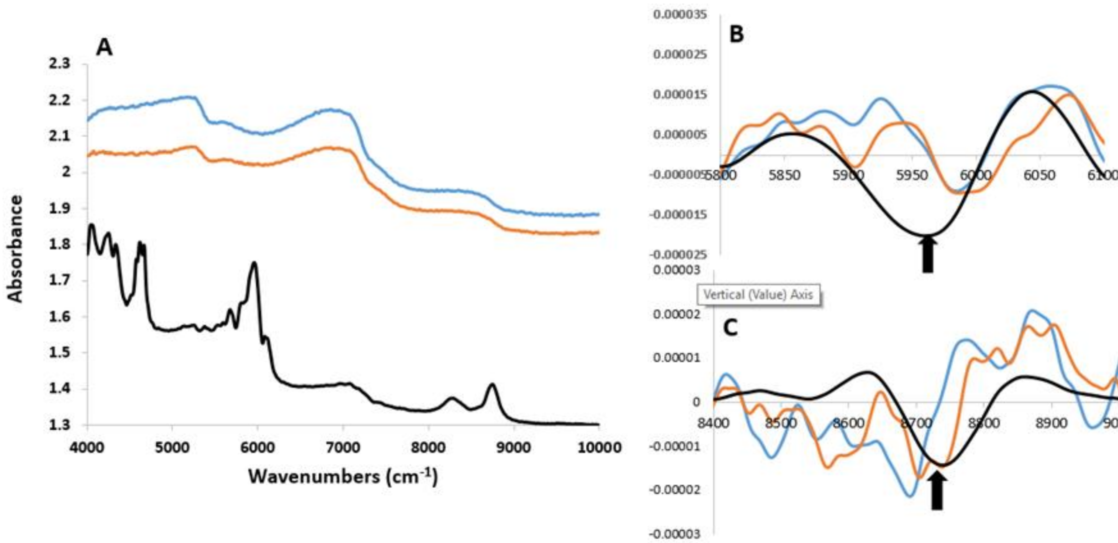

Figure 28: (A) Comparison of raw NIR spectra from 3 mm thick ACL with polystyrene (orange and without polystyrene (blue) along with polystyrene spectra (black). Second derivatives of NIR spectra from 3 mm thick ACL with polystyrene (orange) and without polystyrene (blue) along with polystyrene spectra (black) compared in 5000-6000 cm^{-1} (B) and 8000-9000 cm^{-1} (C). The polystyrene spectrum was divided by a factor of 7 to bring all spectra on the same scale.

4.13 Conclusion:

The results from this study demonstrated that the depth of penetration of NIR radiation into rabbit MCL, ACL and patellar tendon varies throughout the spectral range, 4000-10000 cm^{-1}. The tissue have different collagen organizations, and therefore, it was expected that NIR radiation will have varying depth of penetration. In MCL it was found that the NIR was able to penetrate through the entire thickness of the MCL in the 5000-10000 cm^{-1} range. However, NIR radiation in the range of 4000-5000 cm^{-1} was not able to penetrate through the entire thickness of ~ 1 mm. Therefore the optimal NIR range for collection of spectral data from rabbit MCLs without underlying bone contributions would be 4000-5000 cm^{-1}. For ACL and tendons that are ~3 mm thick, similar to what is found in humans, the entire NIR spectrum would be optimal without any bone or posterior cruciate ligament (PCL) absorbance contribution.

The results from the first aim showed that mid-IR spectroscopy was able to differentiate ligament and tendon composition. However, these are two different tissues and during ligamentization, there will be subtle changes in the remodeling tissue. It has been shown that the graft remodeling starts from the peripheral region of the tissue and progresses towards the center of the graft. Mid-IR spectroscopy will be able to detect the changes in the graft in these initial phase, however, as the graft progresses towards the center, NIR depth wise analysis of the tissue could provide more insight about the remodeling process.

CHAPTER 5

5.0 SPECIFIC AIM 3:

Correlate infrared spectral data obtained from ligament regions with varying composition with mechanical properties.

Significance: The results from this aim would validate that infrared spectral data correlates to functional properties of ligaments. Mechanical properties of the remodeling graft are always of interest. Even if the graft remodels significantly, the mechanical properties are never the same as in the native ACL. Previous studies have used mechanical uniaxial tensile testing as a method of analysis to study ligament graft properties, but this method requires tissue harvesting. A non-destructive method such as spectroscopic assessment that correlates to mechanical properties of the ligament and tendon would aid in furthering understanding of the remodeling process, and could also aid in selecting allograft or autograft replacements.

Prepared as a manuscript for submission to Journal of Orthopaedic Research

Near Infrared Spectroscopic Assessment of Ligament Composition Provides Insight into Regional Differences in Mechanical Properties

5.1 Introduction:

Ligament rupture is the most common injury in young athletes [116]. In female athletes the occurrence of ligament injury is thrice the male athletes [117]. A torn ligament is often reconstructed with an allograft tendon or an autograft tendon [16, 118]. It has been shown that the graft never returns to the 100% of its mechanical strength [86]. The process of transformation of a graft tendon in a structure similar to native ligament is known as ‘ligamentization’ [22]. Along with the chemical changes occurring during ligamentization, mechanical properties of the remodeling graft are often of interest. In order to improve the mechanical properties of the remodeling graft, the mechanical properties of the normal tissue must be studied. All biomechanical data about the remodeling graft or the native tissue is obtained from the experimental data on the dissected tissue.

In-vivo mechanical behavior of the tissue could provide more physiologically relevant information. Additionally, a non-destructive method for assessment of graft composition and mechanical strength could be implemented in a clinical setting. There have been efforts to determine mechanical properties of the ligament and tendon in-vivo in the human during regular activity. Ultrasound has been used to measure mechanical properties of various tendons [40, 41, 119]. In one study, sonography was used to get the dimensions of the tendon while the force was measured with a dynamometer. The findings from this study were similar to the percent strain obtained from laboratory experimental data [33]. These studies are promising and could possibly be translated clinically. However, these studies had some limitations as well. In a detailed systematic review by Seynnes et al, the authors highlighted some of the limitations of the current approach to determine in-vivo tendon force measurements [119]. It was found that the outcomes from the studies showed large discrepancies, and there were several possible sources of errors, including tracking of the elongation, simplification of 3D deformation of tendon, and importantly, ignoring the time dependency of the tendon behavior. The cross-sectional area obtained from the sonography images were two dimensional areas compared to the three dimensional volume of the tendon. And further, the protocols required highly skilled personal to carry out the test each time [40, 41, 119].

In contrast, Fourier transform infrared (FT-IR) spectroscopy exhibits a high degree of specificity to molecular structure and compositional changes in tissue. The mid infrared (mid-IR) spectral absorbances from connective tissues are well understood and have been used to study several connective tissues [47, 48, 54, 120]. An FT-IR spectrometer with a microscope attachment, infrared spectral imaging, can be used to acquire spectral images from histological tissue sections and to study regional differences within the tissue at high spatial resolution, ~ 6 micron. When a fiber optic probe is attached to the spectrometer, spectral data could be directly obtained from tissues with minimal sample preparation, making them ideal for clinical use. Our group has utilized spectral imaging as well as non-destructive infrared fiber optic probes to study musculoskeletal tissues. Recent studies by our group have studied cartilage degeneration and repair with mid-IR fiber optic probes [79]. Previous studies by our group have shown that mid-IR fiber optic probe spectral parameters correlate with cartilage histological grading [52, 53]. Therefore, these studies strongly support the use of FT-IR fiber optic probes as an important tool for the non-destructive evaluation of tissue.

The drawback of mid-IR is its limited depth of penetration, up to ~10 µm only [50, 51]. In contrast to mid-IR, radiation in the NIR spectral range has a depth of penetration up to centimeters [121]. It was found that the depth of penetration of NIR radiation into articular cartilage varies throughout the spectral range, 4000-10000 cm^{-1}, from 0.5 mm to 5 mm. It has been shown that NIR spectra correlate with cartilage matrix composition [58, 69, 89], thickness [90], degradation enzymatically [59], as well as histological grading systems, such as Mankin score system [60, 61]. In addition, several studies are advocating the use of NIR probes arthroscopically to evaluate early cartilage degeneration [60, 88]. To our knowledge, NIR has never been used to study ligament composition and structural properties.

Thus, the purpose of this study was to determine if IR spectroscopy has the potential to be used as a non-destructive tool to characterize mechanical properties of ligaments by directly comparing regional IR-derived compositional parameters of rabbit ligament to mechanical properties from the same specimens. There were two reasons to choose MCLs as a ligament of interest: 1) A previous study has shown that the composition of rabbit MCL varies in different regions of the MCL [77], and 2) The MCL would be readily accessible to the infrared fiber optic probes used in the study, since it is on the exterior of the bones it connects. In the current study, NIR and mid-IR fiber optic data were collected from different regions of rabbit MCLs. After IR data collection, tensile tests were performed on the bone-ligament-bone complex to obtain mechanical properties, including stiffness and modulus, from the same regions where the IR data were collected.

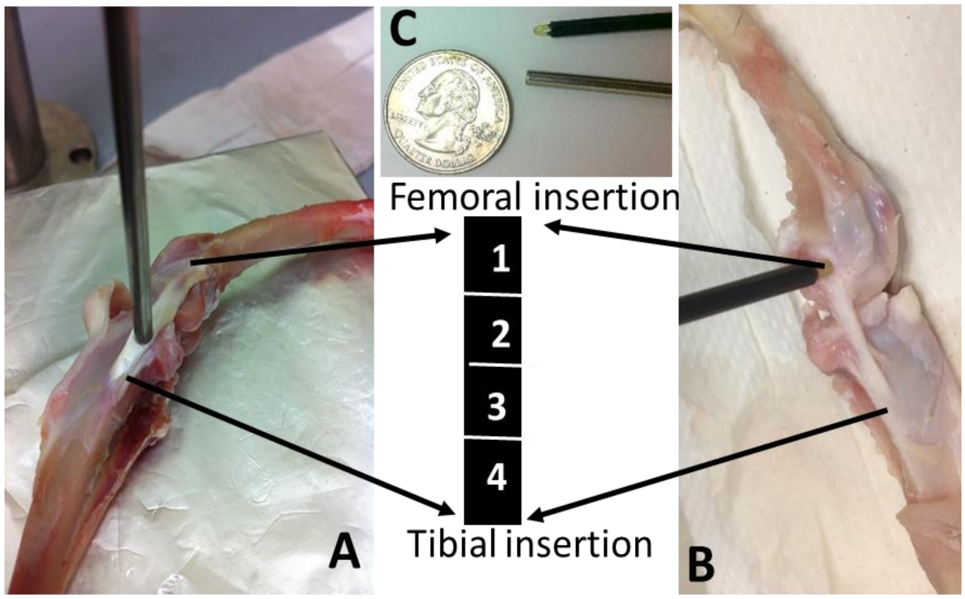

Figure 29: The experimental set up for fiber optic data collection. Spectral data were collected from four different regions from the femoral insertion to tibial insertion. (A) NIR data collection, (B) Mid-IR data collection and (C) size of the fiber optic probes used in the study (mid-IR top, NIR bottom). These probes are custom designed to glide through arthroscope portals.

5.2 Material and methods:

5.2.1 Materials:

Medial collateral ligaments (MCLs, n = 13) were harvested from Dutch-Belted female rabbits ~ 6 months of age under an IACUC-approved protocol, and stored in PBS and PI at -20°C until infrared data collection. NIR and mid-IR spectra were obtained from the MCLs as described below, and the ligaments were again frozen until mechanical testing studies were performed. Thus, each tissue went through two freeze-thaw cycles.

5.2.2: Near infrared fiber optic probe data collection:

Prior to mechanical testing, NIR spectra were obtained from four regions of each MCL (femoral insertion, tibial insertion, two mid-substance regions) using a 3 mm diameter silica glass diffuse reflectance NIR probe (Art Photonics, Berlin, Germany) coupled to a Matrix-F infrared spectrometer with a TEInGaAs detector (Bruker, MA). NIR data were collected in diffuse reflectance mode from 4000-10000 cm^{-1} at 8 cm^{-1}, and 128 co-added scans. At each location three replicate spectra were collected thus resulting in 12 spectra per MCL. A light pressure was used during data collection to ensure contact with the sample. A NIR background was collected from the Spectralon standard prior to sample data collection with spectral range from 4000-10000 cm^{-1}, at 8 cm^{-1}, and 256 co-added scans.

5.2.3: Mid infrared fiber optic probe data collection:

Prior to mechanical testing, mid-IR spectra were collected using a Thermo Scientific Nicolet iS5 FT-IR spectrometer with a TGS detector fitted with a fiber optic coupler (Harrick Scientific Products, Inc., Pleasantville, New York), and a silver halide ATR-loop mid-infrared fiber optic probe of 1 mm diameter. Spectra were ratioed to an air background collected at 8 cm^{-1}, 64 co-added scans and in the frequency range of 1000-1800 cm^{-1}. Similar to the NIR data, mid-IR spectra were collected from insertion sites as well as two locations of the mid substance of MCLs. Spectra were collected at 8 cm^{-1} spectral resolution, with 32 co-added scans in the frequency range of 1000-1800 cm^{-1}. At each data point, 3 replicate spectra were collected resulting in 12 mid-IR spectra per MCL. Care was taken to collect mid-IR data from same regions where NIR data were collected.

5.2.4 Mechanical testing:

Uniaxial tensile testing of the MCLs was performed in the McKay Orthopedic Research Laboratory, University of Pennsylvania, using an Instron 5543 Electromechanical Test

System (Instron, Norwood MA, USA). Cross-sectional areas of the MCLs were measured using a custom made laser device.

At this stage, the excess bone from tibial end and femoral end was cut off with a saw. Holes were drilled on the both ends approximately half way between. A small wire piece was inserted in this hole to take care of the change in diameter towards the end of the bone. This wire was used to help the polymethylmethacrylate cement (PMMA) to hold the

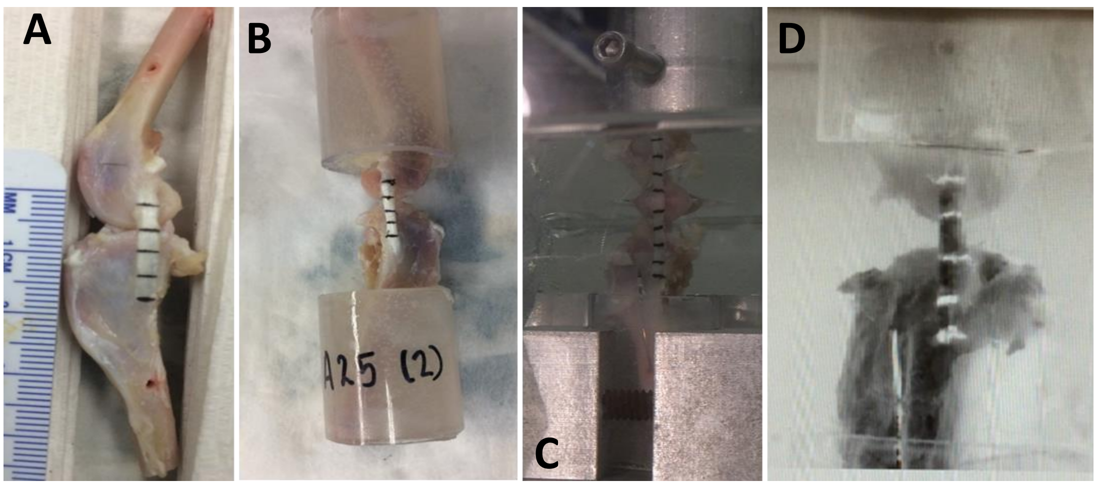

Figure 30: Sample preparation for mechanical testing: A) Stain lines were drawn on the MCL mm apart. B) MCL potted in PMMA C) Fixed in a custom made fixture for mechanical testing D) during data analysis

ligament during tensile testing. The bone –ligament-bone complexes were potted in PMMA and gripped in custom made fixtures. Care was taken during potting to keep any part of the ligament from touching the PMMA. During the testing the MCLs were immersed in a PBS bath. To obtain regional properties of the MCLs, stain lines (Verhoeff's stain) were drawn 4mm apart on the MCL. The stain lines were tracked during mechanical testing by a video analyzer to obtain regional stiffness, which was normalized by cross sectional area to obtain modulus [122].

Prior to the main experiment, a pilot experiment was conducted to determine the typical failure load of the MCL. The specimens were preloaded to 0.1N, followed by

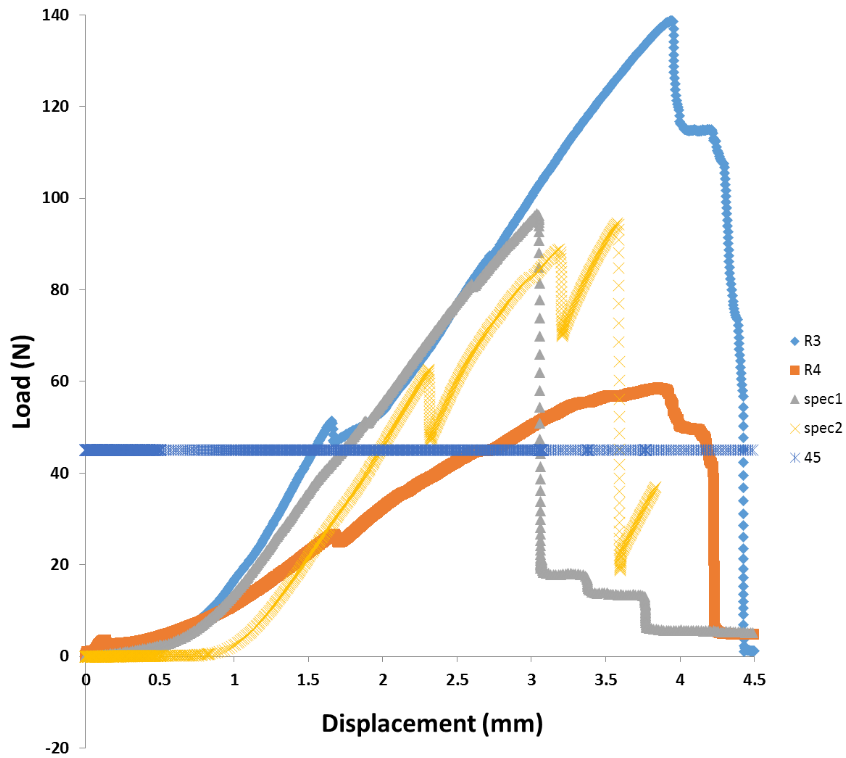

Figure 31: The load-displacement curves for 4 samples used in the pilot study. All samples showed linear characteristics in the 0-45N load range except one sample. From these results, we decided to use load limit of 45N for our study.

preconditioning (0.0 to 0.5 mm, 10 cycles, 10mm/min). This was followed by a hold of 300 seconds prior to a ramp to failure at a rate of 10mm/min. Four MCLs were ramped to failure and it was found that the failure load was found to be in the range of 50-140N. From this experiment we found out that all samples showed linear behavior in the 0-45N range, therefore in the main experiment, the load was restricted to 45N.

5.2.5 Water content:

After mechanical testing, each MCL was cut into four pieces that corresponded to the four regions from which spectral data were acquired. Each piece was weighed and wet weight was noted. Following that, the MCL pieces were lyophilized and the dry weights were obtained. Percent water content was determined by:

Water content (%) = (sample wet weight – sample dry weight) / (sample wet weight) * 100

5.2.6 Sulfated glycosaminoglycan (sGAG) content:

Sulfated glycosaminoglycan (sGAG) content (reflecting PG content) was determined using a dimethylmethylene blue (DMMB) assay. Briefly, 1,9-DMMB (pH 3) (Sigma Aldrich) was added to the digest solution at 10–1 ratio and absorption recorded at 525 nm using a Tecan plate reader (Tecan Systems Inc., San Jose, CA). A series of chondroitin sulfate (Sigma Aldrich) solutions with known concentrations were used to plot a standard curve (absorbance vs. concentration) and the concentration of sGAG in the samples was calculated using the standard curve equation [123].

5.2.7 Hydroxyproline content:

Hydroxyproline content (reflecting collagen content) was determined using a chloramine-T based assay. MCL digest solutions were hydrolyzed using 6 M HCl (1:2 ratio) at 110 °C for 18 h. Then, hydroxylate samples were neutralized with 6 M NaOH, decolorized using activated carbon, and subsequently treated with chloramine-T (3:2:5 1-propanol:water:citrate buffer, 15 mM chloramine-T) and Erlich's (47:37:16 1-

propanol:water:perchloric acid, 160 mM pdimethylaminobenzaldehyde) reagent. A series of cis-4-Hydroxy-D-proline (Sigma Aldrich) solutions with different concentrations were used to calculate a standard curve. Absorbance at 550 nm was measured using a Tecan plate reader. The concentration of hydroxyproline in the samples was calculated using the standard curve equation. Hydroxyproline content was converted to collagen content using a factor of 8 [124]. Collagen and PG content obtained from biochemical assays were normalized to MCL dry weight [125].

5.3 Data analysis:

5.3.1 NIR spectral data:

NIR spectra were scatter corrected and second derivatives (Savitzky Golay, 100 point smoothing) were calculated (Unscrambler software, Camo, Norway). Second derivative peak heights were calculated at 7000 cm^{-1}, which reflects the free water in the tissues, and at 4608 cm^{-1} [58] which reflects the overall matrix composition. One way ANOVA was used to investigate whether the differences in the water content were statistically significant at $p < 0.05$.

5.3.2 Mid-IR data analysis:

Mid-IR spectra were analyzed using ISYs 5.0 software (Malvern Instruments, UK). The integrated areas under Amide I, II and 1338 cm^{-1} were calculated at each location for all samples. One way ANOVA was used to investigate whether the differences in areas were statistically significant at $p < 0.05$. A Pearson correlation was done for the infrared spectral paramaeters and mechanical data, with significance at $p < 0.05$.

5.3.3 Mechanical properties:

During the tensile testing, load-time and deformation of the tissue was recorded

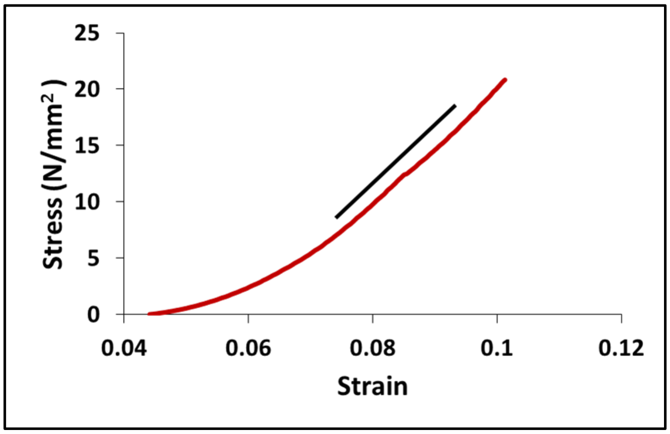

Figure 32: Typical stress strain curve for a rabbit MCL. The black line shows the linear region where the modulus was calculated

simultaneously. A camera was used to collect images which later were analyzed using a custom image processing MATLAB code.

The routine included selection of two stain lines and tracking their relative movement to get the deformation. Stress was determined by dividing the force by area and the strain was obtained by change in length divided by original length. The optical modulus and stiffness were obtained by plotting stress versus strain curve for each region [122]. For each MCL, optical stiffness and optical modulus were calculated at the femoral and tibial insertion sites, and at mid substance. One way ANOVA was used to investigate whether the differences in parameters for each region were statistically significant at $p < 0.05$

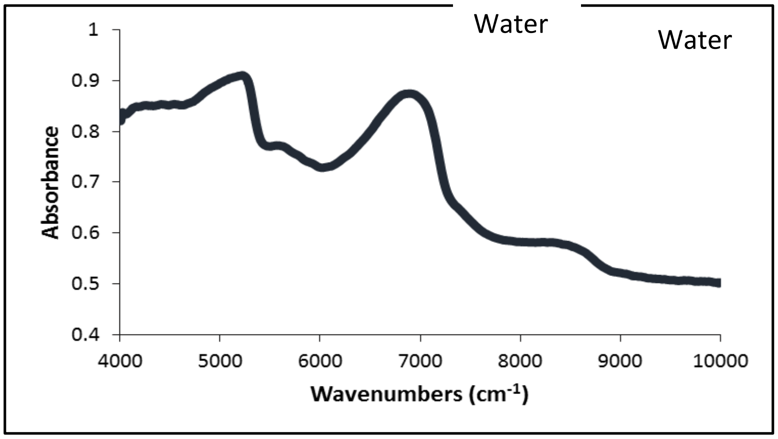

Figure 33: Typical NIR spectrum from rabbit MCL

5.4 Results:

5.4.1 NIR results:

The NIR spectra from different regions of MCLs were dominated by water absorbances at 5200 cm^{-1} and 7000 cm^{-1}.

It was found that the second derivative peak height at 7000 cm^{-1}, reflecting free water content, varied throughout the MCL regions. The free water content at the femoral insertion was significantly higher compared to the other regions of the MCL.

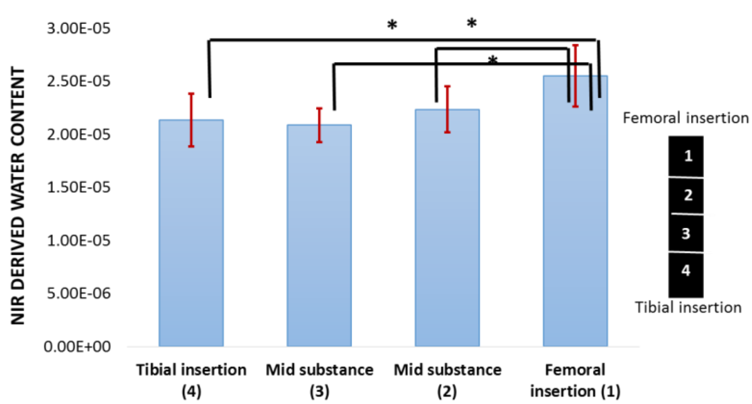

*Figure 34: NIR derived water content results showed variation in the different regions of MCL. It was found that the femoral insertion site showed significantly higher water compared to the other regions. * significance at $p<0.05$*

5.4.2 Mid-IR results:

The Mid-IR spectra from different regions of rabbit MCL were dominated by collagen peaks at collagen peaks at 1650 (amide I), 1550 (amide II), 1338 (side chains) and 1240

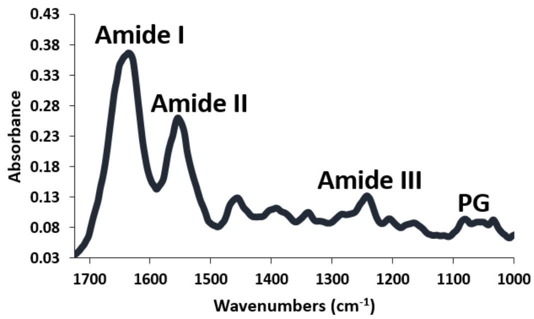

Figure 35: Typical Mid-IR spectra of rabbit MCL where Amide I, II and III arise from collagen and PG arises from sugar chains

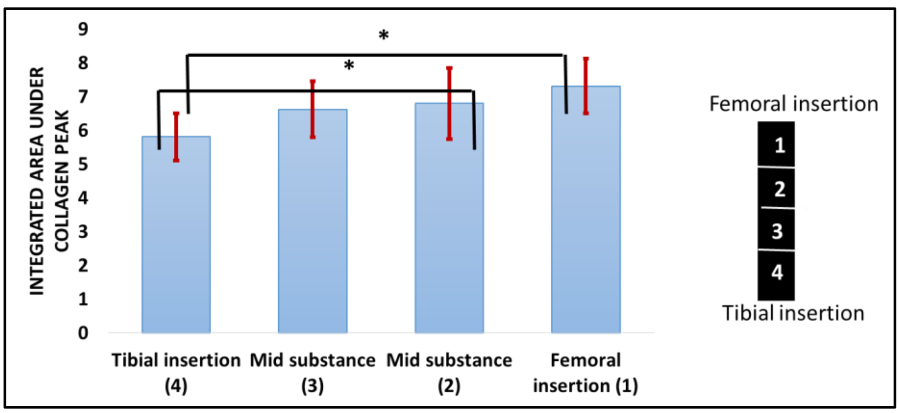

Figure 36: Integrated area under Amide II (collagen content) showed variations at different locations of rabbit MCL

cm^{-1} (amide III) which result from vibrations of the peptide bonds (also present to lesser amounts in proteoglycans, (PG) (Figure 35). It was found that the integrated area under Amide I, II and 1338 were significantly different in different regions of rabbit MCL, with tibial insertion sites containing a lower collagen content. However only Amide II results are shown here (Figure 36).

5.4.3 Mechanical testing results:

Uniaxial tensile testing showed regional variations in the MCL. Tibial insertion sites showed significantly higher values of stiffness as well as modulus when compared with the other regions of MCL (Figure 37).

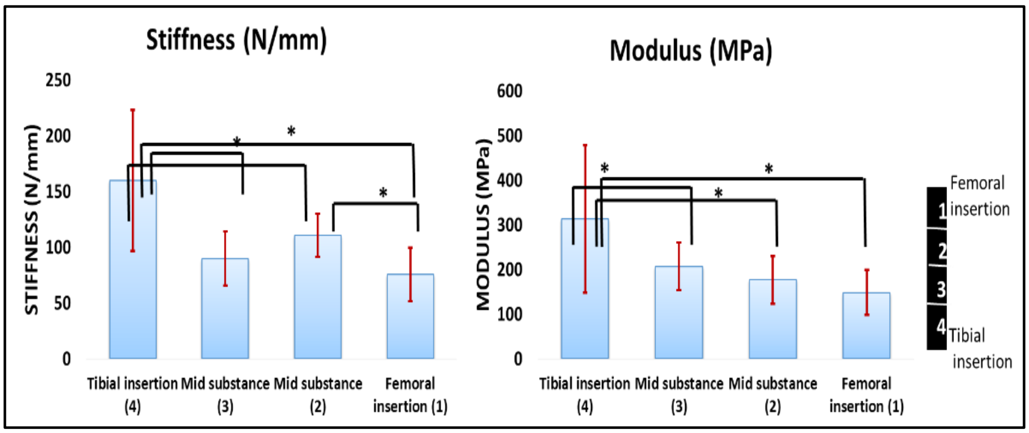

Figure 37: Results from the mechanical testing showed regional variation in the different regions of MCL. It was found that the tibial insertion showed significantly higher values when compared to the rest of the regions.

** significance at $p < 0.05$*

5.4.4: Biochemical analysis results:

The water content from different regions of rabbit MCLs varied from 57- 69%. These water content results are consistent with the literature, and the differences were statistically significant among the different regions. The water content of the tibial insertion site was significantly lower than the mid substance adjacent to the tibial insertion site. The sGAG and collagen content also varied throughout the tissue, however, the differences were not significant (data not shown).

5.4.5: Correlations of Mid-IR parameters with the mechanical testing results:

The area under the amide I absorbance (reflecting collagen content) was negatively correlated with the modulus values from the rabbit MCL (Figure 38). Further, it was found that the sGAG content from the tissue also showed a negative correlation with the modulus of the tissue (Figure 39).

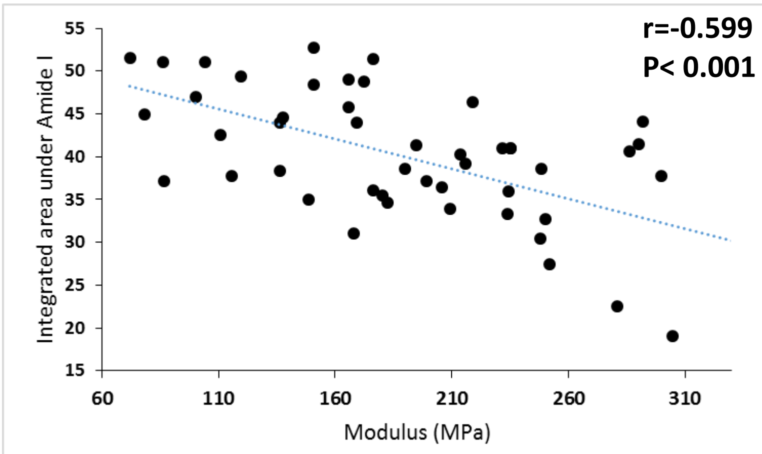

Figure 38: There was a negative correlation between the integrated area under amide I (reflecting collagen content) and modulus of the tissue.

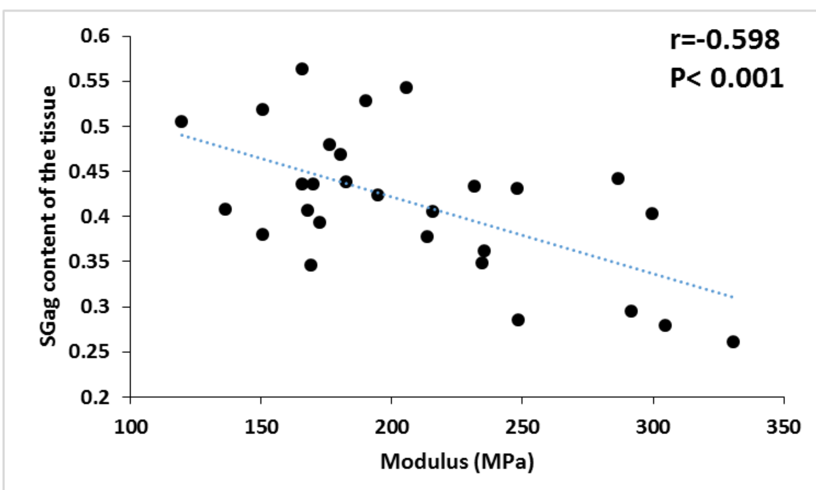

Figure 39: There was a negative correlation between sGAG content of the tissue and modulus of the tissue.

5.5: Discussion:

The current methods of assessing graft remodeling relies on indirect methods such as patient's response and the movement of the joint or the visual assessment by arthroscopy. This study has shown that NIR as well as mid-IR spectroscopic assessments have the potential to provide data that reflect mechanical properties of ligament and tendon in a non-destructive manner. In the future, this methodology has the potential to provide information on the progression of remodeling during an arthroscopic evaluation, which would aid in choosing therapeutic and rehabilitation protocols. In animal studies, fiber optic probes would allow longitudinal study of the healing graft in the same animal resulting in better understanding of the changes during ligamentization.

A previous study has shown that the composition of the rabbit MCL varies throughout the entire length; the water content at the femoral insertion was found to be the greatest and it decreased approximately 10% towards the tibial insertion site [77]. Our results from NIR derived water content showed a similar trend.

In our study we observed that there was a large variation in the mechanical properties of the MCL insertion sites. It was found that the tibial insertion showed significantly higher stiffness and modulus. A previous study by Woo et al. has reported large differences in MCL insertion sites of different species. In rabbits, the strains at tibial insertion failure were twice the femoral insertion [126]. In that study, skeletally mature rabbit MCL samples were tensile tested to failure. This is not consistent with the results of our current study, which could be due to the fact that in our experiment, MCLs were stretched only in the linear region, as opposed to the ramped to failure test in that study. Another possibility is that the strain rate used in that study (2 cm/min) was much higher than the strain rate (10 mm/min) used in our current study.

In our results, we observed that the mechanical behavior of the two insertion sites was significantly different. This could be due to the fact that in MCLs, the ligament attaches to the femoral site by direct insertion, but at the tibial site, it is by indirect insertion [127]. In direct insertion site, there are four different zones between ligament and bone. A direct insertion site allows stress concentration distribution between ligament and bone. In indirect insertion sites, there is no fibrocartilage zone. Therefore at femoral insertion, the ligament can dissipate the loads and resulted in reduced modulus of the tissue.

We also found a negative correlation between the integrated areas under the amide I absorbance (relative collagen content) and the modulus of the tissue, indicating that the stiffness or modulus decreased as protein content increased. It is not obvious why an increase in collagen content could lead to decreased stiffness or modulus, but there are several possibilities. This could be due to differences in crosslinking in different regions of the rabbit MCL. However, it was not investigated in this study, and to our knowledge has not been previously reported.

Another factor that is reported to influence mechanical properties is collagen type. Rabbit MCLs are composed of type I and type III collagen, and type III collagen is significantly higher in the central part of the ligament compared to the peripheral area. The diameter of collagen fibrils are found to be significantly different from proximal to central to distal part of MCL as well [128]. In a recent study, the ratios of collagen content and mechanical properties of the tissue were studied in the mid-substance regions of rabbit MCLs of different ages [129]. It was shown that the ratio of collagen type I and type III were directly correlated with the mechanical properties of the MCL. In our current study, we did not investigate collagen type, but it is possible that such differences could contribute to varying mechanical properties.

The results from hydroxyproline assay did not show significant differences in collagen content among different regions of rabbit MCL, in contrast to our spectral data. This could be attributable to different possibilities, including the fact that the differences are below the sensitivity of the assay, or, that our spectral data did not accurately reflect collagen amount, or it reflected the total protein in the tissue and not just collagen, or lastly, due to an artifact from the ATR data collection method. An ATR spectrum depends on the contact between the probe and the tissue, and the contact improves with the hydration of the tissue [130]. It was observed that the rabbit MCL was thicker and more hydrated at the femoral insertion than the tibial insertion site. Thus, the more hydrated femoral insertion tissue could conceivably have greater contact with the probe tip used in this study, compared to the tibial insertion site. In the future, a flat tip ATR probe could be utilized, which would potentially overcome this artifact, if present. The reason this would address this artifact is that the flat tip will have only one crystal surface for the contact with the tissue as opposed to the loop like multiple contact surfaces as the probe used in this study. Thus, a maximum contact with the probe should be obtained regardless of small differences in hydration of tissues.

There were some limitations to our study as well. To imitate the actual in-vivo data collection conditions, we collected the NIR data without separating the MCL from the bone. Our previous study showed that the NIR radiation was able to penetrate through the rabbit MCL in the water absorbance region. Therefore the absorbance recorded could have had some absorbance from the bone as well. A separate experiment was performed by collecting NIR spectra of MCL regions with and without the bone underneath (N = 3). NIR spectra were collected from MCLs with bone underneath, followed by separation of the MCL from the bone, placement of the MCL on a dark non- reflective surface (black anodized aluminum alloy), and collection of NIR spectra from the same regions. Second derivative spectra of MCL with and without bone underneath the ligament were also compared, and the ratios of water absorbances at 5200 and 7000 cm^{-1} for MCL with and without bone underneath compared. It was found that the ratios of water peaks from MCLs with bone underneath and without bone were not significantly different (data not shown). It is important to note that in humans, the thickness of the MCL is approximately 4 mm [131], and in this case, the absorbances from the bone would not interfere with the data collected from the ligament by NIR spectroscopy.

Another limitation addresses the presence of fluid during standard arthroscopy procedures, where the knee joint is filled with pressurized saline to rinses off the synovial fluid, which gives the surgeon a clearer view of the ligament, and keeps the joint open. In that case the probe will be surrounded by saline, which may interfere during data collection. To address this issue, NIR and mid-IR spectra were collected from MCLs in phosphate buffer saline (PBS), and compared to spectra collected from hydrated ligaments not submerged in PBS. A separate NIR spectrum of PBS was collected as a reference. A constant pressure of 0.24lb was applied during mid-IR data collection to ensure consistent contact with the tissue.

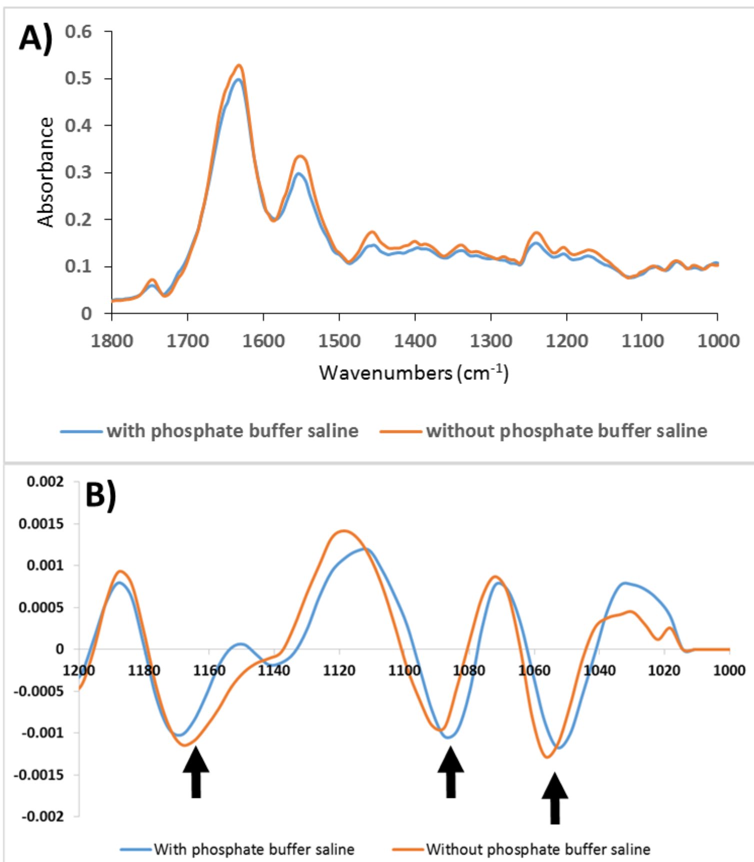

Figure 40: Comparison of mid-IR spectra of MCL in phosphate buffer saline and out of phosphate buffer saline (A). Second derivative comparison in the spectral range 1000-1100 cm^{-1} showed peak shifts as shown by arrows.

In both methods, it was observed that the overall shape of the spectrum from the MCL when collected in PBS was similar to the shape of MCL out of PBS. For mid-IR spectra, when the second derivatives of the MCL spectra with and without PBS were compared, subtle differences were seen in the lower wavenumber regions. Small peak shifts were seen in the 1000-1100 cm^{-1} regions, which is the least sensitive region of the ATR probe (Figure 40). For NIR data, the second derivative of PBS was easily distinguishable from that of MCLs when collected in PBS. The matrix peaks were clearly seen in the 4500 cm^{-1} and between 5700 and 5900 cm^{-1} in the MCL spectra (figure 41).

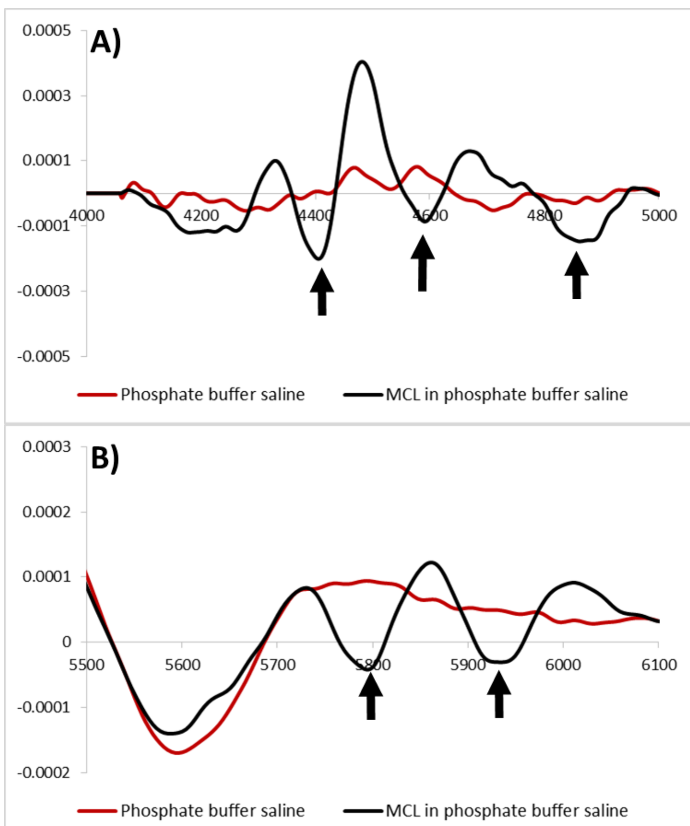

Figure 41: Comparison of second derivatives of NIR spectra of phosphate buffer saline and MCL in phosphate buffer saline. The matrix peaks were seen in 4000-5000 cm^{-1} region (A) and 5500-6000 cm^{-1} (B) as shown by arrows.

Further, we wanted to quantify the differences between the spectra, and hence we looked at the ratios of Amide I/Amide II, Amide I/ 1338 cm^{-1} and Amide II/1338 cm^{-1} for mid-IR

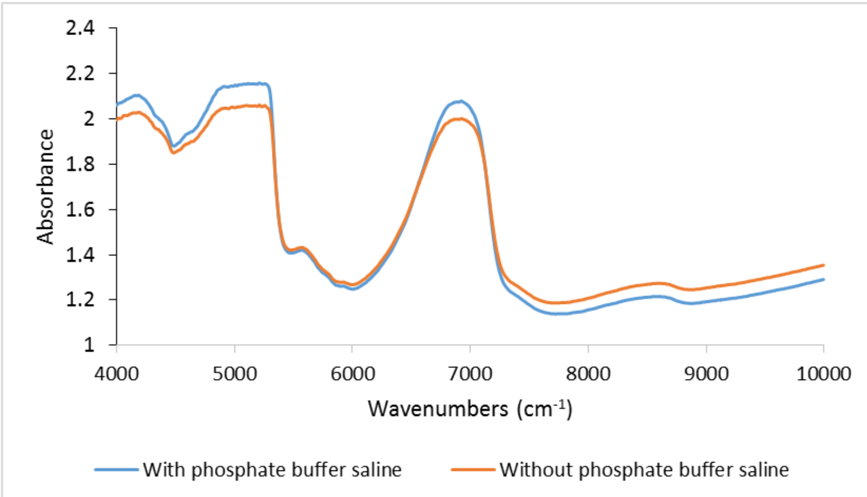

Figure 42: Comparison of NIR spectra of MCL in phosphate buffer saline and out of phosphate buffer saline

data and ratios of 5200 cm^{-1} (free and bound water absorbance) to 7000 cm^{-1} (free water absorbance) for NIR data. For mid-IR data, our results indicated that the ratios of Amide I/Amide II were not significantly different for the samples collected in PBS and out of PBS. However, the ratios of Amide II/ 1338 cm^{-1} were slightly higher ($p=0.079$) in the samples collected in PBS. In the case of NIR data, the ratios of water absorbances didn't show a clear trend between the MCL spectra in PBS or out of PBS.

5.6 Conclusion:

It was found that the NIR, mid-IR and mechanical properties of the MCL varied throughout the length of MCL, and thus this ligament was a good model for assessment of correlations of spectral and mechanical properties. Together, the results from this study demonstrate that non-destructive infrared spectroscopic data reflect mechanical properties of the ligament, and ultimately, could also reflect those of a remodeling graft. In future studies, for more accurate representation of the in-vivo scenario, spectral data should be collected in a PBS environment. In addition, future studies will investigate data collection in a synovial fluid environment.

CHAPTER 6

6.0 CONCLUSION:

The purpose of this thesis was to assess whether infrared fiber optic methods could be utilized to differentiate tendons and ligaments, as a first step towards arthroscopic use for assessment of ligament repair. Our results showed that mid-IR spectroscopy was able to differentiate between ligament and tendon composition, which represent the two extreme ends of the ligamentization process. Partial least square regression discriminant analysis correctly classified 94% sample into ACL or tendon. A non-destructive modality will improve understanding of the changes that occur during ligamentization and could lead to advancement of surgical reconstruction techniques, biologic adjunctive therapies and postoperative rehabilitation protocols. In an animal study, fiber optic probes would allow longitudinal study of the healing graft in the same animal resulting in better understanding of the changes during ligamentization. Better understanding of ligamentization could lead toward improved therapeutic interventions and post-operative protocols.

In the next specific aim, we established the depth of penetration of the NIR radiation into different connective tissues such as articular cartilage, ACL, patellar tendon (bovine tissue) and MCL (rabbit tissue). Our results showed that the depth of penetration of NIR radiation into different tissues differed throughout the NIR spectral range. The results from this study demonstrated that the depth of penetration of NIR radiation into articular cartilage varies throughout the spectral range, 4000-10000 cm^{-1}, from 0.5 mm to at least 5 mm. The optimal NIR frequency range to ensure the absorbances being evaluated are only from cartilage and not from the subchondral bone is no higher than 7000 cm^{-1}.

In rabbit MCL, the NIR radiation was not able to penetrate through the 1 mm thick tissue in the spectral range of 4000-5000 cm^{-1}. However, it was able to penetrate through 5000-10000 cm^{-1}, indicating that in this range there will possibly be interference from bone absorbances. The thickness of human ACL is on average 3-3.5 mm; therefore, the entire NIR spectrum should be optimal for NIR evaluation without underlying bone absorbances contributing to the spectra.

In the last specific aim of this thesis, NIR and mid-IR spectroscopy derived parameters were evaluated and correlated to mechanical properties of the rabbit MCL. It was found that the NIR, mid-IR and mechanical properties of the MCL varied throughout the length of MCL. The water content in the femoral insertion site was significantly higher compared to other regions of the MCL. The tibial insertion site showed higher values for stiffness and modulus. It has been shown that in the initial stage of ligament healing the water content and GAGs concentration increases in the healing tissue and decreases as the tissue heals [132]. Since NIR spectroscopy offers a non-destructive method to determine water content of the tissue, could prove valuable tool to study ligament healing.

Together, these studies from this thesis will lay the foundation for a minimally invasive method for evaluation of healing ligament injuries, which will ultimately aid in clinical decision making.

CHAPTER 7

FUTURE STUDIES:

The purpose of the studies in this thesis was to develop a protocol to use non-destructive infrared fiber optic methods to study ligamentization in a clinical setting. The results from these studies are very encouraging and here are some future directions from which this project can benefit from.

1) Cadaveric studies:

The overall goal of this project is to be able to use a non-destructive method which will be enable us to get better understanding of the changes that occur during human ligamentization. However, in this thesis the main approach was to do the ground work which will lead to this overall goal of this big project. Here all the experiments were done on the harvested tissues. In order to use these fiber optic probes in a clinical setting, there are several questions still need to be answered. The only way an infrared fiber optic probe could be used to study ligamentization in a clinical setting will be through an arthroscope portal. The future studies will need to focus on the optimal contact of the probes with the tissues, and may include improved design of the fiber optic probes.

2) Animal studies:

Animal studies could really benefit from a non-destructive method. A non-destructive method offers a tool to understand the ligamentization process of the same animal over a long period of time. In the first aim of this thesis, mid-IR spectroscopy was able to differentiate between ligament and tendon composition. However, these are two extreme ends of the ligamentization process and now it will be important to see if spectroscopy has the potential to monitor the entire ligamentization process.

3) Engineering ligament assessment:

Although autografts do provide a good solution for ACL reconstruction, they nevertheless they do present some problems such as donor site morbidity and muscle weakness, and thus tissue engineering of the ligament could be another solution. There have been several studies showing promising results in ligament tissue engineering, however, there are several challenges still need to be resolved to optimize the engineered tissue. A non-destructive method could be used to compare the outcomes of engineered ligament with different scaffolds, different stimuli (growth factors, ultrasound, and mechanical stimuli) and cell based therapies.

REFERENCES:

[1] M. M. Murray and B. C. Fleming, "The Biology of the Normal ACL," in *The ACL Handbook*, ed: Springer, 2013, pp. 63-72.

[2] V. Sanchis-Alfonso, S. Zaffagnini, E. Roselló-Sastre, M. Carmen Carda, and M. Carlos Monteagudo, "Graft Healing in ACL Reconstruction: Can We Enhance It in Clinical Practice?," in *The ACL-Deficient Knee*, ed: Springer, 2013, pp. 113-129.

[3] V. Duthon, C. Barea, S. Abrassart, J. Fasel, D. Fritschy, and J. Ménétrey, "Anatomy of the anterior cruciate ligament," *Knee surgery, sports traumatology, arthroscopy,* vol. 14, pp. 204-213, 2006.

[4] M. M. Murray, "ACL Injury Epidemiology," in *The ACL Handbook*, ed: Springer, 2013, pp. 3-17.

[5] L. Lohmander, A. Östenberg, M. Englund, and H. Roos, "High prevalence of knee osteoarthritis, pain, and functional limitations in female soccer players twelve years after anterior cruciate ligament injury," *Arthritis & Rheumatism,* vol. 50, pp. 3145-3152, 2004.

[6] C. Domnick, M. J. Raschke, and M. Herbort, "Biomechanics of the anterior cruciate ligament: Physiology, rupture and reconstruction techniques," *World journal of orthopedics,* vol. 7, p. 82, 2016.

[7] W. Petersen and T. Zantop, "Anatomy of the anterior cruciate ligament with regard to its two bundles," *Clinical orthopaedics and related research,* vol. 454, pp. 35-47, 2007.

[8] T. Iwahashi, K. Shino, K. Nakata, N. Nakamura, Y. Yamada, H. Yoshikawa*, et al.*, "Assessment of the “functional length” of the three bundles of the anterior cruciate ligament," *Knee Surgery, Sports Traumatology, Arthroscopy,* vol. 16, pp. 167-174, 2008.

[9] R. Siebold, D. Dejour, and S. Zaffagnini, *Anterior Cruciate Ligament Reconstruction: A Practical Surgical Guide*: Springer Science & Business, 2014.

[10] S. H. Liu, R.-S. Yang, R. Al-Shaikh, and J. M. Lane, "Collagen in Tendon, Ligament, and Bone Healing: A Current Review," *Clinical orthopaedics and related research,* vol. 318, pp. 265-278, 1995.

[11] T. J. Lujan, C. J. Underwood, N. T. Jacobs, and J. A. Weiss, "Contribution of glycosaminoglycans to viscoelastic tensile behavior of human ligament," *Journal of Applied Physiology,* vol. 106, pp. 423-431, 2009.

[12] C. Frank, D. Amiel, S. L. Woo, and W. Akeson, "Normal ligament properties and ligament healing," *Clinical orthopaedics and related research*, vol. 196, pp. 15-25, 1985.

[13] S. P. Reese and J. A. Weiss, "Tendons and Ligaments: Current State and Future Directions," in *Multiscale Modeling in Biomechanics and Mechanobiology*, ed: Springer, 2015, pp. 159-206.

[14] M. M. Murray, "The Biology of Impaired Healing of Joint Tissues," in *The ACL Handbook*, ed: Springer, 2013, pp. 101-112.

[15] F. H. Fu, C. H. Bennett, C. Lattermann, and C. B. Ma, "Current trends in anterior cruciate ligament reconstruction part 1: biology and biomechanics of reconstruction," *The American Journal of Sports Medicine,* vol. 27, pp. 821-830, 1999.

[16] J. Marrale, M. C. Morrissey, and F. S. Haddad, "A literature review of autograft and allograft anterior cruciate ligament reconstruction," *Knee surgery, sports traumatology, arthroscopy,* vol. 15, pp. 690-704, 2007.

[17] K. P. Spindler, J. E. Kuhn, K. B. Freedman, C. E. Matthews, R. S. Dittus, and F. E. Harrell, "Anterior cruciate ligament reconstruction autograft choice: Bone-tendon-bone versus hamstring does it really matter? a systematic review," *The American Journal of Sports Medicine,* vol. 32, pp. 1986-1995, 2004.

[18] M. V. Hogan, Y. Kawakami, C. D. Murawski, and F. H. Fu, "Tissue engineering of ligaments for reconstructive surgery," *Arthroscopy: The Journal of Arthroscopic & Related Surgery,* vol. 31, pp. 971-979, 2015.

[19] S. W. Meisterling, R. J. Schoderbek, and J. R. Andrews, "Anterior cruciate ligament reconstruction," *Operative techniques in sports medicine,* vol. 17, pp. 2-10, 2009.

[20] D. Amiel, C. Frank, F. Harwood, J. Fronek, and W. Akeson, "Tendons and ligaments: a morphological and biochemical comparison," *Journal of Orthopaedic Research,* vol. 1, pp. 257-265, 1983.

[21] P. P. Provenzano and R. Vanderby, "Collagen fibril morphology and organization: implications for force transmission in ligament and tendon," *Matrix Biology,* vol. 25, pp. 71-84, 2006.

[22] D. Amiel, J. B. Kleiner, R. D. Roux, F. L. Harwood, and W. H. Akeson, "The phenomenon of "ligamentization": anterior cruciate ligament reconstruction with autogenous patellar tendon," *J Orthop Res,* vol. 4, pp. 162-72, 1986.

[23] A. N. Mastrangelo, B. M. Haus, P. Vavken, M. P. Palmer, J. T. Machan, and M. M. Murray, "Immature animals have higher cellular density in the healing anterior cruciate ligament than adolescent or adult animals," *Journal of Orthopaedic Research,* vol. 28, pp. 1100-1106, 2010.

[24] H. O. Mayr, A. Stoehr, M. Dietrich, R. von Eisenhart-Rothe, R. Hube, S. Senger, *et al.*, "Graft-dependent differences in the ligamentization process of anterior cruciate ligament grafts in a sheep trial," *Knee Surgery, Sports Traumatology, Arthroscopy,* vol. 20, pp. 947-956, 2012.

[25] S. Claes, P. Verdonk, R. Forsyth, and J. Bellemans, "The “Ligamentization” Process in Anterior Cruciate Ligament Reconstruction What Happens to the Human Graft? A Systematic Review of the Literature," *The American Journal of Sports Medicine,* vol. 39, pp. 2476-2483, 2011.

[26] L. Pauzenberger, S. Syré, and M. Schurz, "“Ligamentization” in Hamstring Tendon Grafts After Anterior Cruciate Ligament Reconstruction: A Systematic Review of the Literature and a Glimpse Into the Future," *Arthroscopy: The Journal of Arthroscopic & Related Surgery,* vol. 29, pp. 1712-1721, 2013.

[27] R. P. Janssen and S. U. Scheffler, "Remodeling of Hamstring Tendon Grafts After ACL Reconstruction," in *Anterior Cruciate Ligament Reconstruction,* ed: Springer, 2014, pp. 257-265.

[28] S. Oakley, I. Portek, Z. Szomor, R. Appleyard, P. Ghosh, B. Kirkham*, et al.*, "Arthroscopy–a potential “gold standard” for the diagnosis of the chondropathy of early osteoarthritis," *Osteoarthritis and cartilage,* vol. 13, pp. 368-378, 2005.

[29] N. Maffulli, U. G. Longo, S. Campi, and V. Denaro, "Meniscal Tears (Meniscectomy, Meniscopexy, Meniscal Transplants/Scaffolds)," *Evidence-Based Orthopedics,* pp. 803-811, 2012.

[30] R. Crawford, G. Walley, S. Bridgman, and N. Maffulli, "Magnetic resonance imaging versus arthroscopy in the diagnosis of knee pathology, concentrating on meniscal lesions and ACL tears: a systematic review," *British medical bulletin,* vol. 84, pp. 5-23, 2007.

[31] L. David, E. S. Grood, F. R. Noyes, and R. E. Zernicke, "Biomechanics of ligaments and tendons," *Exercise and sport sciences reviews,* vol. 6, pp. 125-182, 1978.

[32] C. T. Laurencin and J. W. Freeman, "Ligament tissue engineering: an evolutionary materials science approach," *Biomaterials,* vol. 26, pp. 7530-7536, 2005.

[33] R. B. Martin, D. B. Burr, N. A. Sharkey, and D. P. Fyhrie, "Mechanical properties of ligament and tendon," in *Skeletal Tissue Mechanics,* ed: Springer, 2015, pp. 175-225.

[34] R. Jones, N. Nawana, M. Pearcy, D. Learmonth, D. Bickerstaff, J. Costi*, et al.*, "Mechanical properties of the human anterior cruciate ligament," *Clinical Biomechanics,* vol. 10, pp. 339-344, 1995.

[35] N. Chandrashekar, H. Mansouri, J. Slauterbeck, and J. Hashemi, "Sex-based differences in the tensile properties of the human anterior cruciate ligament," *Journal of biomechanics,* vol. 39, pp. 2943-2950, 2006.

[36] G. Milano, P. D. Mulas, F. Ziranu, S. Piras, A. Manunta, and C. Fabbriciani, "Comparison between different femoral fixation devices for ACL reconstruction with doubled hamstring tendon graft: a biomechanical analysis," *Arthroscopy: The Journal of Arthroscopic & Related Surgery,* vol. 22, pp. 660-668, 2006.

[37] S. U. Scheffler, N. P. Südkamp, A. Göckenjan, R. F. Hoffmann, and A. Weiler, "Biomechanical comparison of hamstring and patellar tendon graft anterior cruciate ligament reconstruction techniques," *Arthroscopy: The Journal of Arthroscopic & Related Surgery,* vol. 18, pp. 304-315, 2002.

[38] A. Debandi, A. Maeyama, S. Lu, C. Hume, S. Asai, B. Goto*, et al.*, "Biomechanical comparison of three anatomic ACL reconstructions in a porcine model," *Knee Surgery, Sports Traumatology, Arthroscopy,* vol. 19, pp. 728-735, 2011.

[39] B. Beynnon and A. A. Amis, "In vitro testing protocols for the cruciate ligaments and ligament reconstructions," *Knee Surgery, Sports Traumatology, Arthroscopy,* vol. 6, pp. S70-S76, 1998.

[40] C. N. Maganaris, "Tensile properties of in vivo human tendinous tissue," *Journal of biomechanics,* vol. 35, pp. 1019-1027, 2002.

[41] C. N. Maganaris and J. P. Paul, "In vivo human tendon mechanical properties," *The Journal of physiology,* vol. 521, pp. 307-313, 1999.

[42] N. Saupe, L. M. White, M. M. Chiavaras, J. Essue, I. Weller, M. Kunz*, et al.*, "Anterior Cruciate Ligament Reconstruction Grafts: MR Imaging Features at Long-term Follow-up—Correlation with Functional and Clinical Evaluation 1," *Radiology,* vol. 249, pp. 581-590, 2008.

[43] R. Mohankumar, L. M. White, and A. Naraghi, "Pitfalls and Pearls in MRI of the Knee," *American Journal of Roentgenology,* vol. 203, pp. 516-530, 2014.

[44] P. Van Dyck, F. M. Vanhoenacker, J. L. Gielen, L. Dossche, J. Van Gestel, K. Wouters*, et al.*, "Three tesla magnetic resonance imaging of the anterior cruciate ligament of the knee: can we differentiate complete from partial tears?," *Skeletal radiology,* vol. 40, pp. 701-707, 2011.

[45] S. Gohil, P. Annear, and W. Breidahl, "Anterior cruciate ligament reconstruction using autologous double hamstrings: a comparison of standard versus minimal debridement techniques using MRI to assess revascularisation A RANDOMISED PROSPECTIVE STUDY WITH A ONE-YEAR FOLLOW-UP," *Journal of Bone & Joint Surgery, British Volume,* vol. 89, pp. 1165-1171, 2007.

[46] A. M. Chaudhari, E. A. Zelman, D. C. Flanigan, C. C. Kaeding, and H. N. Nagaraja, "Anterior Cruciate Ligament–Injured Subjects Have Smaller Anterior Cruciate Ligaments Than Matched Controls A Magnetic Resonance Imaging Study," *The American journal of sports medicine,* vol. 37, pp. 1282-1287, 2009.

[47] A. Boskey and N. Pleshko Camacho, "FT-IR imaging of native and tissue-engineered bone and cartilage," *Biomaterials,* vol. 28, pp. 2465-2478, 2007.

[48] A. L. Boskey and R. Mendelsohn, "Infrared spectroscopic characterization of mineralized tissues," *Vib Spectrosc,* vol. 38, pp. 107-114, 2005.

[49] H. Büning-Pfaue, "Analysis of water in food by near infrared spectroscopy," *Food Chemistry,* vol. 82, p. 9, 2003.

[50] I. Notingher and R. E. Imhof, "Mid-infrared in vivo depth-profiling of topical chemicals on skin," *Skin Research and Technology,* vol. 10, pp. 113-121, 2004.

[51] S. Wartewig and R. H. Neubert, "Pharmaceutical applications of Mid-IR and Raman spectroscopy," *Advanced drug delivery reviews,* vol. 57, pp. 1144-1170, 2005.

[52] P. A. West, M. P. Bostrom, P. A. Torzilli, and N. P. Camacho, "Fourier transform infrared spectral analysis of degenerative cartilage: an infrared fiber optic probe and imaging study," *Appl Spectrosc,* vol. 58, pp. 376-81, Apr 2004.

[53] A. Hanifi, X. Bi, X. Yang, B. Kavukcuoglu, P. C. Lin, E. Dicarlo*, et al.*, "Infrared Fiber Optic Probe Evaluation of Degenerative Cartilage Correlates to Histological Grading," *Am J Sports Med,* vol. 40, p. 9, Oct 29 2012.

[54] J. P. Spalazzi, A. L. Boskey, N. Pleshko, and H. H. Lu, "Quantitative Mapping of Matrix Content and Distribution across the Ligament-to-Bone Insertion," *PloS one,* vol. 8, p. e74349, 2013.

[55] J. Lammertyn, A. Peirs, J. De Baerdemaeker, and B. Nicolaı, "Light penetration properties of NIR radiation in fruit with respect to non-destructive quality assessment," *Postharvest Biol Technol,* vol. 18, pp. 121-132, 2000.

[56] F. Faris, M. Thorniley, Y. Wickramasinghe, R. Houston, P. Rolfe, N. Livera*, et al.*, "Non-invasive in vivo near-infrared optical measurement of the penetration depth in the neonatal head," *Clin Phys Physiol Meas,* vol. 12, p. 353, 1991.

[57] W. A. P. Luck, ""Structure of water and aqueous solutions" " in *Proceedings of the International Symposium held at in July 1973*, Marburg, 1974, pp. 247-284.

[58] U. P. Palukuru, C. M. McGoverin, and N. Pleshko, "Assessment of hyaline cartilage matrix composition using near infrared spectroscopy," *Matrix Biology,* 2014.

[59] C. P. Brown, J. C. Bowden, L. Rintoul, R. Meder, A. Oloyede, and R. W. Crawford, "Diffuse reflectance near infrared spectroscopy can distinguish normal from enzymatically digested cartilage," *Phys Med Biol,* vol. 54, pp. 5579-94, Sep 21 2009.

[60] I. Afara, I. Prasadam, R. Crawford, Y. Xiao, and A. Oloyede, "Non-destructive evaluation of articular cartilage defects using near-infrared (NIR) spectroscopy in osteoarthritic rat models and its direct relation to Mankin Score," *Osteoarthr Cartilage,* 2012.

[61] McGoverin CM, Lewis K, Yang X, Bostrom MPG, and P. N, "The Contribution of Bone and Cartilage to the Near Infrared Spectrum of Osteochondral Tissue," *Applied Spectroscopy,* vol. 68, p. 1168, 2014.

[62] M. Hoffmann, M. Lange, F. Meuche, T. Reuter, H. Plettenberg, G. Spahn, *et al.*, "Comparison of Optical and Biomechanical Properties of Native and Artificial Equine Joint Cartilage under Load using NIR Spectroscopy," *Biomed Tech,* vol. 57, p. 1, 2012.

[63] G. O. Hofmann, J. Marticke, R. Grossstuck, M. Hoffmann, M. Lange, H. K. Plettenberg, *et al.*, "Detection and evaluation of initial cartilage pathology in man: A comparison between MRT, arthroscopy and near-infrared spectroscopy (NIR) in their relation to initial knee pain," *Pathophysiology,* vol. 17, pp. 1-8, Feb 2010.

[64] N. Dupuy, O. Galtier, Y. Le Dréau, C. Pinatel, J. Kister, and J. Artaud, "Chemometric analysis of combined NIR and MIR spectra to characterize French olives," *Eur J Lipid Sci Technol,* vol. 112, pp. 463-475, 2010.

[65] N. Dupuy, O. Galtier, D. Ollivier, P. Vanloot, and J. Artaud, "Comparison between NIR, MIR, concatenated NIR and MIR analysis and hierarchical PLS model. Application to virgin olive oil analysis," *Analytica chimica acta,* vol. 666, pp. 23-31, 2010.

[66] C. Armstrong and V. Mow, "Variations in the intrinsic mechanical properties of human articular cartilage with age, degeneration, and water content," *J Bone Joint Surg Am,* vol. 64, pp. 88-94, 1982.

[67] P. Timmins and J. Wall, "Bone water," *Calcified tissue research,* vol. 23, pp. 1-5, 1977.

[68] D. Howell, *Etiopathogenesis of osteoarthritis, in McCarty DJ(ed): Arthritis and Allied Conditions*. Philadelphia,: McCarty, D.J., ed. Lea and Febiger, , 1989.

[69] M. V. Padalkar, R. G. Spencer, and N. Pleshko, "Near Infrared Spectroscopic Evaluation of Water in Hyaline Cartilage," *Ann Biomed Eng,* vol. 41, pp. 1-11, 2013/07/04 2013.

[70] S. Chaudhury, C. Dicko, M. Burgess, F. Vollrath, and A. Carr, "Fourier transform infrared spectroscopic analysis of normal and torn rotator-cuff tendons," *Journal of Bone & Joint Surgery, British Volume,* vol. 93, pp. 370-377, 2011.

[71] Å. Rinnan, F. v. d. Berg, and S. B. Engelsen, "Review of the most common pre-processing techniques for near-infrared spectra," *TrAC Trends in Analytical Chemistry,* vol. 28, pp. 1201-1222, 2009.

[72] K. H. Esbensen, *Multivariate Data Analysis - in Practice: An Introduction to Multivariate Data Analysis and Experimental Design*, 5Th ed. Woodbridge: CAMO Sosftware, 2010.

[73] M. Zeaiter, J.-M. Roger, and V. Bellon-Maurel, "Robustness of models developed by multivariate calibration. Part II: The influence of pre-processing methods," *TrAC Trends in Analytical Chemistry,* vol. 24, pp. 437-445, 2005.

[74] G. V. Kamath, J. C. Redfern, P. E. Greis, and R. T. Burks, "Revision anterior cruciate ligament reconstruction," *The American journal of sports medicine,* vol. 39, pp. 199-217, 2011.

[75] B. S. Delay, R. J. Smolinski, W. M. Wind, and D. S. Bowman, "Current practices and opinions in ACL reconstruction and rehabilitation: results of a survey of the American Orthopaedic Society for Sports Medicine," *The American journal of knee surgery,* vol. 14, pp. 85-91, 2000.

[76] D. Farlay, M.-E. Duclos, E. Gineyts, C. Bertholon, S. Viguet-Carrin, J. Nallala, *et al.*, "The ratio 1660/1690 cm− 1 measured by infrared microspectroscopy is not specific of enzymatic collagen cross-links in bone tissue," *PLoS One,* vol. 6, p. e28736, 2011.

[77] P. Sabiston, "Biochemical heterogeneity within the maturing rabbit medial collateral ligament," 1988.

[78] S. Oakley, I. Portek, Z. Szomor, A. Turnbull, G. Murrell, B. Kirkham, *et al.*, "Poor accuracy and interobserver reliability of knee arthroscopy measurements are improved by the use of variable angle elongated probes," *Annals of the rheumatic diseases,* vol. 61, pp. 540-543, 2002.

[79] M. P. O'Brien, M. Penmatsa, U. Palukuru, P. West, X. Yang, M. P. Bostrom, *et al.*, "Monitoring the Progression of Spontaneous Articular Cartilage Healing with Infrared Spectroscopy," *Cartilage,* p. 1947603515572874, 2015.

[80] S. G. Kazarian and K. A. Chan, "ATR-FTIR spectroscopic imaging: recent advances and applications to biological systems," *Analyst,* vol. 138, pp. 1940-1951, 2013.

[81] A. Wall and T. Board, "Chemical Basis for the Histological Use of Safranin O in the Study of Articular Cartilage," in *Classic Papers in Orthopaedics*, ed: Springer, 2014, pp. 433-435.

[82] D. Ballabio and V. Consonni, "Classification tools in chemistry. Part 1: linear models. PLS-DA," *Analytical Methods,* vol. 5, pp. 3790-3798, 2013.

[83] C. K. Kuo, J. E. Marturano, and R. S. Tuan, "Novel strategies in tendon and ligament tissue engineering: Advanced biomaterials and regeneration motifs," *BMC Sports Science, Medicine and Rehabilitation,* vol. 2, p. 20, 2010.

[84] R. Cheheltani, C. M. McGoverin, J. Rao, D. A. Vorp, M. F. Kiani, and N. Pleshko, "Fourier transform infrared spectroscopy to quantify collagen and elastin in an in vitro model of extracellular matrix degradation in aorta," *Analyst,* vol. 139, pp. 3039-3047, 2014.

[85] B. Rougraff, K. D. Shelbourne, P. K. Gerth, and J. Warner, "Arthroscopic and histologic analysis of human patellar tendon autografts used for anterior cruciate

ligament reconstruction," *The American journal of sports medicine,* vol. 21, pp. 277-284, 1993.

[86] S. Scheffler and R. Becker, "Graft Remodeling and Bony Ingrowth After Anterior Cruciate Ligament Reconstruction," *Sports Injuries: Prevention, Diagnosis, Treatment and Rehabilitation,* pp. 1077-1087, 2015.

[87] K. Marumo, M. Saito, T. Yamagishi, and K. Fujii, "The “Ligamentization” Process in Human Anterior Cruciate Ligament Reconstruction With Autogenous Patellar and Hamstring Tendons A Biochemical Study," *The American journal of sports medicine,* vol. 33, pp. 1166-1173, 2005.

[88] G. Spahn, H. Plettenberg, E. Kahl, H. M. Klinger, T. Muckley, and G. O. Hofmann, "Near-infrared (NIR) spectroscopy. A new method for arthroscopic evaluation of low grade degenerated cartilage lesions. Results of a pilot study," *BMC Musculoskelet Disord,* vol. 8, p. 47, 2007.

[89] D. Baykal, O. Irrechukwu, P. C. Lin, K. Fritton, R. G. Spencer, and N. Pleshko, "Nondestructive assessment of engineered cartilage constructs using near-infrared spectroscopy," *Appl Spectrosc,* vol. 64, pp. 1160-6, Oct 2010.

[90] I. Afara, S. Singh, and A. Oloyede, "Application of near infrared (NIR) spectroscopy for determining the thickness of articular cartilage," *Med Eng Phys,* vol. 35, pp. 88-95, 2012.

[91] S. Vahur, A. Teearu, and I. Leito, "ATR-FT-IR spectroscopy in the region of 550â€“230cmâˆ’ 1 for identification of inorganic pigments," *Spectrochimica Acta Part A: Molecular and Biomolecular Spectroscopy,* vol. 75, pp. 1061-1072.

[92] A. R. Poole, T. Kojima, T. Yasuda, F. Mwale, M. Kobayashi, and S. Laverty, "Composition and structure of articular cartilage - A template for tissue repair," *Clinical Orthopaedics and Related Research,* pp. S26-S33, Oct 2001.

[93] M. Huber, S. Trattnig, and F. Lintner, "Anatomy, biochemistry, and physiology of articular cartilage," *Investigative Radiology,* vol. 35, pp. 573-580, Oct 2000.

[94] T. Neogi and Y. Zhang, "Epidemiology of osteoarthritis," *Rheumatic Disease Clinics of North America,* vol. 39, pp. 1-19, 2013.

[95] M. Huber, S. Trattnig, and F. Lintner, "Anatomy, biochemistry, and physiology of articular cartilage," *Invest Radiol,* vol. 35, pp. 573-80, Oct 2000.

[96] A. I. Caplan, M. Elyaderani, Y. Mochizuki, S. Wakitani, and V. M. Goldberg, "Principles of cartilage repair and regeneration," *Clin Orthop Relat Res,* pp. 254-69, Sep 1997.

[97] G. Spahn, H. M. Klinger, M. Baums, U. Pinkepank, and G. O. Hofmann, "Reliability in arthroscopic grading of cartilage lesions: results of a prospective blinded study for evaluation of inter-observer reliability," *Archives of orthopaedic and trauma surgery,* vol. 131, pp. 377-381, 2011.

[98] G. Spahn, H. M. Klinger, and G. O. Hofmann, "How valid is the arthroscopic diagnosis of cartilage lesions? Results of an opinion survey among highly experienced arthroscopic surgeons," *Archives of orthopaedic and trauma surgery,* vol. 129, pp. 1117-1121, 2009.

[99] A. Billaud, A. Moreau-Gaudry, D. Girardeau-Montaut, F. Billet, D. Saragaglia, and P. Cinquin, "Navigated intra-articular us probe for 3d arthroscopic knee cartilage evaluation: In-vitro thickness measurement and cadaveric feasibility," *J Bone Joint Surg Proc,* vol. 95, pp. 26-26, 2013.

[100] M. F. Koff, K. K. Amrami, and K. R. Kaufman, "Clinical evaluation of T2 values of patellar cartilage in patients with osteoarthritis," *Osteoarthritis Cartilage,* vol. 15, pp. 198-204, Feb 2007.

[101] S. Lusse, H. Claassen, T. Gehrke, J. Hassenpflug, M. Schunke, M. Heller*, et al.*, "Evaluation of water content by spatially resolved transverse relaxation times of human articular cartilage," *Magn Reson Imaging,* vol. 18, pp. 423-30, May 2000.

[102] W. Marik, S. Apprich, G. Welsch, T. Mamisch, and S. Trattnig, "Biochemical evaluation of articular cartilage in patients with osteochondrosis dissecans by means of quantitative T2-and T2*-mapping at 3T MRI: A feasibility study," *European Journal of Radiology,* vol. 81, pp. 923-927, 2012.

[103] Ding C, F. C, and a. G. J, "How important is MRI for detecting early osteoarthritis?," *Nat Clin Pract Rheumatol,* vol. 4, pp. 4-5, 2008.

[104] M. P. Recht, D. W. Goodwin, C. S. Winalski, and L. M. White, "MRI of articular cartilage: revisiting current status and future directions," *AJR Am J Roentgenol,* vol. 185, pp. 899-914, Oct 2005.

[105] I. O. Afara and A. Oloyede, *Near Infrared Spectroscopy Evaluation of Articular Cartilage: Decision-Making in Arthroplasty: Real-Time Assessment of Articular Cartilage*: LAP Lambert Academic Publishing 2012.

[106] G. Spahn, H. Plettenberg, H. Nagel, E. Kahl, H. M. Klinger, T. Muckley*, et al.*, "Evaluation of cartilage defects with near-infrared spectroscopy (NIR): an ex vivo study," *Med Eng Phys,* vol. 30, pp. 285-92, Apr 2008.

[107] I. Afara, S. Singh, and A. Oloyede, "Load-unloading response of intact and artificially degraded articular cartilage correlated with near infrared (NIR) absorption spectra," *J Mech Behav Biomed,* pp. 249-258, 2012.

[108] G. Spahn, G. Felmet, and G. O. Hofmann, "Traumatic and degenerative cartilage lesions: arthroscopic differentiation using near-infrared spectroscopy (NIRS)," *Arch Orthop Trauma Surg,* vol. 133, pp. 1-6, 2013.

[109] I. Afara, I. Prasadam, R. Crawford, Y. Xiao, and A. Oloyede, "Non-destructive evaluation of articular cartilage defects using near-infrared (NIR) spectroscopy in

osteoarthritic rat models and its direct relation to Mankin score," *Osteoarthr Cartil,* vol. 20, pp. 1367-1373, 2012.

[110] G. Li, S. E. Park, L. E. DeFrate, M. E. Schutzer, L. Ji, T. J. Gill*, et al.*, "The cartilage thickness distribution in the tibiofemoral joint and its correlation with cartilage-to-cartilage contact," *Clinical biomechanics,* vol. 20, pp. 736-744, 2005.

[111] D. Shepherd and B. Seedhom, "Thickness of human articular cartilage in joints of the lower limb," *Annals of the rheumatic diseases,* vol. 58, pp. 27-34, 1999.

[112] R. Karvonen, W. Negendank, R. Teitge, A. Reed, P. Miller, and F. Fernandez-Madrid, "Factors affecting articular cartilage thickness in osteoarthritis and aging," *The Journal of rheumatology,* vol. 21, pp. 1310-1318, 1994.

[113] H. Büning-Pfaue, "Analysis of water in food by near infrared spectroscopy," *Food Chemistry,* vol. 82, pp. 107-115, 2003.

[114] H. Cen and Y. He, "Theory and application of near infrared reflectance spectroscopy in determination of food quality," *Trends in Food Science & Technology,* vol. 18, pp. 72-83, 2007.

[115] D. M. Swenson, C. L. Collins, T. M. Best, D. C. Flanigan, S. K. Fields, and R. Comstock, "Epidemiology of knee injuries among US high school athletes," 2005.

[116] J. M. Hootman, R. Dick, and J. Agel, "Epidemiology of collegiate injuries for 15 sports: summary and recommendations for injury prevention initiatives," *Journal of athletic training,* vol. 42, p. 311, 2007.

[117] K. M. Sutton and J. M. Bullock, "Anterior cruciate ligament rupture: differences between males and females," *Journal of the American Academy of Orthopaedic Surgeons,* vol. 21, pp. 41-50, 2013.

[118] L. S. Beasley, D. E. Weiland, A. F. Vidal, A. Chhabra, A. S. Herzka, M. T. Feng, *et al.*, "Anterior cruciate ligament reconstruction: a literature review of the anatomy, biomechanics, surgical considerations, and clinical outcomes," *Operative Techniques in Orthopaedics,* vol. 15, pp. 5-19, 2005.

[119] O. R. Seynnes, J. Bojsen-Møller, K. Albracht, A. Arndt, N. J. Cronin, T. Finni, *et al.*, "Ultrasound-based testing of tendon mechanical properties: a critical evaluation," *Journal of Applied Physiology,* vol. 118, pp. 133-141, 2015.

[120] X. Bi, G. Li, S. Doty, and N. Camacho, "A novel method for determination of collagen orientation in cartilage by Fourier transform infrared imaging spectroscopy (FT-IRIS)," *Osteoarthritis and Cartilage,* vol. 13, pp. 1050-1058, 2005.

[121] F. Faris, M. Thorniley, Y. Wickramasinghe, R. Houston, P. Rolfe, N. Livera*, et al.*, "Non-invasive in vivo near-infrared optical measurement of the penetration depth in the neonatal head," *Clinical Physics and Physiological Measurement,* vol. 12, p. 353, 1991.

[122] K. A. Derwin, L. J. Soslowsky, W. Green, and S. H. Elder, "A new optical system for the determination of deformations and strains: calibration characteristics and experimental results," *Journal of biomechanics*, vol. 27, pp. 1277-1285, 1994.

[123] R. W. Farndale, D. J. Buttle, and A. J. Barrett, "Improved quantitation and discrimination of sulphated glycosaminoglycans by use of dimethylmethylene blue," *Biochimica et Biophysica Acta (BBA)-General Subjects*, vol. 883, pp. 173-177, 1986.

[124] J. Eastoe and A. Leach, "A survey of recent work on the amino acid composition of vertebrate collagen and gelatin," in *Recent advances in gelatin and glue research*, ed: Pergamon Press London, 1958, pp. 173-178.

[125] C. D. Hoemann, J. Sun, V. Chrzanowski, and M. D. Buschmann, "A multivalent assay to detect glycosaminoglycan, protein, collagen, RNA, and DNA content in milligram samples of cartilage or hydrogel-based repair cartilage," *Analytical biochemistry*, vol. 300, pp. 1-10, 2002.

[126] S. Woo, M. Gomez, Y. Seguchi, C. Endo, and W. Akeson, "Measurement of mechanical properties of ligament substance from a bone-ligament-bone preparation," *Journal of Orthopaedic Research*, vol. 1, pp. 22-29, 1983.

[127] M. Benjamin, H. Toumi, J. Ralphs, G. Bydder, T. Best, and S. Milz, "Where tendons and ligaments meet bone: attachment sites ('entheses') in relation to exercise and/or mechanical load," *Journal of anatomy*, vol. 208, pp. 471-490, 2006.

[128] C. Wan, Z. Hao, and S. Wen, "A quantitative comparison of morphological and histological characteristics of collagen in the rabbit medial collateral ligament," *Annals of Anatomy-Anatomischer Anzeiger*, vol. 195, pp. 562-569, 2013.

[129] C. Wan, Z. Hao, S. Wen, and H. Leng, "A quantitative study of the relationship between the distribution of different types of collagen and the mechanical behavior of rabbit medial collateral ligaments," *PloS one*, vol. 9, p. e103363, 2014.

[130] P. Ducheyne, K. Healy, D. E. Hutmacher, D. W. Grainger, and C. J. Kirkpatrick, *Comprehensive Biomaterials: Online Version*: Elsevier, 2011.

[131] J. I. Lee, I. S. Song, Y. B. Jung, Y. G. Kim, C. H. Wang, H. Yu, *et al.*, "Medial collateral ligament injuries of the knee: ultrasonographic findings," *Journal of ultrasound in medicine*, vol. 15, pp. 621-625, 1996.

[132] R. C. Manske and J. DeWitt, "Ligament Healing," *Fundamental Orthopedic Management for the Physical Therapist Assistant*, vol. 32, p. 155, 2015.

APPENDIX A: RABBIT MCL MECHANICAL TESTING

Material:

#11 blades	Wooden stir sticks
Blade holder	Weigh boats
Jewler's forceps	10-24 hardware
Stain and thread for stainlines	Permanent marker
Metric Ruler	Acrylic tubing (1" OD)
PMMA powder	Duct tape
PMMA catalyst	

Potting Preparation Procedure:

1. Cut acrylic tubing into ~1.5" lengths with a bandsaw.
2. Use the sharpie marker to mark the sides of the tubing as medial and lateral. If desired, you may also mark the anterior and posterior sides of the tubes.
3. Tap 2 10-24 holes on two sides of the tube, half way away from the top edge. This will be useful for placing the specimen during PMMA potting.
4. Cover the bottom of the pots with duct tape. This will prevent liquid PMMA from oozing out of the bottom of the pot.
5. Set tubes aside for later use.

General Specimen Preparation Procedure

1. Remove desired bone-ligament-bone complexes from freezer (specimens have already been dissected and frozen by Scott and Mugdha at Temple).
2. Place specimens, still in their plastic bags, in sink. Wait overnight or until completely thawed.
3. Label weigh boats by writing on the underside in permanent marker. Each specimen should have its own weigh boat.
4. Place the thawed samples into their respective weigh boats which are filled with PBS.
5. Ensure that the medial/lateral and anterior/posterior sides of the bone plugs can be readily identified on the femur and the tibia.
6. Drill a 1/8" medial/lateral hole in the femoral bones, less than 1" away from the distal-most edge of the bone.
7. Place the specimen into the PBS bath to prevent them from drying out.

Fine Dissection Procedure:

1. Remove the gauze from the ligament and inspect visually.
2. If necessary, remove any remaining musculature, connective tissue, and/or extraneous ligamentous tissue by using the jeweler's forceps and size 11 scalpel blade.
3. If necessary, determine the medial/lateral and anterior/posterior sides of the bone plugs and mark the bone plugs with a Sharpie marker.
4. Clean up the rest of the ligament, particularly the insertion site.

5. Place the complex back into the PBS bath and repeat steps 1-4 for remaining samples.

Stain Lines:

1. Create stain by mixing 100μL hematoxylin with 50μL FeCl and 50μL Wiegert's solution in a slanted weigh boat.
2. Orient specimen such that the insertion to the bone can be clearly visualized.
3. Remove the specimen from the PBS bath and dry the MCL with a Kim Wipe.
4. Place stain lines at the insertion site of the tibia and make another stain line proximally 2.5 mm away from the insertion line. Repeat the process for the insertion to the femur.
5. Use Kim Wipe to gently remove any excess stain from the ligament.
6. Place the sample back into the PBS bath. Repeat steps 2-5 for remaining samples.
7. Cross-sectional area measurement
8. Remove the specimen from the PBS bath, and blot MCL with Kim Wipe to remove excess PBS without drying the tendon.
9. Do your best to ensure that the ligament is laying flat. If necessary, use a small block of plastic to support the ligament from underneath to ensure good measurements.
10. To the best of your ability, use GisMO to measure the thickness of the ligament at the mid-substance.
11. Record all measurements.

12. Submerge the ligament in the PBS bath and repeat steps 1-4 for remaining samples.
13. Post-process in MATLAB using the script called gismo_area to determine the cross-sectional areas of the mid-substances for each ligament.

Potting:

1. In a disposable cup, mix PMMA powder and PMMA primer until a pourable liquid is created. Use your best judgment to create a mixture that is neither too thick nor too thin.
2. Remove ligament from PBS bath.
3. Using the hardware and the tapped holes, secure the tibia into a pot.
4. Wrap the exposed ligament with a PBS-soaked gauze pad.
5. Pour the PMMA mixture into the pot, taking care not to pour over the ligament.
6. Wipe all surfaces that may have been unintentionally covered with PMMA. The pots will not go into the fixtures properly if there is any slop on the outside of the pots.
7. Allow to dry for 30-45 minutes, or until the PMMA has cured.
8. Repeat entire procedure for all specimens.
9. Be sure to continue to spray the gauze with PBS solution to keep the ligament moist. Once all of the pots have cured you are ready to test.

Image Capture Set-Up:

1. Get a Basler Scout camera out of the cabinet, attach the lens, and plug in the firewire cable.
2. Log in to image capture computer (computer on the right).
3. Find folder on image capture computer desktop called “Software”. Open folder and click on Digivlepo->Table->BaslerScout.vi to open software.
4. Set “cam X”, depending on which camera you chose to use.
5. Run Labview module.
6. Create directory and new folder for image capture using the folder button. Change specimen name, keeping “~” at the end of the file name.

Instron Set-Up

1. Turn on Instron 5542.
2. Use a 5000 N load cell.
3. Ensure that Bluehill and the Instron are communicating properly.
4. Open Test Method Called Hast_Rabbit_MCL.
5. Affix the femoral grip by attaching it to the Instron crosshead.
6. Affix the tibial grip by screwing it into the base of the Instron machine.
7. Load the femur into the femoral bone grip. Secure by screwing the set screws tightly.
8. Load the tibial pot into the tibial grip. Make sure that the MCL is aligned with the crosshead. This ensures that the uniaxial force passes through the ligament, and a moment is not being applied to the ligament.
9. Lock the tibial pot into place by securing the set screws.

10. With tendon slack, balance the load.
11. Apply a preload of ~0.01 N and reset gauge length.

Mechanical Testing Protocol

1. 5 second hold under position control
2. Ramp to 45N at 0.05mm/s

Image Prep:

1. Move camera stand forward/backwards for "zoom" and up/down and left/right to center the tendon.
2. Move light so that it is lighting the ligament well and doesn't not create obstructive shadows.
3. Ensure that image is zoomed out enough so that the whole complex is still captured in the image, even when ramping to failure.

Start Test

1. Start test by simultaneously pressing "OK" to start test for Instron and "zero time" on image capture.
2. Press Record Image button when test reaches ramp to failure step in protocol.
3. Test is ~2 minutes in duration.

End Test

1. At end of test, gently increase displacement to visualize how ligament failed. Record failure method.

2. Take a calibration image with the prefix “Cal~” by using the mm side of a ruler. Be sure to set up the correct directory to save this image.
3. Transfer Instron and image files to appropriate drive.
4. Clean up all materials and return equipment to its proper storage areas.

APPENDIX B: TISSUE PROCESSING PROTOCOL FOR RABBIT MCL

Rabbit MCLs were dissected and stored in PBS and PI in the freezer at -4C. After mechanical testing the MCL was cut and was fixed with formalin for 12 hours. After that it was rinsed thrice to remove all formalin. The tissues were processed in a processor with following parameters:

70% ethanol (30 minutes) X 2

95% ethanol (30 minutes) X 2

100% ethanol (1hour and 15 minutes) X 2

Xylene (1and half hour total)

Paraffin (1 hour 24 minutes) X 2

Adapted from: Animal protocols

Then the tissues were embedded in paraffin cross-sectionally.

APPENDIX C: PROTOCOL FOR HISTOLOGY

Immerse in d-H20 for 2 min.

Immerse in 3% acetic acid for 3 min.

Immerse in Alcian blue for 7 min

First immerse in acid alcohol for 2 min

Second immerse in acid alcohol for 2 min

Immerse in tap water for 1 min

Immerse in Hematoxylin for 5 min

Wash in tap water until water is clear.

Immerse in Eosin for 10-20 seconds.

First immerse in 95% alcohol for 1 min.

Second immerse in 95% alcohol for 1 min.

Immerse in 100% alcohol for 1 min.

Immerse in Xylene for 1 min.

Immerse the sections in another Xylene, which will act as a hold.

Mount cover slip with Permount.

APPENDIX D: PERMISSION TO USE COPYRIGHT MATERIAL

Springer

01_02

PERMISSION LETTER

April 14, 2016

Springer reference

The ACL-Deficient Knee
pp 113-129
Date: 06 October 2012
Graft Healing in ACL Reconstruction: Can We Enhance It in Clinical Practice?
Vicente Sanchis-Alfonso, Stefano Zaffagnini, Esther Roselló-Sastre, Carmen Carda, Carlos Monteagudo
© Springer-Verlag London 2013
DOI 10.1007/978-1-4471-4270-6_10
Print ISBN 978-1-4471-4269-0
Online ISBN 978-1-4471-4270-6

Material to be used: Figures 10.1, 10.2 and 10.3

Knee Surgery, Sports Traumatology, Arthroscopy
March 2006, Volume 14, Issue 3, pp 204-213
Anatomy of the anterior cruciate ligament
V. B. Duthon, C. Barea, S. Abrassart, J. H. Fasel, D. Fritschy, J. Ménétrey
© Springer-Verlag 2005
DOI 10.1007/s00167-005-0679-9
Print ISSN 0942-2056
Online ISSN 1433-7347
Journal No: 00167

Material to be used: Figure 1

The ACL Handbook
pp 63-72
Date: 21 March 2013
The Biology of the Normal ACL
Martha M. Murray, Braden C. Fleming
© Springer Science+Business Media New York 2013
DOI 10.1007/978-1-4614-0760-7_5
Print ISBN 978-1-4614-0759-1
Online ISBN 978-1-4614-0760-7

Material to be used: Figure 5.5

Your project

Requestor:	Mugdha Padalkar
	tub84972@temple.edu
University:	Temple University
Purpose:	Dissertation/Thesis

With reference to your request to reuse material in which Springer controls the copyright, our permission is granted free of charge under the following conditions:

Springer material

- represents original material which does not carry references to other sources (if material in question refers with a credit to another source, authorization from that source is required as well);

Springer

01_02

PERMISSION LETTER

- requires full credit (Springer book/journal title, chapter/article title, volume, year of publication, page, name(s) of author(s), original copyright notice) to the publication in which the material was originally published by adding: "With permission of Springer";
- figures, illustrations, and tables may be altered minimally to serve your work. Any other abbreviations, additions, deletions and/or any other alterations shall be made only with prior written authorization of the author;
- Springer does not supply original artwork or content.

<u>This permission</u>

- is non-exclusive;
- is valid for one-time use only for the purpose of defending your thesis limited to university-use only and with a maximum of 100 extra copies in paper. If the thesis is going to be published, permission needs to be reobtained.
- includes use in an electronic form, provided it is an author-created version of the thesis on his/her own website and his/her university's repository, including UMI (according to the definition on the Sherpa website: http://www.sherpa.ac.uk/romeo/);
- is subject to courtesy information to the author (address is given in the publication);
- is personal to you and may not be sublicensed, assigned, or transferred by you to any other person without Springer's written permission;
- is only valid if no personal rights, trademarks, or competitive products are infringed.

This license is valid only when the conditions noted above are met.

Permission free of charge does not prejudice any rights we might have to charge for reproduction of our copyrighted material in the future.

Rights and Permissions
Springer
Tiergartenstr. 17
69121 Heidelberg
Germany

Branch of Springer-Verlag GmbH, Heidelberger Platz 3, 14197 Berlin, Germany | Amtsgericht Berlin-Charlottenburg, HRB 91881 B
Managing Directors: Derk Haank, Martin Mos, Peter Hendriks | Springer is part of Springer Science+Business Media